NTNU – Trondheim
Norwegian University of
Science and Technology

Atmospheric mercury speciation and aerosol properties at Ny-Ålesund

Pan Wang

Environmental Toxicology and Chemistry
Submission date: May 2015
Supervisor: Torunn Berg, IKJ

Norwegian University of Science and Technology
Department of Chemistry

NTNU – Trondheim
Norwegian University of
Science and Technology

Atmospheric mercury speciation and aerosol properties at Ny-Ålesund

Pan Wang

May 2015

MASTER THESIS

Department of Chemistry

Norwegian University of Science and Technology

Supervisor 1: Torunn Berg, IKJ, NTNU

Supervisor 2: Johan Ström, Stockholm University

Preface

This is a Master Thesis in Chemistry Department of NTNU as a part of the Environmental Toxicology and Chemistry study programme. Besides, it is a part of a joint project "Mercury in the Arctic: The roles that atmosphere, aerosols, snow and ground play on the mercury cycle at Ny-Ålesund". This joint project is carried out by Norwegian University of Science and Technology (NTNU), Norwegian Institute for Air Research (NILU), Norwegian Institute for Water Research (NIVA), Stockholm University (SU), and Environment Canada.

The joint project is started in July 2013, and it is led by Professor Torunn Berg. It is also an integrated part of Arctic Monitoring and Assessment Programme (AMAP). The data and results generated from this joint project will help to improve the understanding of atmospheric mercury and its effect on the Arctic ecosystem and human health.

Trondheim, 20.04.2015

Pan Wang

Pan Wang

Acknowledgment

I would like to thank my supervisor Torunn Berg for teaching me of theoretical background and the mechanism of Tekran instruments, and helping me revise my thesis. And I would like to thank my supervisor Johan Ström for teaching me of aerosol chemistry. Without the help from my supervisors, I would not be able to finish my thesis.

I would like to thank the scientists and technical staff at the Norwegian Polar Institute (Sverdrupstasjonen) for maintaining the instruments in Zeppelin station. Without their help, I could not get the precise data from Zeppelin station.

Thanks to Katrine Aspmo Pfaffhuber at NILU for providing me the mercury data from NILU's mercury speciation unit at Zeppelin station.

I would also like to thank Tekran company for providing me Tekran HgLogger Plus software so that I could combine the raw daily mercury data into one file.

Thanks to all of the team members of this joint project, I got a lot of help and inspiration from the plenary meetings.

P. W.

Abstract

Gaseous elemental mercury (GEM), reactive gaseous mercury (RGM) and particulate bound mercury (PHg) measurements at Zeppelin station, Ny-Ålesund, Svalbard were analyzed for the correlations with meteorological conditions and aerosol number concentrations.

During the study period from 1 April 2007 to 31 December 2011, a full atmospheric mercury depletion event (AMDE) only appeared at a temperature range of -23 to $-12\,^{\circ}$C. The highest monthly median values of RGM concentrations appeared in April (11 pg m^{-3}) and June (6 pg m^{-3}). PHg concentrations were generally higher in winter-spring period (November-April), and the highest monthly median values appeared in February (17 pg m^{-3}) and April (13 pg m^{-3}).

The meteorological conditions including temperature, relative humidity and precipitation were intimately correlated with the concentrations of GEM, RGM and PHg. AMDEs had a general trend to occur under low temperature, high relative humidity, and low precipitation. It has been found that either very high relative humidity (around 98%) or no accumulated precipitation during the recent few hours backward trajectory would seem to provide a good condition for the high PHg concentrations to occur.

The accumulation mode aerosols with a size range between 100 and 562 nm in diameter seemed to be most characteristic for hosting PHg, and mercury might not tend to associate with particles smaller than 100 nm in diameter. PHg might consist of much cloud associated mercury during AMDEs.

Contents

Chapter 1

Introduction

1.1 Background

There is a significant amount of mercury entering the Arctic through long-distance transportation, and a substantial amount of mercury is from anthropogenic origin at lower latitudes (AMAP, 2011; Dietz et al., 2009). Due to the traditional diet of eating local animals, Arctic's indigenous people are facing a potential risk by exposure to mercury (AMAP, 2011).

During the recent two decades, scientists have increased the attention to mercury chemistry in the Arctic (Steffen et al., 2014). In the springtime, there is an interesting phenomenon happening in the high Arctic, referred to as atmospheric mercury depletion events (AMDEs): the AMDEs occur during a period of just a few weeks, where the long-lived gaseous elemental mercury (GEM) are converted to more quickly deposited reactive gaseous mercury (RGM) and if there are particles available, the RGM may be bound to those as particulate mercury (PHg) (Steffen et al., 2008). Both RGM and PHg may deposit quickly onto any surface such as snowpack and sea ice, and finally be delivered to Arctic ecosystem (AMAP, 2011).

The three different types of mercury have very different physical and chemical properties. GEM is the predominant form of the total atmospheric mercury, but when considering the atmospheric deposition, RGM and PHg species are more important because of the large dry deposition velocities and scavenging coefficients (Shannon and Voldner, 1995; Kim et al., 2012). The removal of atmospheric mercury is intimately related to the pre-existing aerosol, and thus it is important to investigate the aerosol distribution and properties (Pirrone and Mahaffey, 2005).

1.2 Objectives

The understanding between the relation of atmospheric mercury species and aerosol properties is still very poor. Thus, the overall aim of this thesis is to investigate the relations between mercury speciation in the atmosphere and aerosol properties by using the data from Zeppelin station, Ny-Ålesund. And it can be subdivided into several objectives:

1. To investigate what particle size range is most characteristic for hosting particulate mercury;
2. To investigate how meteorological conditions affect mercury concentrations and the associations between mercury and aerosols;
3. To improve the understanding of AMDEs and mercury speciation at Ny-Ålesund.

1.3 Mercury

Mercury (Hg), commonly known as quicksilver, is the only liquid metallic element that under standard conditions for temperature and pressure (273.15 K, 100 kPa) (Nabi, 2014). Mercury is easy to evaporate at normal temperature, and thus entering the atmosphere (Baukal Jr, 2004).

1.3.1 The source and transport of mercury

Mercury is an extremely rare element in the nature, and it has only 0.08 parts per million (ppm) of an average crustal abundance by mass (Ehrlich and Newman, 2008). The emissions of mercury to the atmosphere can be either from natural sources or anthropogenic sources. The emissions from natural sources include the contribution from primary natural sources such as volcanoes, and re-emission of previously deposited mercury on water or land surfaces. The estimated annual mercury contribution from natural processes is estimated to be 5207 $\mathrm{Mg\,yr^{-1}}$ which represent almost 70% of the total emission budget (Pirrone et al., 2010). The most important source is the ocean which accounts for 36% of the global emission budget. And then biomass burning accounts for 9% followed by deserts, non-vegetated zones and metalliferous (7%), grassland and tundra (6%), forests (5%) and re-emission after AMDEs (3%) (Pirrone et al., 2010). The emissions

from man-made sources can be divided into primary anthropogenic sources such as mining and burning of fossil fuels, and secondary anthropogenic sources where emissions occur from intentional use of mercury, for example mercury use in industrial processes (Pacyna et al., 2010).

When mercury is emitted into the atmosphere, it is advected by winds. And due to the long residence time of GEM, it can be transported fairly long distances. Although the life time of RGM and PHg is relatively very short, they can be reduced to GEM and re-emitted. As a result, the deposition and re-emission processes will eventually make mercury able to be transported to anywhere on the world (Durnford et al., 2010).

1.3.2 Mercury in the Arctic

Mercury is transported to the Arctic by air currents (within a few days), ocean currents (may take decades) and rivers (AMAP, 2011). It is shown from atmospheric models that Asia contributes most to the mercury seen in the Arctic (Durnford et al., 2010). In the Arctic, mercury is mainly deposited in inorganic forms, but it can also be transformed to methylmercury form which is more toxic and more readily bioaccumulated in the Arctic food webs. A schematic diagram is shown in Figure 1.1.

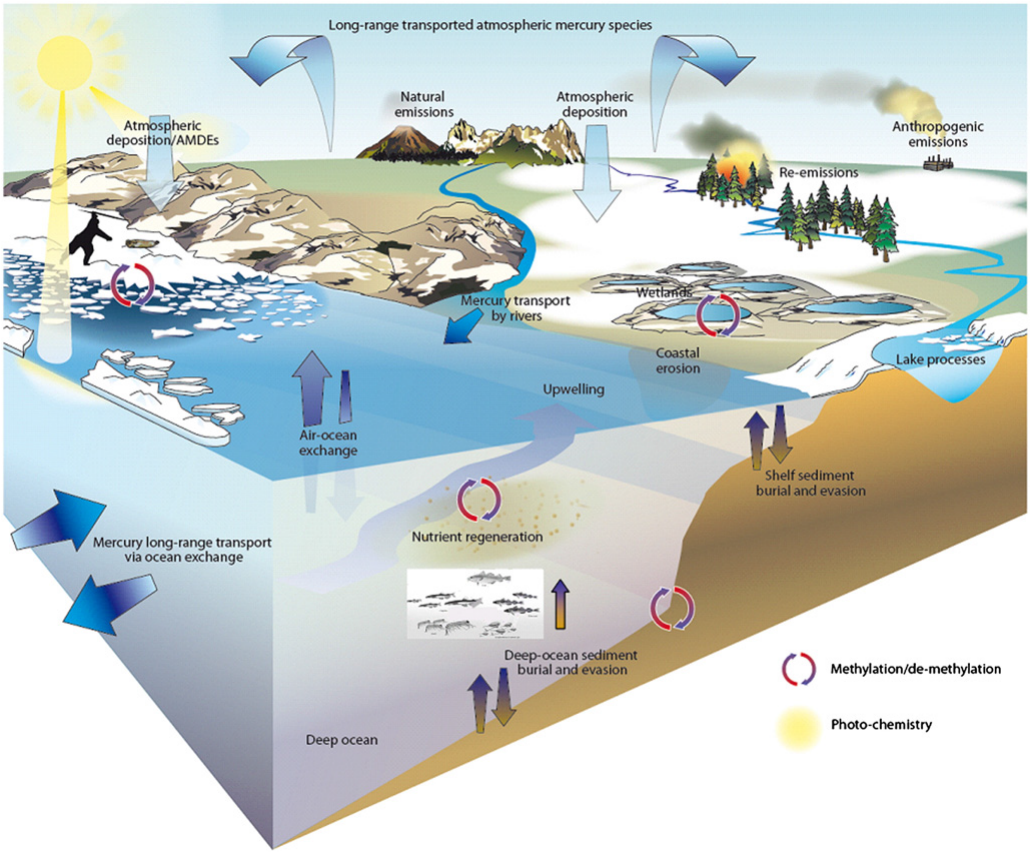

Figure 1.1: Cycling of mercury in the Arctic ecosystem (Stern et al., 2012).

Climate-related variables can influence mercury transformation processes anywhere between global emissions and the accumulation of methylmercury in food web (Stern et al., 2012). Climate change has more severe impact impact in the Arctic than most of the other places in the world, and the average Arctic temperatures have increased almost twice of the global average during the past 100 years (Bernstein et al., 2007). It is shown that climate change also have significant impact on mercury transport pathways, speciation and cycling in the Arctic ecosystems (Stern et al., 2012).

1.3.3 Atmospheric mercury

Mercury exists in three oxidation states: 0, +1 and +2. In the atmosphere, the elemental form (Hg (0)) and +2 oxidation state of mercury (Hg (II)) are predominant, while the +1 oxidation state is very rare (Schroeder and Munthe, 1998).

Atmospheric mercury can be operationally subdivided into three different fractions: gaseous elemental mercury (GEM or Hg^0), reactive gaseous mercury (RGM or GOM as gaseous oxidized mercury) and particulate bound mercury (PHg or PBM).

GEM

Gaseous elemental mercury (GEM) is the predominant form of atmospheric mercury, and it is the most stable form with a residence time from months up to 1 year due to its high vapor pressure and low solubility in water (Hedgecock and Pirrone, 2004; Selin et al., 2007; Corbitt et al., 2011). The long residence time of GEM allows homogeneous mixing within the hemisphere of origin, and it is expected to be a concentration gradient between the two hemispheres since anthropogenic sources of mercury emissions are mostly in northern hemisphere (Steffen et al., 2008). The global background concentration of GEM is 1.5-1.7 $ng\,m^{-3}$ in the northern hemisphere and 0.9-1.3 $ng\,m^{-3}$ in the southern hemisphere (Ebinghaus et al., 2002; Slemr et al., 2003; Temme et al., 2004; Kock et al., 2005; Pfaffhuber et al., 2012). Hg^0 can be oxidized to RGM by reaction with many oxidants which include ozone (O_3) (Hall, 1995; Calvert and Lindberg, 2005), hydroxyl radicals (OH) (Sommar et al., 2001; Calvert and Lindberg, 2005), and halogen atoms (Holmes et al., 2006, 2010; Stephens et al., 2012; Feddersen et al., 2012).

RGM

Reactive gaseous mercury (RGM) is a gaseous fraction of oxidized mercury, and it is operationally defined as the fraction that can be sampled by denuder measurement method (Landis et al., 2002; Steffen et al., 2008). RGM has a much shorter lifetime than GEM, with less volatility and more water solubility, and it is much easier to deposit. It is a minor part of the total atmospheric mercury, and it can deposit to the surface or be adsorbed to particles forming particulate mercury (Sheu and Mason, 2004; Lindberg et al., 2007; Steffen et al., 2008; Amos et al., 2012). RGM is assumed to consist gaseous neutral complexes such as $HgCl_2$, $HgBr_2$, and HgOBr by laboratory studies (Balabanov and Peterson, 2003; Sheu and Mason, 2004). RGM can bind to particles to create PHg . Further, RGM can be reduced back to Hg^0 by SO_2 and sunlight (Lindberg and Stratton, 1998; Feddersen et al., 2012).

PHg

Particulate mercury (PHg) is operationally defined as the atmospheric mercury fraction that can be sampled by a filter system (Gustin and Jaffe, 2010). The actual chemical identities of both

RGM and PHg are still not well determined (Steffen et al., 2014). PHg deposits much faster than GEM but slightly slower than RGM, and its deposition velocity strongly depends on the particle size, meteorological conditions (wind speed, relative humidity, and atmospheric stability), and characteristics of the deposition surface (Poissant et al., 2004; Zhang et al., 2009). Comparing to GEM and RGM, very little is known about PHg and its size distribution in the atmosphere (Feddersen et al., 2012).

1.3.4 Atmospheric mercury depletion events

In the Arctic springtime, the concentration of GEM suddenly plunges from the background level to undetectable level during a short period, and it is called atmospheric mercury depletion events (AMDEs). This phenomenon was first reported by Schroeder and Munthe (1998), and it was then confirmed that AMDEs occurred throughout the Arctic, sub-Arctic and Antarctic coasts (Lindberg et al., 2001; Ebinghaus et al., 2002; Berg et al., 2003, 2008; Poissant and Pilote, 2003; Steffen et al., 2005).

Several studies have shown a close correlation between ozone depletion events (ODEs) and AMDEs (Schroeder et al., 1998; Lindberg et al., 2002; Temme et al., 2003; Gauchard et al., 2005; Sommar et al., 2007). It is now believed that GEM is converted to more reactive species and associated to particles in the air and deposited to the environment during AMDEs, which is performed through a series of photo-chemical reactions involving halogens (Steffen et al., 2008).

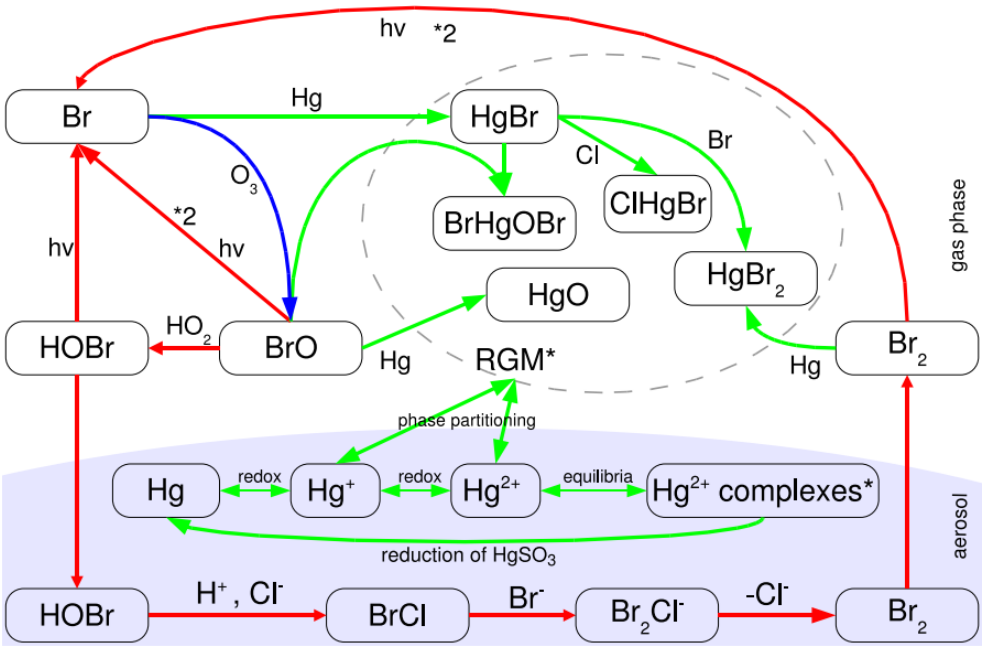

Figure 1.2: Simulated mercury and halogen chemistry. Red arrows show bromine chemistry, Hg chemistry in green arrows show mercury chemistry, and ozone destruction is in blue. RGM* refers to all mercury species in gas phase except elemental Hg, and Hg^{2+} complexes* refers to several chemical forms of Mercury which include sulfited, chlorinated and brominated forms of mercury (Xie et al., 2008).

Simplified halogen and mercury chemical reactions are shown as Figure 1.2 (Xie et al., 2008). These reactions are derived by using atmospheric chemistry box Model MECCA (Module Efficiently Calculating the Chemistry of the Atmosphere) provided by Sander et al. (2005), which contains a comprehensive atmospheric reaction mechanism including O_3, HO_x and halogen chemistry in the Arctic area. Mercury chemistry is added to this model by Xie et al. (2008), and the simulation shows the reactions between halogens and mercury in both gas phase and aerosol phase.

It has been found that the reaction of Hg with Br dominates the GEM concentration decreases during AMDEs, and BrHgOBr is the most abundant reactive mercury species in both RGM and PHg (Xie et al., 2008).

1.3.5 Atmospheric mercury emission events

Besides the appearing of AMDEs in springtime, it has been found that GEM concentration is very high during the summertime in the Canadian High Arctic (Steffen et al., 2005). It is similarly defined as atmospheric mercury emission events (AMEEs), but the mechanisms for AMEEs is lack of understanding. The origin of AMEEs is currently not known, but it might be dependent on meteorological conditions (Cole and Steffen, 2010). The high GEM concentration in summertime at Alert station is thought to be probably due to the emission of Hg from snow surfaces and tundra (Steffen et al., 2005).

1.4 Aerosol

An aerosol is technically defined as a suspension of fine solid or liquid particles in a gas, and it has a range in size from a few nanometers to tens of micrometers in diameter (Pandis and Seinfeld, 2006). According to the size, aerosols can be divided into several groups. Aerosol particles larger than 2.5 µm in diameter are referred to as coarse particles and those smaller than 2.5 µm in diameter are fine particles. Fine particles can be subdivided into several modes by different size intervals. Particles with diameters less than 10 nm are referred to as nucleation (or nuclei) mode. The Aitken mode has a size range from 10 nm to 100 nm in diameter. Nuclei and Aitken modes of aerosols are predominant of aerosols by number but only a few percent by mass (Pandis and Seinfeld, 2006). The accumulation mode has a size range from 0.1 µm to 2.5 µm in diameter, and it accounts for most of the particle surface area and a large part by mass (Pandis and Seinfeld, 2006).

The nuclei mode of aerosols have relatively short lifetimes (around hours or less), and they are formed from condensation of hot vapors and the nucleation of atmospheric species (Pandis and Seinfeld, 2006; Oliver, 2005). The nuclei mode particles can rapidly coagulate with themselves or other particles to form larger accumulation mode particles. The removal mechanisms for accumulation mode particles are least efficient, and this mode of particles can exist in the atmosphere of days or more so that they can be transported in a relatively long distance (Pandis and Seinfeld, 2006; Oliver, 2005). The coarse mode particles are formed by mechanical processes, and they have sufficiently large sedimentation velocities to be removed in a relatively

short time (Pandis and Seinfeld, 2006). In the Arctic, both nucleation mode and coarse mode aerosols are considered locally formed because of their short lifetimes.

Aerosols are very important constituents in the atmosphere, and they may act as cloud condensation nuclei (CCN) for cloud formation in the presence of a supersaturation of water vapor. The minimum CCN aerosol diameter is 50-140 nm for the formation of marine stratiform clouds, and the majority of CCNs are formed by accumulation mode aerosols (Pandis and Seinfeld, 2006; Penner et al., 2001).

At Ny-Ålesund, the number size distribution has a clear seasonal variation, and there are three different periods during the Arctic year: the haze period (March-May) which is dominated by the accumulation mode particles; the sunlit summer period (June-August) which has large abundance of small particles but less accumulation mode aerosols; and the rest of the year (September-February) which contains relatively low abundance of accumulation mode aerosols and negligible amount of the nuclei and Aitken mode aerosols (Tunved et al., 2013).

Chapter 2

Method

2.1 Zeppelin station

Ny-Ålesund is a research village, and it is one of the most northern human settlements on the world (GAWSIS, 2014). It is located in Kongsfjorden, which is on the northwest coast of Spitsbergen, Svalbard. Zeppelin Observatory (78°54'29" N, 11°52'53" E, 478 m a.s.l.) is located 1.5 km south of the settlement Ny-Ålesund. It has an altitude of 478 m on Zeppelin Mountain, which makes it hardly influenced by local contaminants. It is owned by the Norwegian Polar Institute, and Norwegian Institute for Air Research (NILU) is responsible for scientific coordination (NPI, 2014). The location of Zeppelin station is shown in Figure 2.1.

Figure 2.1: The location of Zeppelin Observatory (Source from NILU).

2.2 Mercury measurements

There are currently two separate instruments for the measurements of atmospheric mercury in Zeppelin station. One is run by NTNU, and it measures the concentrations of three different mercury species, namely GEM, RGM and PHg (Steen et al., 2009). Another one is run by NILU, and it only measures GEM (Berg et al., 2013).

Tekran products have been used to measure the ambient air mercury, and they have the capabilities for automated, continuous and relatively unattended measurements (Tekran, 2015). A Tekran 1130 denuder module and a Tekran 1135 particulate module are attached to the front end of a Tekran 2537A analyzer and provide semi-continuous concentrations of RGM and PHg. The Tekran 1130, 1135 and 2537A are therefore named the speciation system (Steen et al., 2009).

The speciation system is programmed to collect one-hour composite RGM and PHg, while the pre-concentrated RGM and PHg are determined in the following hour (Tekran method 35-2L5) (Steen et al., 2011). The schematic diagram is shown as Figure 2.2.

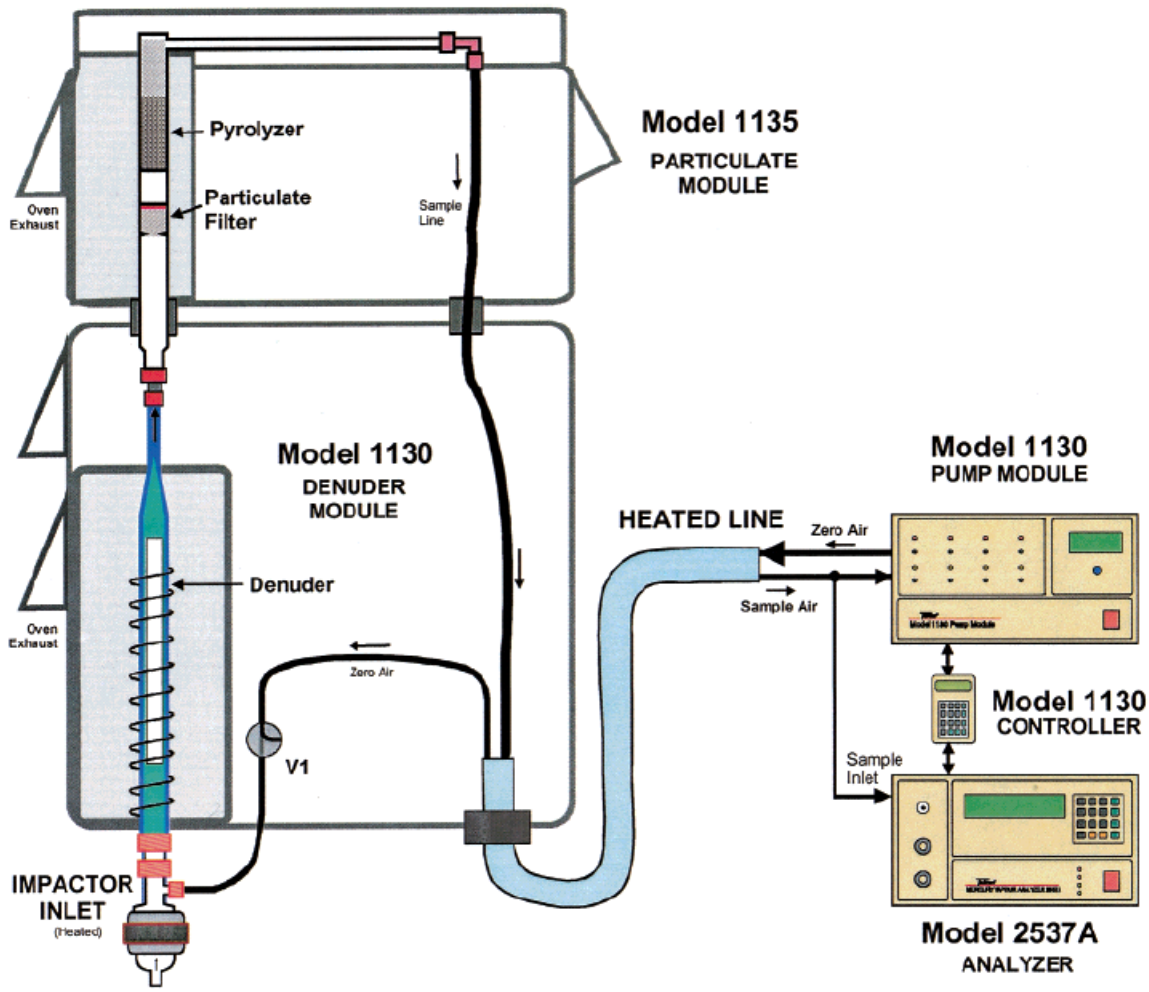

Figure 2.2: Tekran 2537-1130-1135 Atmospheric Mercury Speciation System (Lindberg et al., 2001).

Tekran Model 2537A Mercury Vapor Analyzer is used for the measurement of atmospheric Hg^0. It uses gold traps to pre-concentrate Hg^0, and then mercury is thermally desorbed and detected by using Cold Vapor Atomic Fluorescence Spectrometry (CVAFS) (Lindberg et al., 2002). It is set inside Zeppelin station and connecting Model 1130 and Model 1135 which are on the roof of the station through a heated line.

Tekran Model 1130 Oxidized Mercury Speciation Unit is used for the measurement of RGM. It generates mercury free air (Zero Air) for use in the system by passing ambient air through a series of mercury scrubbing filters. RGM is captured on a KCl-coated Thermal Annular Denuder while Hg^0 can pass through (Tekran, 2008a).

Tekran Model 1135 Particulate Mercury Unit is used for the measurement of PHg. It is conjunct with Model 1130, and fine particles (diameter is less than or equals to 2.5 µm) are trapped on the regenerable particulate filter (RPF) and they are captured by a pyrolyzer while Hg^0 can pass through. The coarse particles (diameter is larger than 2.5 µm) are captured by a heated impactor to be prevented from entering (Tekran, 2008b).

The data points of GEM are presented as the means of every 5 minutes sampling. RGM and PHg concentrations are generally very low, and they are concentrated in the denuder and particle modules first before analyzing. The captured reactive phase mercury is desorbed and transformed to elemental form that are detected in the 2537A analyzer. The instrumental operation for the measurement of RGM and PHg is shown in Table 2.1.

Cycle ID	Cycle description	Event flag
A	Flushing with blank sample	1
B	Flushing with blank sample	1
C	Flushing with blank sample	1
D	Pyrolyzer heating	2
E	RPF heating	3
F	RPF heating	3
G	RPF heating	3
H	Denuder heating	4
I	Denuder heating	5
J	Denuder heating	5
K	Cooling with blank sample	1
L	Cooling with blank sample	1

Table 2.1: Tekran 2537A cycles of operation for RGM and PHg measurements.

The concentrations of PHg and RGM were calculated by equation (2.1) and equation (2.2).

$$\mathrm{PHg}(\mathrm{pg\,m^{-3}}) = \mathrm{Cycle(D)} + \mathrm{Cycle(E)} + \mathrm{Cycle(F)} + \mathrm{Cycle(G)} - 3 \cdot (\mathrm{Cycle(B)} + \mathrm{Cycle(C)})/2 \tag{2.1}$$

$$\mathrm{RGM}(\mathrm{pg\,m^{-3}}) = \mathrm{Cycle(H)} + \mathrm{Cycle(I)} + \mathrm{Cycle(J)} - 3 \cdot (\mathrm{Cycle(B)} + \mathrm{Cycle(C)})/2 \tag{2.2}$$

NILU's GEM measurements were continuously carried out by using only the Tekran Model 2537A, which was set up with a heated sampling line and an extra Teflon filter at the inlet of the sampling line. A sampling time of 5 min and a flow rate of 1.5 L min^{-1} were used. The 5 min means of GEM were averaged to hourly or daily means and provided by NILU (Berg et al., 2013).

Although the Tekran instruments could automatically record the concentrations of the three species of mercury, the data needed to be checked frequently and gathered all together and calibrated. Mercury data from NTNU's mercury speciation unit in the period of 23.08.2013 to 01.08.2014 was downloaded by using TeamViewer, and it was collected together by using Tekran HgLogger Plus and Microsoft Excel. Mercury data for the study period of 01.04.2007 to 31.12.2011 were provided by both Katrine Aspmo Pfaffhuber at NILU and Torunn Berg.

2.3 Meteorological conditions

Meteorological data was provided by Johan Ström and obtained from the Hybrid Single-Particle Lagrangian Integrated Trajectory Model (HYSPLIT) by the National Oceanic and Atmospheric Administration (NOAA) (ARL, 2015). The HYSPILIT model shows the air parcel trajectories, as well as the meteorological data along them. Temperature, relative humidity (RH) and precipitation data was used for further analysis in this thesis. The meteorological data was not local data, but trajectory data instead. The temperature data used was the average value of the most recent one hour before the air parcel arrived to Zeppelin station. Relative humidity data used the same of most recent one hour average as temperature data did. Precipitation data was the accumulated precipitation for 10 days backwards of the arrived air parcel which was also used in previous study (Tunved et al., 2013). Some other meteorological data was also considered to have influence on mercury concentrations, such as wind, air pressure, etc. But due to the large

sample size and limited time, only temperature, relative humidity and precipitation data was analyzed in this thesis by using Microsoft Excel.

2.4 Aerosol measurements

The aerosol number size distribution was measured also at Zeppelin station using a Differential Mobility Particle Sizer (DMPS) (GAWSIS, 2014). A DMPS system consists of a Differential Mobility Analyzer (DMA) and a Condensation Particle Counter (CPC) (Winklmayr et al., 1991). DMA classifies particles according to their sizes, and then CPC counts the numbers of the classified particles (Hari and Kulmala, 2008). The particles larger than the size range to be investigated were removed by a pre-impactor and dried to a relative humidity below 40% (TROPOS, 2015). Aerosol data was provided by Johan Ström, and it was hourly average value and covered a range of 10 nm to 562 nm in diameter. Aerosol data has been analyzed by using Microsoft Excel.

2.5 Statistical analysis

2.5.1 Method detection limit

The method detection limit (MDL) is defined as the minimum concentration of a substance that can be measured and reported with 99% confidence that the analyte concentration is greater than 0 and is determined from analysis of a sample in a given matrix containing the analyte (CFR, 1986). The MDL has been considered for the concentrations of GEM, RGM and PHg in this thesis. For GEM, the MDL was used as the low detection limit of Model 2537A which was 0.1 $\mathrm{ng\,m^{-3}}$. And for RGM and PHg, the MDL equaled to the standard deviation of blank samples multiplied by 3 (Steen et al., 2011). The values less than the MDL were considered as half of the MDL.

Standard deviation (SD) was calculated by the function of Microsoft Excel, and it was theoretically calculated by the equation (2.3) and equation (2.4).

$$\mathrm{SD} = \sqrt{\frac{1}{(n-1)}\sum_{i=1}^{n}(X_i - \overline{X})^2} \tag{2.3}$$

$$\mathrm{X} = 3 \times \frac{\mathrm{Cycle(B)} + \mathrm{Cycle(C)}}{2} \tag{2.4}$$

X indicated the blank sample, and it equaled to the 3 times the average of Cycle(B) and Cycle(C) in Table 2.1.

2.5.2 Correlation coefficient

To compare the relations between two different parameters, correlation coefficient (R) has been calculated to describe the relations. Correlation coefficient was calculated by the function of Microsoft Excel, and it was using Pearson Product-Moment Correlation Coefficient (Calmorin, 2006). It was calculated by equation (2.5).

$$R = \frac{\sum(x-\overline{x})(y-\overline{y})}{\sqrt{\sum(x-\overline{x})^2\sum(y-\overline{y})^2}} \tag{2.5}$$

Here, x and y are the two arrays for comparing, and the correlation coefficient R has a range from -1 to 1. The value of R close to 1 means a strong positive correlation between the two arrays, and close to -1 means a strong negative correlation. If R is close to 0, it means the two arrays are not so correlated with each other. It is considered to have not clear correlations if R value is in between -0.4 and 0.4 (Wierig, 2004). However, the value of R is also dependent on the sample size, if the sample size is too small, R has a trend to be more close to 1 or -1 (Rubin, 2012). In this thesis, none of the correlation coefficients were calculated within too small sample size, so the R values were considered rather reliable.

2.6 Quality control

For GEM measurements, auto calibrations were carried out everyday using the internal calibration source for both Tekran 2537A instruments, and they were verified by manual injections every 3 to 4 months (Berg et al., 2013). A soda lime trap was installed in line before the instrument filter, and it was changed every two weeks. A soda lime trap can scrub deleterious compounds that may be generated when the denuder and RPF are heated during the analytical cycle, and it is essential in Tekran 2537-1130-1135 speciation system (Tekran, 2009). The denuder and RPF were replaced monthly.

The instruments were frequently checked and maintained, and every time it was recorded on the log in Zeppelin station. According to the log, several times of mechanical failures happened during the period of 2013 to 2014. And as a consequence, the instruments either stopped measuring or provided unreliable data during those times. Thus the unreliable data of those periods were considered as outliers and were removed.

Unnatural high RPF concentration might be seen when the glassware ware was changed. This might possibly be due to damaged glass frit in the RPF or that GEM was adsorbed in the glassware. Sometimes lower GEM values might be seen during those periods with strange high values (Berg et al., personal comm.). When the soda lime trap was changed, GEM, RGM and PHg might be affected depending on where in the measurement cycle the instrument was.

The MDLs for RGM and PHg were calculated and shown in Table 2.2.

	2007	2008	2009	2010	2011	2013-2014
MDL for RGM & PHg (pg m^{-3})	4	9	21	11	7	19

Table 2.2: MDL for RGM and PHg from 2007 to 2011 and 2013-2014.

Landis et al. (2002) reported that the MDL for one-hour sampling of RGM with KCl-coated denuder was 6.2 pg m^{-3} through laboratory and field evaluations. However, the calculated yearly based MDL varied from year to year, and it was relatively very high for the periods of 2009 and 2013-2014. According to the log, problems happened several times with the Zero Air generation system during 2009. And it had a trend to increase the values of blank sample during each sampling cycle, which might increase the standard deviation thus increase the MDL. During 2013-2014, snow was filled inside Tekran 1130 model in December, and it was found several times of

leakage in the system which might increase also the values of blank sample thus increased the MDL.

Chapter 3

Results and discussion

3.1 Mercury data of 2013-2014 from NTNU's speciation unit

The mercury data from NTNU's speciation unit was collected from 23.08.2013 to 01.08.2014, and it is shown in Figure 3.1 and Figure 3.2.

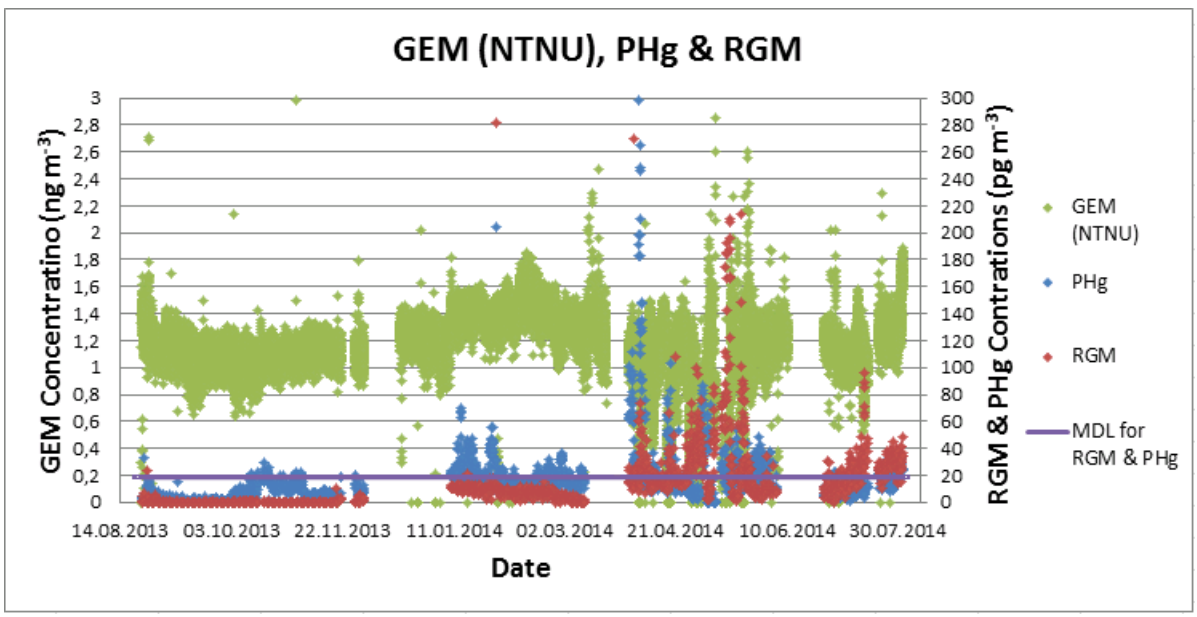

Figure 3.1: GEM, PHg, RGM concentrations measured by NTNU's speciation unit from 23.08.2013 to 01.08.2014.

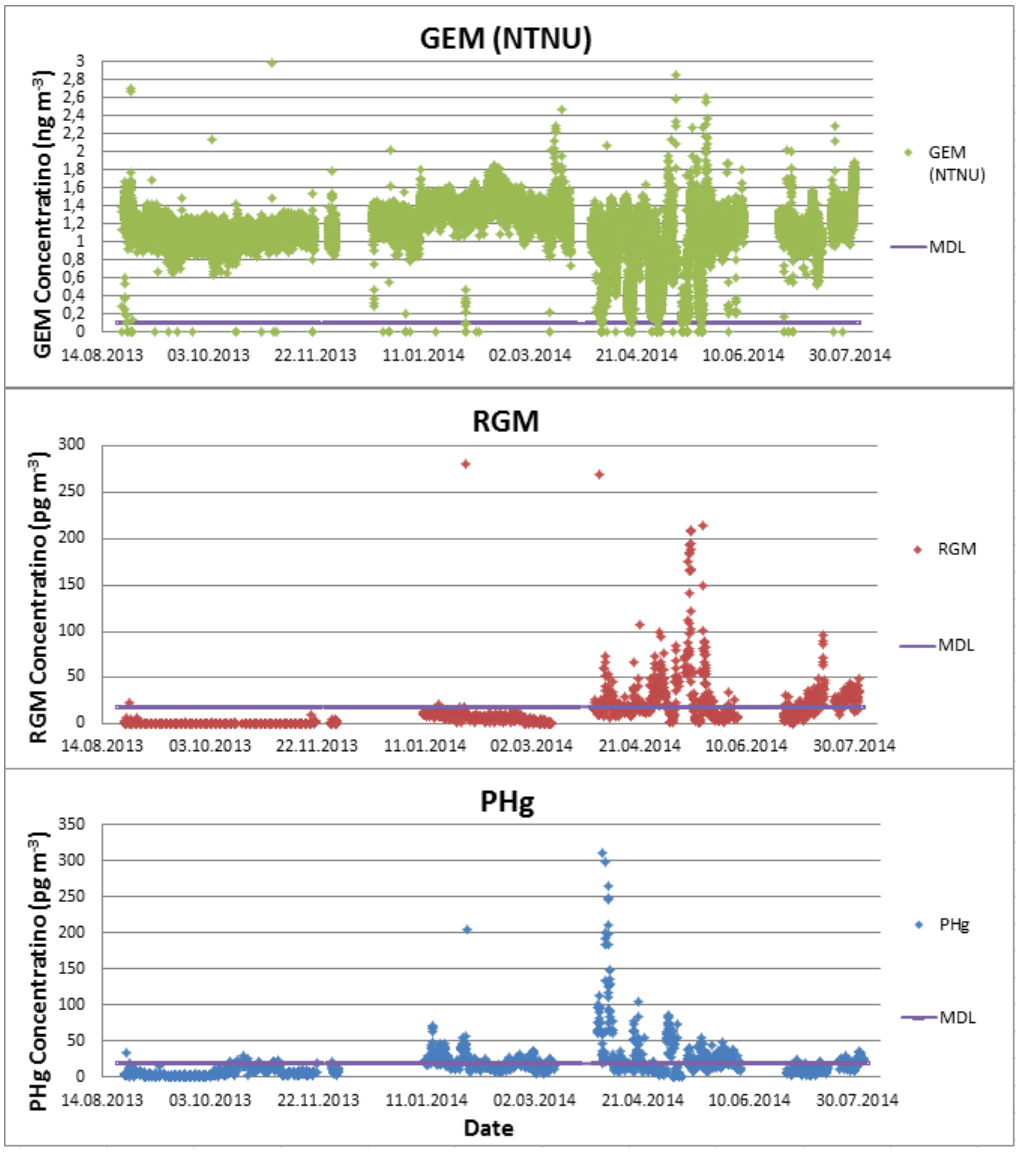

Figure 3.2: separated GEM, PHg, RGM concentrations from 23.08.2013 to 01.08.2014.

As can be seen, several times of AMDEs happened during April to June as GEM concentration decreased below the MDL. There were also some GEM data points that were below the MDL in other periods, but most of them could be considered as outliers and should be removed for further study. For RGM and PHg, they had relatively higher concentrations during AMDEs. Quite many data points were below the MDL for RGM and PHg, and there were more blank periods than for GEM. The medians, averages, number of data points and data points below the MDL for GEM, RGM and PHg have been calculated and they are shown in Table 3.1.

	Median	Average	Data points	MDL	Date points <MDL
GEM	1.19 ng m^{-3}	1.16 ng m^{-3}	38594	0.1 ng m^{-3}	769 (2%)
RGM	7 pg m^{-3}	12 pg m^{-3}	2530	19 pg m^{-3}	2033 (80%)
PHg	13 pg m^{-3}	16 pg m^{-3}	2564	19 pg m^{-3}	1867 (73%)

Table 3.1: The medians, averages, number of data points and data points below MDL for GEM, RGM and PHg during 2013-2014.

The MDL for GEM was 0.1 ng m^{-3}, and for RGM and PHg it was calculated to be 19 pg m^{-3}. A large proportion of data points were below the MDL and thus should be considered as half of the MDL. The median and average values of PHg were higher than that of RGM, but both were below the MDL. The data points of RGM and PHg were much less than that of GEM, and some data points of RGM and PHg have been removed due to abnormally high values caused by changing the glassware. Figure 3.3 shows how PHg concentrations were affected by changing the glassware.

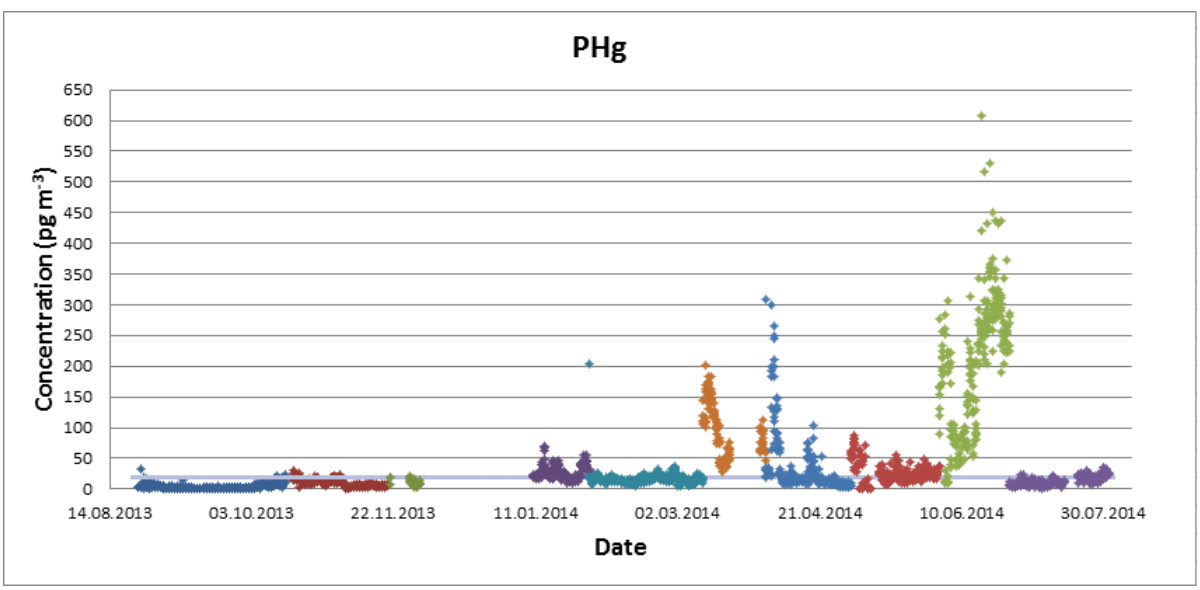

Figure 3.3: PHg concentration from 23.08.2013 to 01.08.2014. The change of color indicates the change of glassware.

It shows that the change of glassware might lead to an abnormally increasing of PHg concentrations, which appeared during the middle of March and June. During these two periods, there

were no AMDEs found according to Figure 3.2, and the high PHg values appeared right after the change of glassware. The reason for the influence of changing glassware has been explained in Section 2.6, and those abnormally high values have been removed.

3.2 Comparison of GEM data from mercury speciation units of NTNU and NILU

There was a difference between GEM concentration obtained from NTNU's speciation unit and from NILU's speciation unit. The comparison is shown in Figure 3.4.

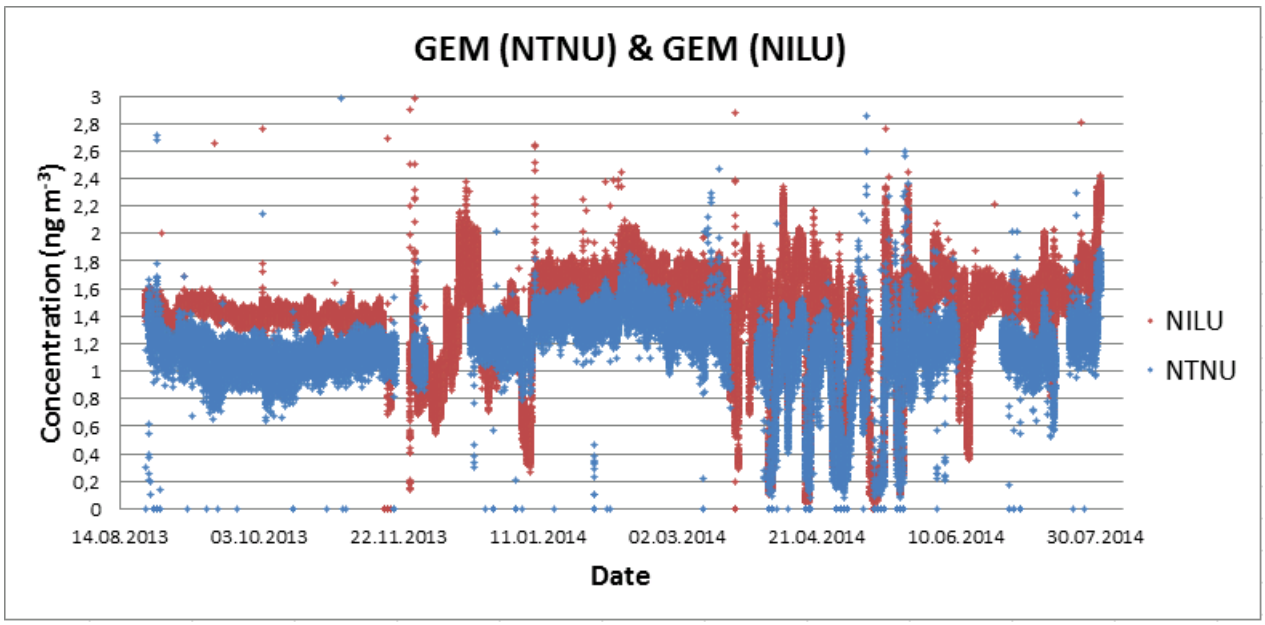

Figure 3.4: The comparison of GEM concentration between mercury speciation units of NTNU and NILU from 23.08.2013 to 01.08.2014.

As can be seen, GEM data obtained from NTNU's speciation unit was generally lower than that from NILU's speciation unit. This was probably due to the different detection methods. As described in Section 2.2, NILU's speciation unit only measured GEM by using Tekran 2537A model, but NTNU's speciation unit measured all the three species of mercury. The air sample came through Model 1130 and Model 1135 before entering Model 2537A, and it might cause

a loss of GEM. Most likely, the loss was in the glassware/impactor since the NILU's speciation unit also had a heating tube quite similar to the NTNU's speciation unit's (Berg et al., personal comm.). GEM data obtained from NILU's speciation unit has been considered more accurate. The medians, averages, number of data points are shown in Table 3.2.

	Median	Average	Data points
GEM (NTNU)	1.19 ng m^{-3}	1.16 ng m^{-3}	38594
GEM (NILU)	1.49 ng m^{-3}	1.42 ng m^{-3}	94320

Table 3.2: The medians, averages, number of data points of GEM from speciation units of NTNU and NILU.

The median value of GEM concentration obtained from NTNU's speciation unit was lower than that from NILU's speciation unit by 0.3 ng m^{-3}. The number of data points for GEM (NILU) was much larger, which was because of continuous measurement of GEM without the break for analyzing RGM and PHg. During December of 2013, GEM data from NTNU's speciation unit was removed due to the influence of snow inside Tekran 1130 model and some leakage problems. GEM data from NILU's speciation unit showed an abnormal increasing in the same period, but the conditions of NILU's speciation unit was not directly shown from the log during that time. The median of GEM concentration from NILU's speciation unit was slightly lower than the global background concentration of GEM in the northern hemisphere, which was considered to be 1.5-1.7 ng m^{-3} (Slemr et al., 2003; Steffen et al., 2008; Temme et al., 2004; Pfaffhuber et al., 2012). The median of total gaseous mercury (TGM) which is the sum of GEM and RGM was then calculated to be around 1.5 ng m^{-3}, and it was also lower than the reported ten-year median TGM from 2000 to 2009 at Zeppelin station which was 1.60 ng m^{-3} (Berg et al., 2013).

3.3 Mercury data of 2007-2011

For the period of 2013-2014, aerosol data was not available, so mercury data from previous years was used for further analysis with the aerosol conditions corresponding to the same period. The overall concentrations of GEM, RGM and PHg are shown in Figure 3.5.

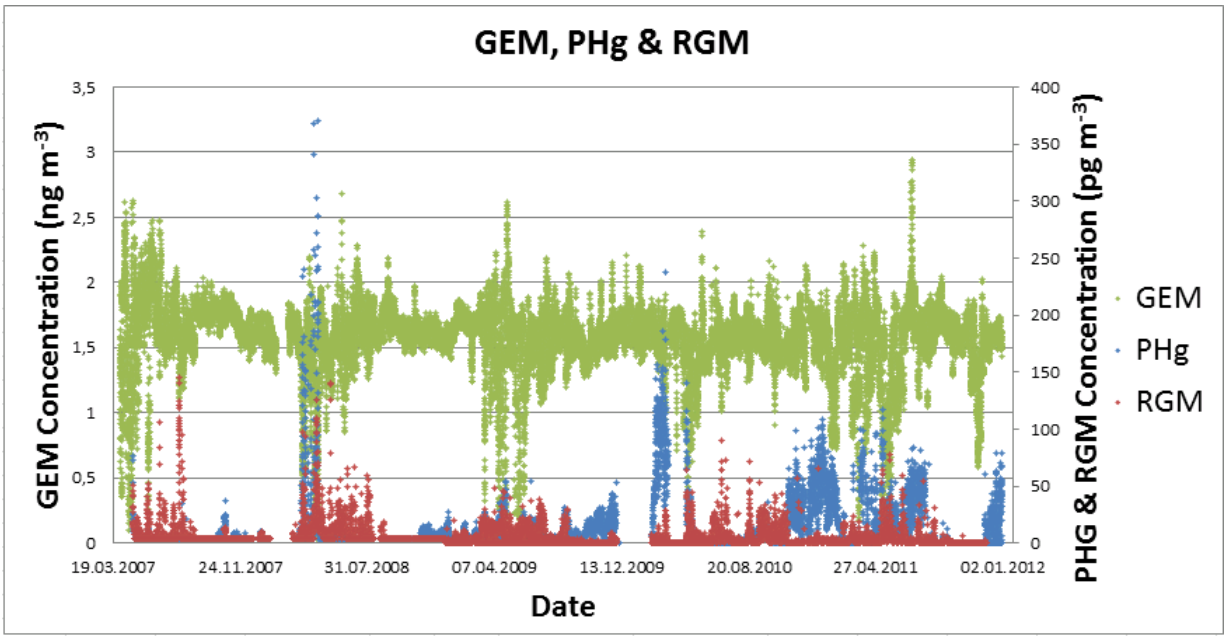

Figure 3.5: GEM, PHg and RGM concentrations from 01.04.2007 to 31.12.2011.

GEM data was used from NILU's speciation unit, and RGM, PHg were used from NTNU's speciation unit. As can be seen from the data, every year AMDEs happened during spring time at Ny-Ålesund, and the situations varied from year to year. The yearly medians and average values of GEM, RGM and PHg concentrations are listed in Table 3.3.

		2007	2008	2009	2010	2011
GEM ($ng\,m^{-3}$)	Median	1.70	1.61	1.60	1.57	1.59
	Average	1.67	1.57	1.55	1.56	1.52
RGM ($pg\,m^{-3}$)	Median	4	4	4	4	3
	Average	7	8	7	7	5
PHg ($pg\,m^{-3}$)	Median	4	4	6	12	24
	Average	4	11	8	26	29

Table 3.3: Yearly medians and average values of GEM, RGM and PHg concentrations from 2007 to 2011.

It shows that GEM concentration had a small decreasing trend over the 5 years from 2007 ($1.70\,ng\,m^{-3}$) to 2011 ($1.59\,ng\,m^{-3}$). If looking at a longer period, it showed a similar result with

previous report by Berg et al. (2013) where TGM had a median of 1.60 ng m^{-3} (while the median of RGM comprises a few percent of TGM) at Zeppelin station during 2000-2009, and it kept very stable each year. The median of GEM corresponded to the background concentration of norther hemisphere which is 1.5-1.7 ng m^{-3} (Slemr et al., 2003; Steffen et al., 2008; Temme et al., 2004; Pfaffhuber et al., 2012). The median of RGM was also very stable each year during 2007-2011, while the median of PHg was very different from year to year. The median of PHg showed an increasing trend from 4 ng m^{-3} to 24 ng m^{-3} during 2007-2011. The high PHg concentrations during 2010-2011 were also reported in previous Master's thesis (Moen, 2012), and it was thought to be due to the change of glassware as explained in Section 2.6.

The monthly medians of GEM, RGM and PHg concentrations are listed in Table 3.4. And the corresponding graph is shown as Figure 3.6

	Jan	Feb	Mar	Apr	May	Jun	Jul	Aug	Sep	Oct	Nov	Dec	overall
GEM (ng m^{-3})	1.61	1.65	1.63	1.48	1.52	1.57	1.63	1.62	1.66	1.59	1.60	1.61	1.61
RGM (pg m^{-3})	3	3	5	11	4	6	4	4	4	4	4	4	4
PHg (pg m^{-3})	9	17	7	13	4	4	4	4	4	4	10	10	4

Table 3.4: Monthly medians of GEM, RGM and PHg concentrations from 2007 to 2011.

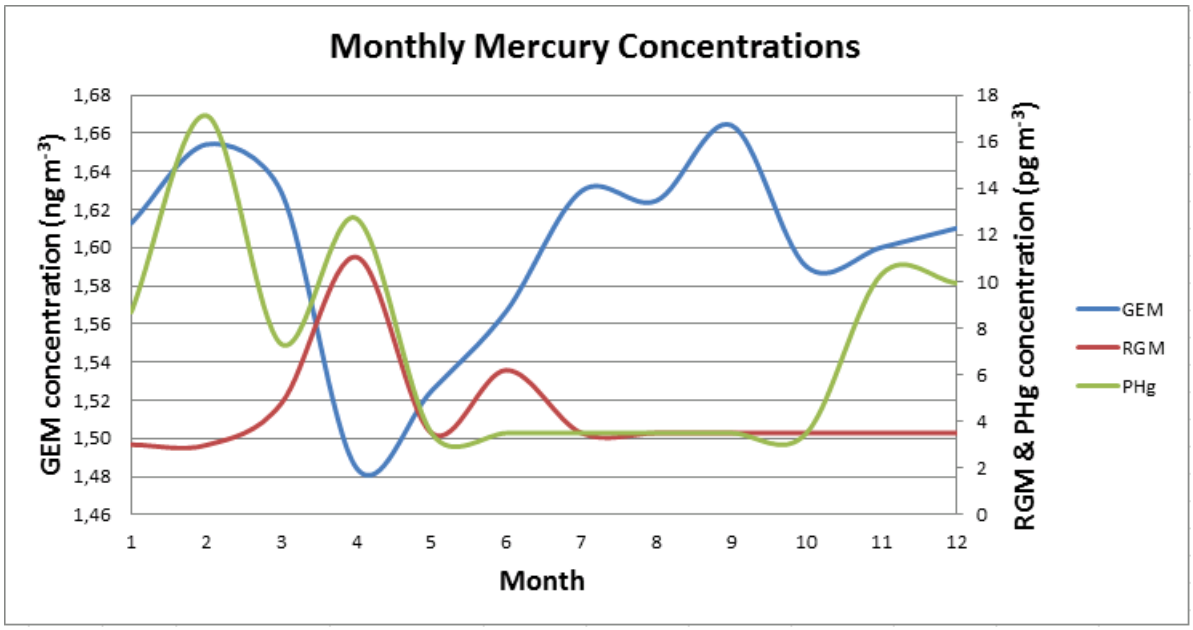

Figure 3.6: Monthly medians of GEM, PHg and RGM concentrations from 2007 to 2011.

The median of GEM concentration for the whole period was 1.61 ng m^{-3}, with the highest in September (1.66 ng m^{-3}) and the lowest in April (1.48 ng m^{-3}) which was during the AMDE periods (Table 3.4). The median of RGM concentration was 4 pg m^{-3} overall, and the highest concentration was in April (11 pg m^{-3}). Only the median values in March, April and June for RGM were higher than the overall value, which corresponded to the AMDE periods. Steen et al. (2011) reported an increased concentration of RGM in summertime at Zeppelin station. However, this phenomenon could not be directly seen from the medians of RGM, and it would be discussed in Section 3.4. The overall median of PHg was the same as RGM which was 4 pg m^{-3}, but the medians from November to April were higher than the overall value. Steen et al. (2011) reported that increased PHg concentrations occurred almost exclusively during March and April at Zeppelin station. However, the high PHg concentrations in wintertime did not correspond to Steen et al. (2011) well. The relatively high values of PHg in wintertime were also previously reported at Alert station by Lu and Schroeder (2004); Steffen et al. (2014) as well, and it was likely a product of aerosol transported from southern latitudes referred to as Arctic haze (Barrie, 1986; Sharma et al., 2013).

3.4 Meteorological data of 2007-2011

To have a general view of the meteorological conditions at Ny-Ålesund, the monthly median values of meteorological data were calculated and they are shown in Table 3.5.

	Temperature (°C)	Relative Humidity (%)	Precipitation (mm)
Jan	-14.3	92.2	6.4
Feb	-14.2	87.5	5.8
Mar	-16.9	91.3	3.7
Apr	-12.8	92.1	3.8
May	-6.1	90.0	2.7
Jun	-2.0	89.5	3.7
Jul	2.0	91.3	6.2
Aug	1.2	91.6	7.0
Sep	-1.3	92.7	9.6
Oct	-8.9	93.1	7.7
Nov	-11.4	91.0	6.3
Dec	-11.5	92.1	7.4
overall	-6.6	91.4	5.7

Table 3.5: Monthly median value of temperature, relative humidity and precipitation from 2007 to 2011.

The lowest and highest temperatures were in March (−16.9 °C) and July (2.0 °C) respectively. The highest relative humidity value appeared in October (93.1%), and the lowest value was in February (87.5%). 10-day accumulated precipitation had a highest value in September (9.6 mm) and a lowest value in May (2.7 mm) respectively. A strong annual variation was reported by Tunved et al. (2013) where the maximum of precipitation were estimated in the summer months (7-8 mm during July-September), and minimum value occurred in the haze period (2-3 mm during March-May) at Zeppelin station. The precipitation data corresponded it very well.

To have a look at the distributions of meteorological data points, the distribution figures of temperature, relative humidity and precipitation have been made and they are shown in Fig-

ure 3.7 to Figure 3.9.

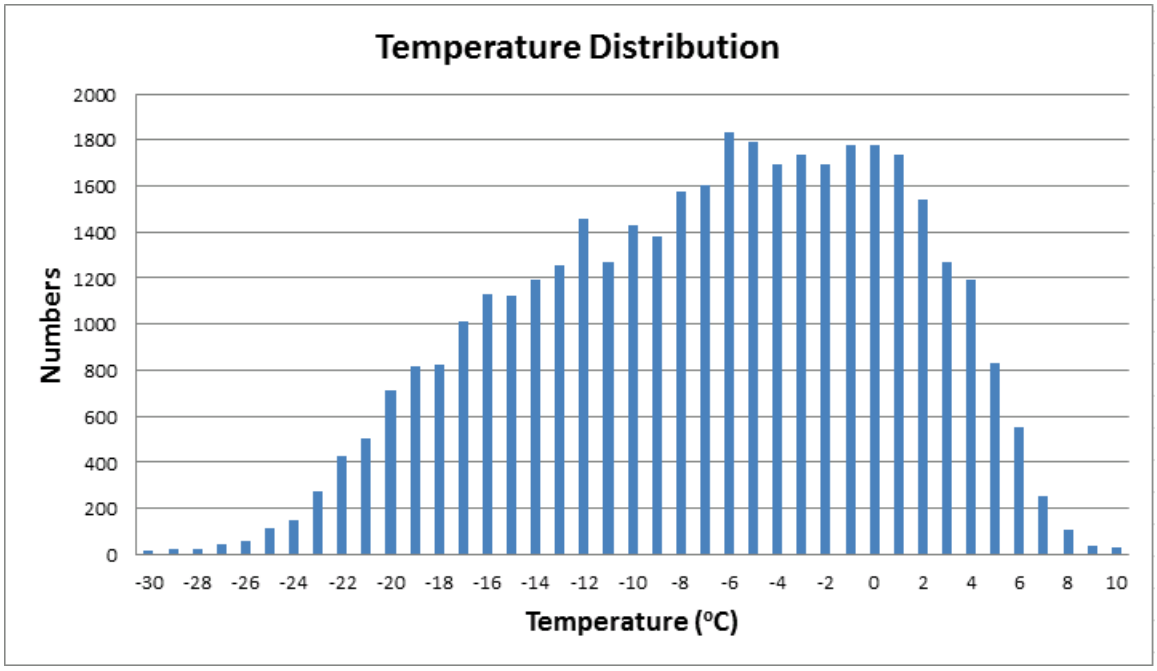

Figure 3.7: Temperature data points distribution from 2007 to 2011.

The distribution of meteorological data are shown in Figure 3.7. As can be seen, temperature varied from around -30 to 10 °C, and the majority of the data points had a temperature range from -22 to 6 °C.

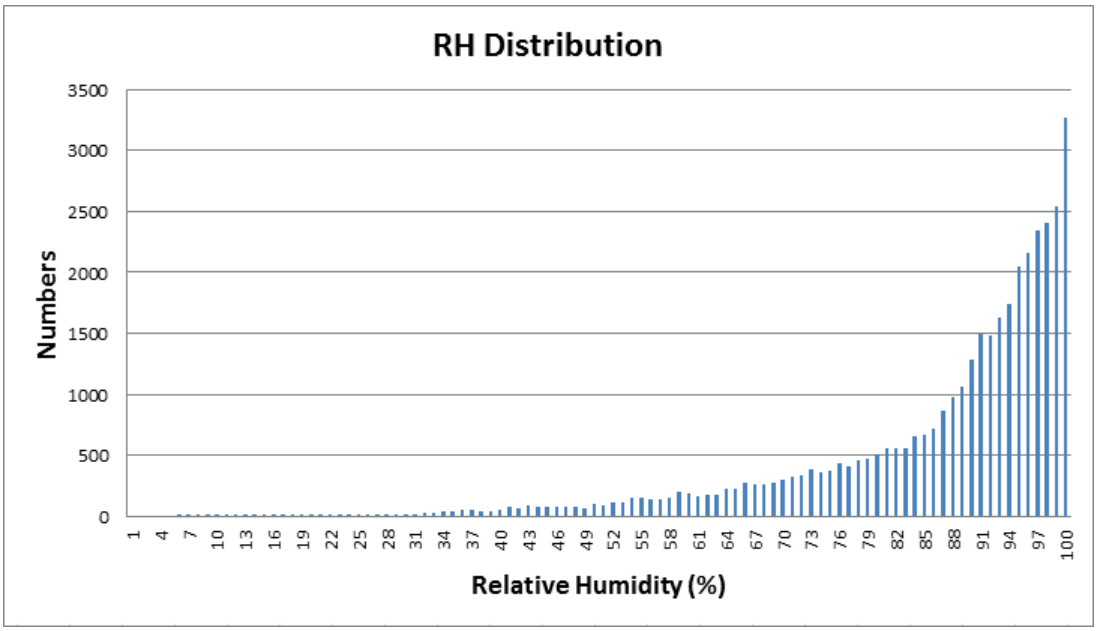

Figure 3.8: Relative humidity data points distribution from 2007 to 2011.

Relative humidity distribution is shown in Figure 3.8. The numbers of relative humidity data points were all the way increasing with the increasing of RH, and most of the data points were within the values of 80 to 100%.

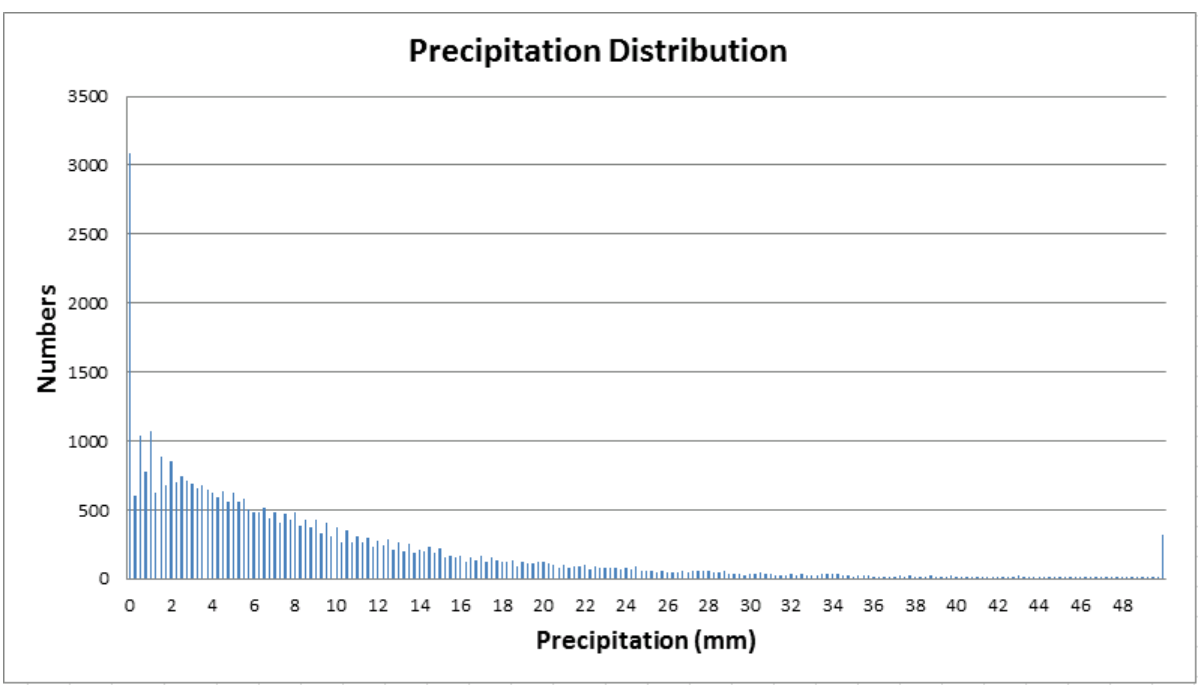

Figure 3.9: Precipitation data points distribution from 2007 to 2011.

Precipitation distribution is shown in Figure 3.9. It had the opposite trend compared with that of RH, and most of the data points had the values between 0 and 10 mm.

To get a general idea of the correlations between meteorological conditions and mercury species, concentrations of all the three species of mercury were plotted as a function of the three series of meteorological data separately during the whole period of 2007-2011. Some regulations were found between the temperature and mercury concentrations, and they are shown in Figure 3.10 to Figure 3.12.

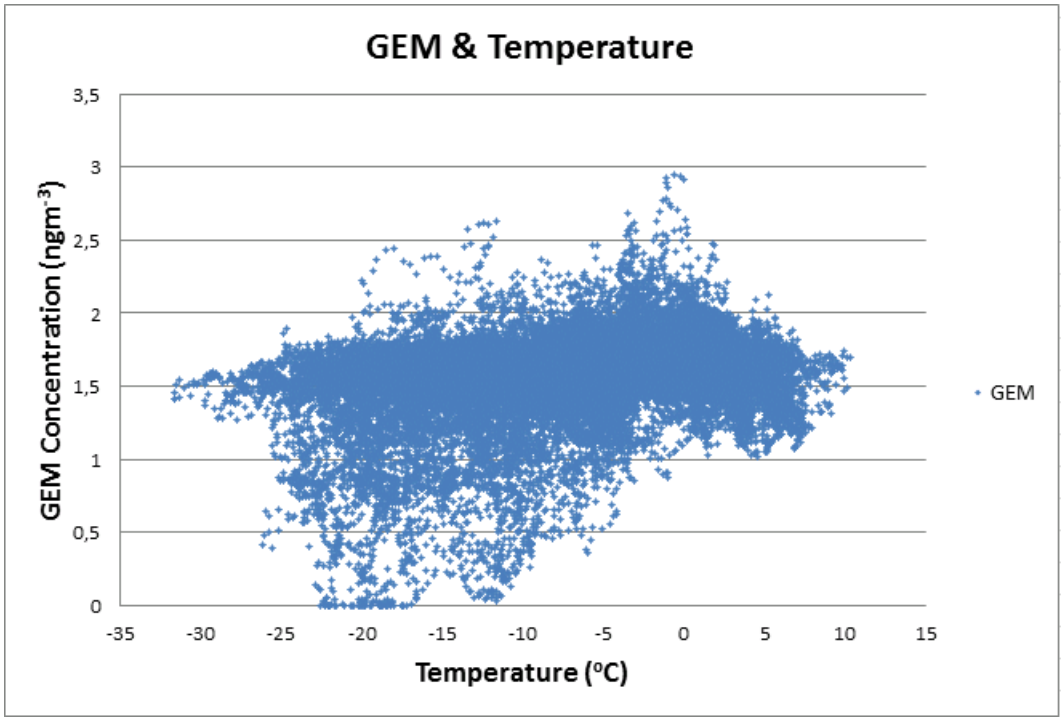

Figure 3.10: GEM concentration distribution as a function of temperature during 2007-2011.

As can be seen in Figure 3.10, the very low GEM values (below MDL) only appeared when the temperature was between -23 and $-12\,^{\circ}$C or so, which meant that a full AMDE might only happened in this temperature range at Zeppelin station. Within the similar temperature range, very high GEM values (above $2\,\mathrm{ng\,m^{-3}}$) also appeared under around -20 to $-12\,^{\circ}$C. This phenomenon might be explained by the rapid reemission processes of GEM from deposited reactive species (Lalonde et al., 2002). The highest concentrations of GEM appeared at around $0\,^{\circ}$C, and this was probably a signal of reemission from snow (Hirdman et al., 2009; Maxwell et al., 2013). The temperature was above 0 during summertime, and no reemission from the ground had ever

been found at Ny-Ålesund during summer. Therefore, the concentration of GEM decreased back when the temperature was above 0. There were two blank areas for low GEM concentrations (below 1 ng m^{-3}) when the temperature was below around −27 °C and when it was above −1 °C. This phenomenon might be explained by the initiation of AMDEs required mercury in the atmosphere, sunlight and reactive halogens. Sea ice or snow might provide a large pool of halogens for the photochemical reactions (Steffen et al., 2008). Arctic summer (with temperature above 0) did not have all of these requirements, neither did the dark season (with very low temperature).

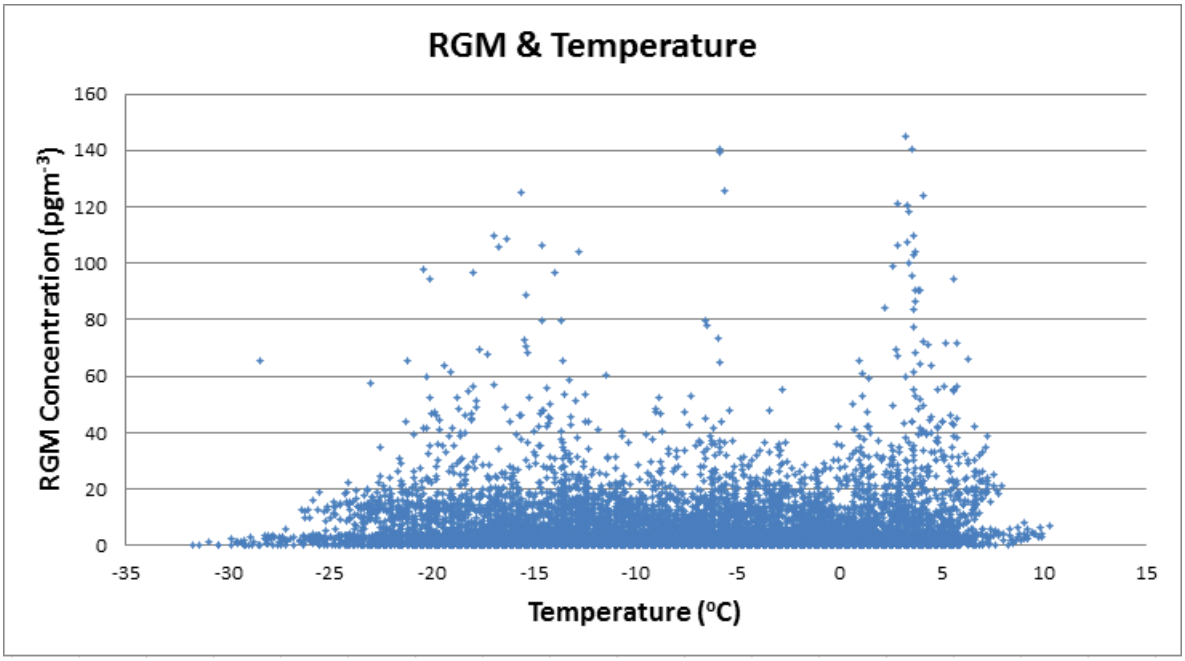

Figure 3.11: RGM concentration distribution as a function of temperature during 2007-2011.

Figure 3.11 shows the general correlations between RGM and temperature, and RGM had some very high concentrations (above 40 pg m^{-3}) at the temperature range of around -23 to −12 °C which shared the same temperature range with low GEM concentrations (Figure 3.10). However, there were also some very high values of RGM at around −6 °C and 0 to 7 °C, and the latter corresponded to the high summer time. Peterson et al. (2009) reported that warmer air temperature, lower relative humidity and more incident light would promote the oxidation of GEM to form RGM in summertime. The high RGM concentrations in summertime was also reported previously by Steen et al. (2011), and it was thought to indicate that RGM formation was photochemically mediated and not solely formed during AMDEs. However, the formation

mechanism for RGM in summertime still remained less clear (Steen et al., 2011).

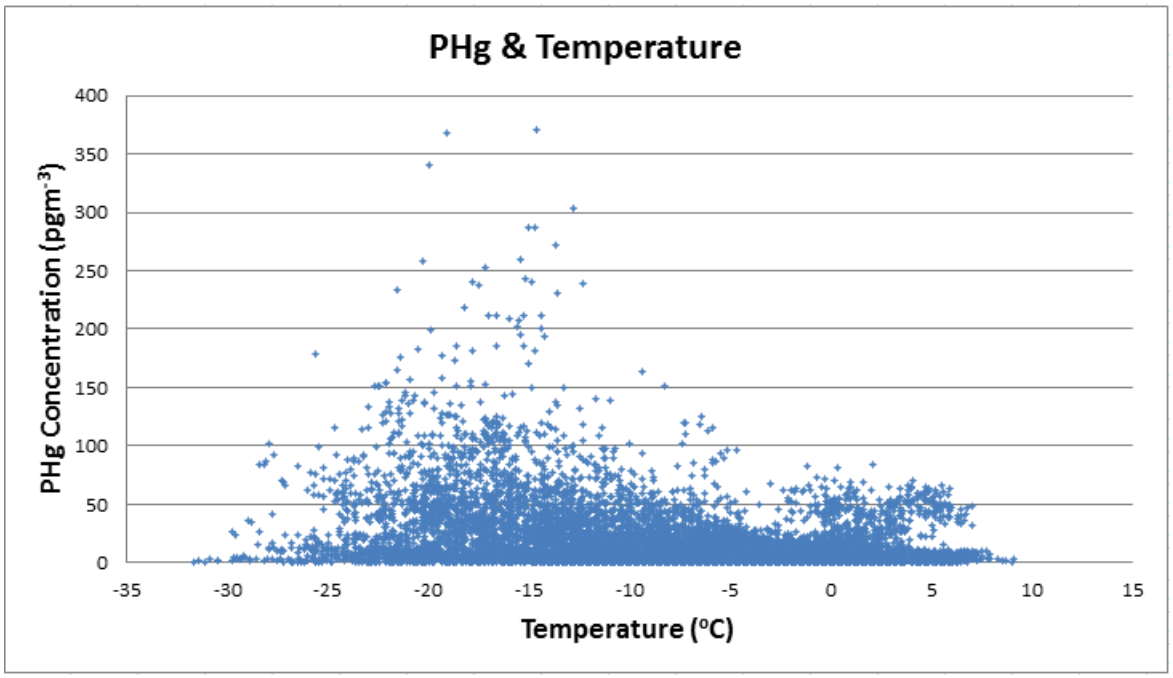

Figure 3.12: PHg concentration distribution as a function of temperature during 2007-2011.

Figure 3.12 shows the general correlations between PHg and temperature, and PHg concentrations also had some very high values (above 200 pg m^{-3}) at the temperature range of -23 to $-12\,°C$ which corresponded to the same temperature range with low GEM concentrations (Figure 3.10). On the other hand, PHg did not show remarkably high concentrations at the high temperatures as RGM did. PHg showed generally high concentrations at relatively low temperature, which might correspond to winter and spring periods as explained in Section 3.3. Cobbett et al. (2007) reported that the elevated PHg concentrations typically occurred when the temperature dropped below $-20\,°C$ at Alert, Nunavut, Canada. However, the study period of 2007-2011 at Zeppelin station showed more elevated PHg concentrations (above 200 pg m^{-3}) occurred between the temperature of -20 and $-15\,°C$.

3.5 Aerosol data of 2007-2011

The aerosol concentrations was measured according to aerosol number size distribution, and the data covered the size range of 10 to 562 nm in diameter during 2007-2011. The measured size

range of aerosols was slightly different from the measurement of other years at Zeppelin station, and for example the size range was 22-500 nm during the beginning of 2000, 20-630 nm during October 2000 to the end of 2002, and 10-790 nm during 2005 (Tunved et al., 2013). The size range of 10-562 nm covered the size of Aitken mode particles (10-100 nm), and a part of accumulation mode particles (100-562 nm). The densities of total detected aerosol were calculated and are shown in the upper part of Figure 3.13, and the size distributions were made and are shown corresponding to the densities.

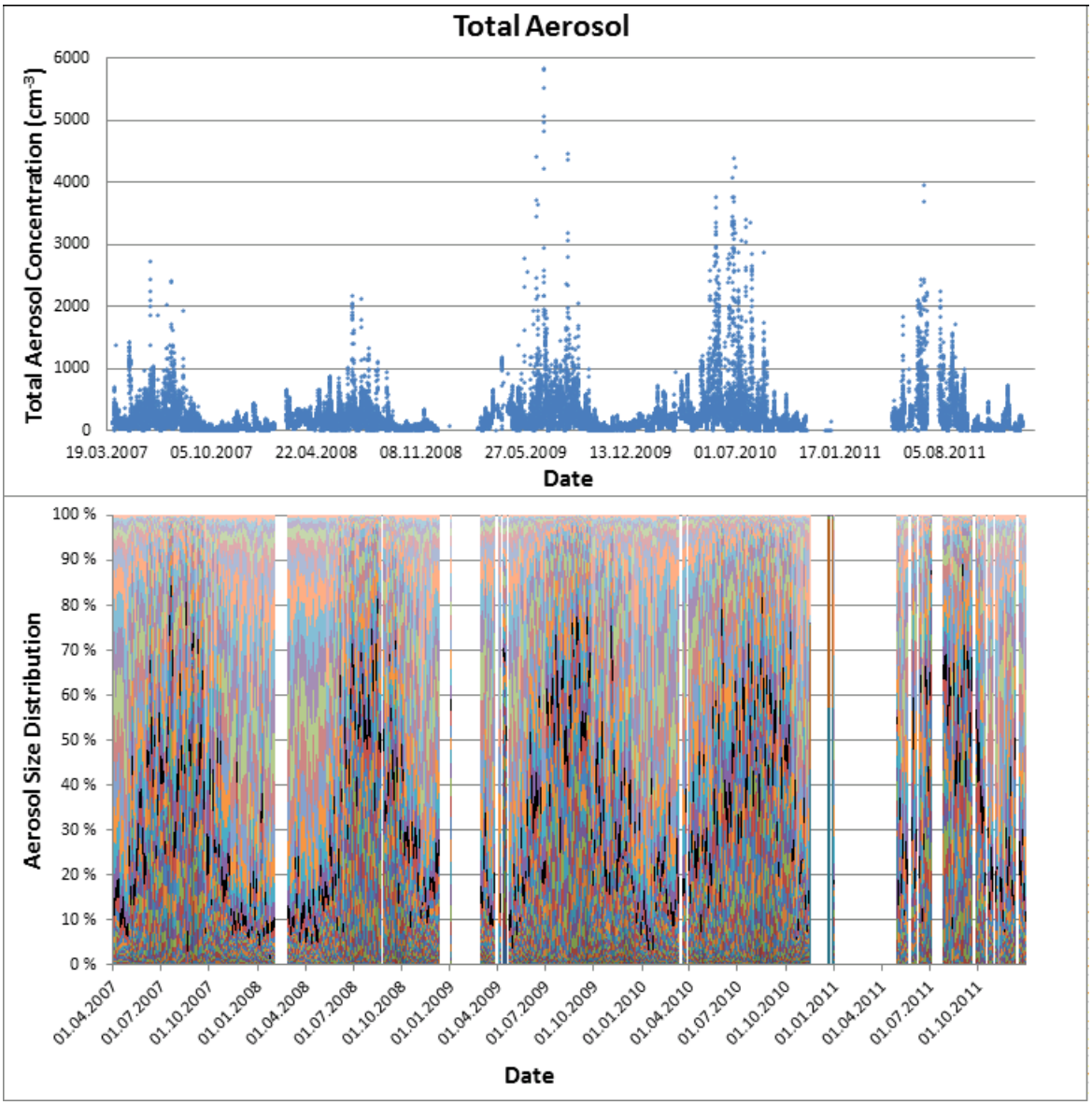

Figure 3.13: Total aerosol concentration and size distribution from 2007 to 2011. The bottom figure is aerosol size distribution along time, different size interval of aerosols are colored and small to large sizes are shown from bottom to top where the black color represents 100 nm as the middle size.

As can be seen in Figure 3.13, the density of aerosol particles had a seasonal distribution, and in general it was high in the summer and low during the winter. The similar seasonal distribution was also previously reported by Ström et al. (2003); Engvall et al. (2008). The large number of particles in summertime was dominated by small particles, which were newly formed un-

der lower aerosol loading, increased photochemistry and biological activity in summer period (Tunved et al., 2013). On the other hand, the Arctic winter was devoid of sunlight, thus reduced photochemical production and new particle formation (Tunved et al., 2013). The monthly median concentrations of aerosols are shown in Table 3.6.

	Total Aerosol ($particles \cdot cm^{-3}$)
Jan	51
Feb	151
Mar	154
Apr	160
May	199
Jun	234
Jul	248
Aug	203
Sep	78
Oct	36
Nov	43
Dec	48
overall	115

Table 3.6: Monthly median values of total aerosol concentrations from 2007 to 2011.

Total aerosol had highest median concentrations in June ($234\,cm^{-3}$) and July ($248\,cm^{-3}$), and lowest concentrations in October ($36\,cm^{-3}$) and November ($43\,cm^{-3}$). This agreed well with Ström et al. (2003) and Tunved et al. (2013), where the number of particles was around $50\,cm^{-3}$ during wintertime and higher in a magnitude in summertime at Zeppelin station. The monthly number of Aitken mode and accumulation mode particles are plotted in Figure 3.14.

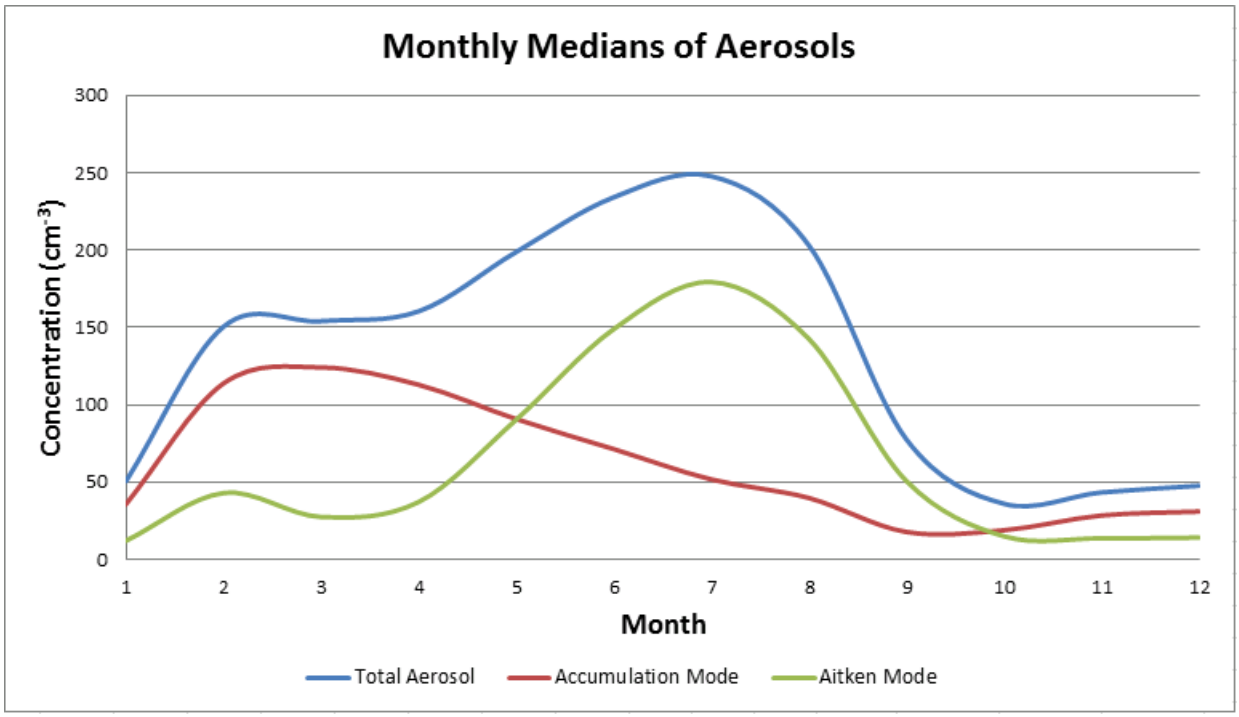

Figure 3.14: Monthly median values of aerosols in different mode from 2007 to 2011.

It can be seen that the accumulation mode particles were more dominant from February to April, and both accumulation mode and Aitken mode particles were relatively equal in May. This was slightly different with the description of Arctic haze period where accumulation mode particles dominated from March to May (Tunved et al., 2013). Aitken mode particles dominated the concentration from June to August 2007-2011 which agreed with the description of sunlit summer period very well (Tunved et al., 2013).

3.6 PHg episodes

To investigate the relations between PHg and aerosol particles, some episodes have been chosen for detailed studies. The episodes were selected for periods within one to three days in which the PHg changed at least 20 pg m^{-3} from and to fairly stable concentrations. The chosen episodes are shown in Table 3.7.

PHg episode	PHg trend	Start time	End time	Start Conc.	End Conc.	Median Conc.	if during AMDEs
1	increasing	23.03.2008 19:30	25.03.2008 23:30	<MDL	52	94	yes
2	increasing	16.04.2008 13:30	18.04.2008 04:10	<MDL	211	186	yes
3	increasing	23.04.2008 06:15	24.04.2008 23:35	52	241	212	yes
4	increasing	25.04.2009 13:10	27.04.2009 19:00	<MDL	44	30	yes
5	decreasing	25.11.2009 13:55	27.11.2009 13:15	43	<MDL	23	no
6	decreasing	21.04.2010 19:30	24.04.2010 00:10	89	29	42	yes
7	increasing	05.11.2010 06:55	07.11.2010 07:55	<MDL	49	38	no
8	increasing	09.05.2011 03:10	11.05.2011 17:10	15	88	74	yes
9	decreasing	19.06.2011 13:10	20.06.2011 19:10	29	<MDL	22	no
10	increasing	21.06.2011 13:50	22.06.2011 11:50	8	38	20	no

Table 3.7: PHg episodes chosen during 2007-2011. The table includes time period of each episode, PHg concentrations of the start time and end time, and the median concentrations of PHg. The unit of the concentration is $\mathrm{pg\,m^{-3}}$.

As shown in Table 3.7, 10 PHg episodes were chosen during 2008-2011, which was because typical PHg episodes had not been found during the period of 2007. 6 of the total 10 episodes happened during AMDEs which were from the end of March to the beginning of June. Both increasing and decreasing trends of PHg concentrations had been considered for further analysis.

The episodes would be discussed more into details in the following parts, and they were divided into 10 subsections. Figure 3.15 to Figure 3.24 are showing the individual episodes and the related parameters.

3.6.1 PHg episode 1

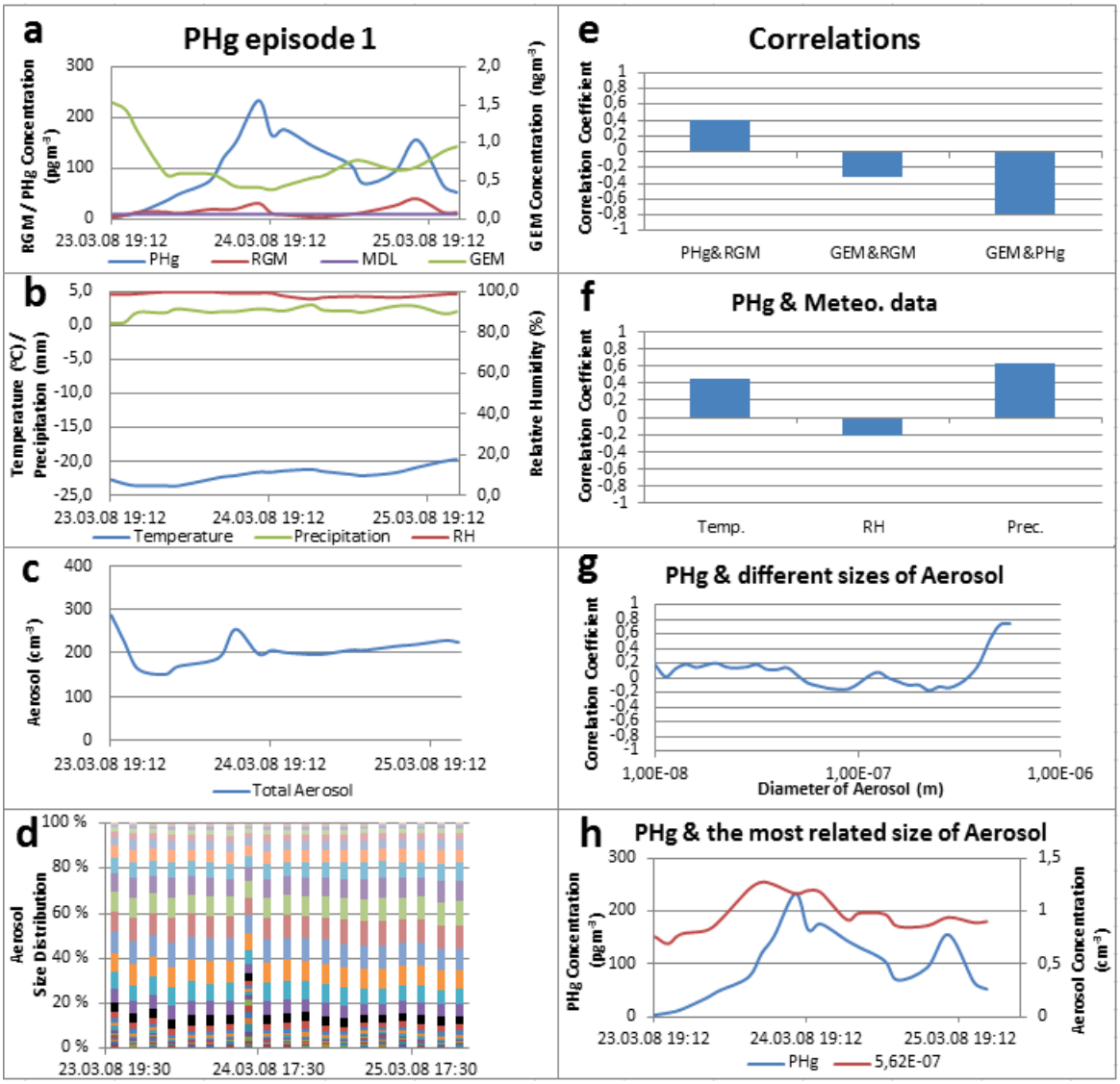

Figure 3.15: PHg episode 1. Figure **a**: Concentrations of GEM, RGM and PHg. Figure **b**: Temperature, relative humidity and 10-day accumulated precipitation. Figure **c**: Number concentration of total detected aerosol. Figure **d**: Aerosol size distribution along time, different size interval of aerosols are colored and small to large sizes are shown from bottom to top where the black color represents 100 nm as the middle size. Figure **e**: Correlations between PHg and RGM, GEM and RGM, GEM and PHg. Figure **f**: Correlations between Temperature and PHg, RH and PHg, precipitation and PHg. Figure **g**: Correlations between aerosols and PHg as a function of particle size. Figure **h**: Concentrations of PHg and aerosols that correlate to PHg the most.

As can be seen from Figure 3.15, PHg concentration increased significantly during the first day from a very low level to more than 200 pg m^{-3}, and then decreased to around 50 pg m^{-3} before staying stable. The concentration of GEM decreased from about 1.5 ng m^{-3} to less than 0.5 ng m^{-3}, and then rose again. It was obviously an GEM depletion event, and the concentration of GEM showed a strong anti-correlation with PHg. While the concentration of RGM did not have significant change, and it kept in a fairly low level at an average value of around 15 pg m^{-3}. RGM only showed a slightly positive correlation with PHg and negative correlation with GEM.

Temperature had an increasing trend from about -24 to $-19\,^{\circ}$C, and it had a positive correlation with PHg but not very much. Relative humidity kept a very high level during the whole period, and it did not show any correlation with PHg. Precipitation showed a positive correlation with PHg, and the correlation coefficient is 0.64.

During episode 1, total aerosol had an average concentration of around 200 particles cm^{-3}, and the accumulation mode particles contributed most of it. It seemed that only the largest detected particles had strong correlation with PHg as shown in figure **g**, and particles smaller than the diameter of 400 nm were not correlated with PHg concentrations very much. The concentration of particles that had a diameter of 562 nm were correlated with PHg concentration the most, and the correlation coefficient was calculated to be 0.74. Although the concentrations of largest aerosols detected were not as high as particles of middle sizes as shown in figure **d**, they showed a relatively high correlation with PHg.

3.6.2 PHg episode 2

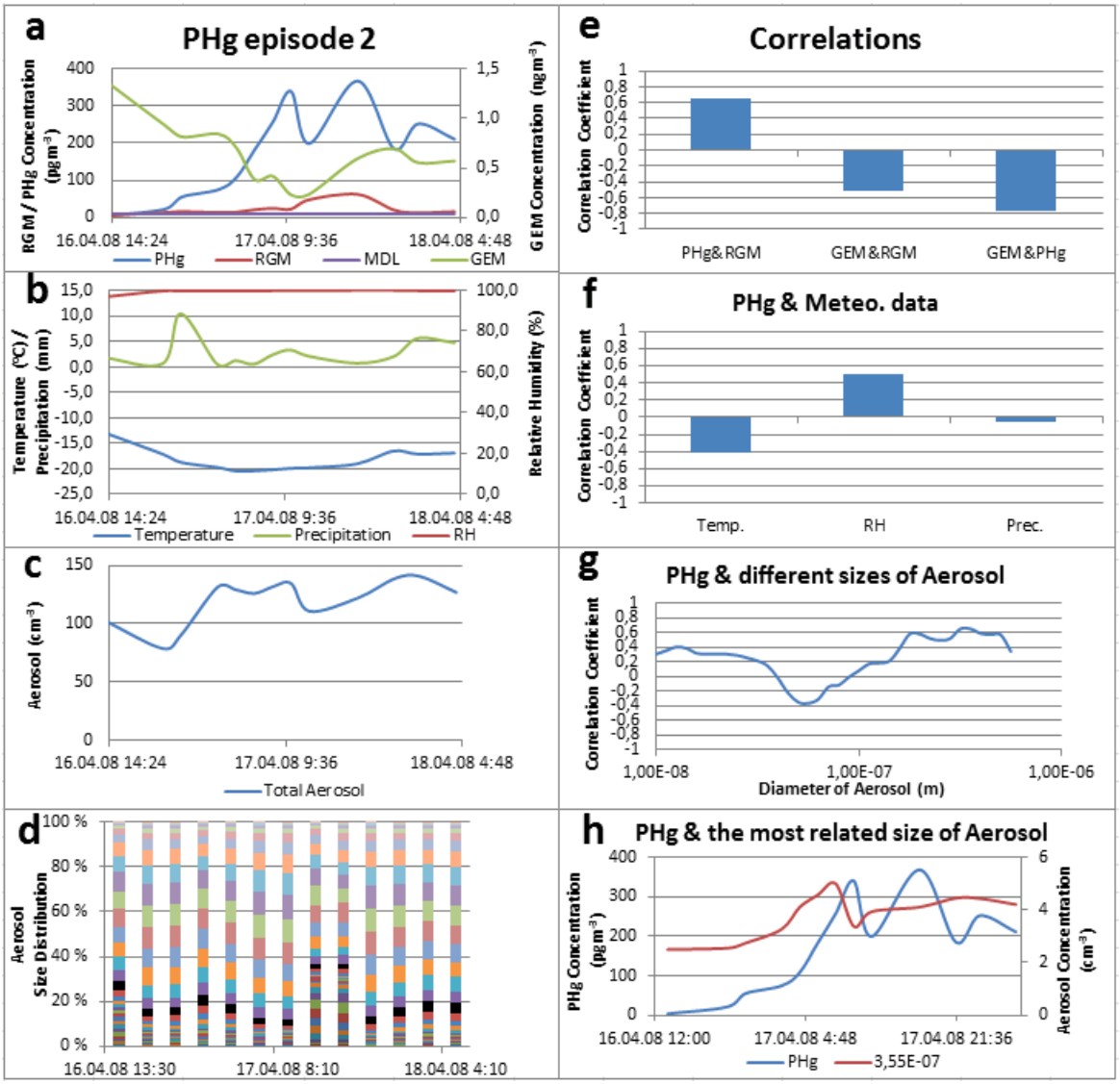

Figure 3.16: PHg episode 2. Figure **a**: Concentrations of GEM, RGM and PHg. Figure **b**: Temperature, relative humidity and 10-day accumulated precipitation. Figure **c**: Number concentration of total detected aerosol. Figure **d**: Aerosol size distribution along time, different size interval of aerosols are colored and small to large sizes are shown from bottom to top where the black color represents 100 nm as the middle size. Figure **e**: Correlations between PHg and RGM, GEM and RGM, GEM and PHg. Figure **f**: Correlations between Temperature and PHg, RH and PHg, precipitation and PHg. Figure **g**: Correlations between aerosols and PHg as a function of particle size. Figure **h**: Concentrations of PHg and aerosols that correlate to PHg the most.

In Figure 3.16, PHg concentration increased from a very low level to more than 300 pg m^{-3} within less than one day, and then fluctuated three times before getting a relatively stable concentration of 200 pg m^{-3} or so. RGM concentration also increased from a low level to about 60 pg m^{-3} then decreased, and it had a correlation coefficient of 0.65 with PHg. GEM decreased from 1.4 to only 0.2 ng m^{-3} then rose up a bit, so it was obviously an AMDE. GEM had negative correlations with both RGM and PHg, and it was stronger with PHg at a correlation coefficient of -0.76.

Temperature decreased from around -13 to $-20\,^{\circ}$C then rose up a bit, and it had a small negative correlation with PHg. Relative humidity kept a very high level during the whole period (> 96%), and it had a small positive correlation with PHg. Precipitation did not show any correlation with PHg during this episode.

Total aerosol concentration was at about the median value of 2007-2011 which was 115 cm^{-3}, and accumulation mode particles dominated the size contribution. The correlation curve between the particle concentration at different sizes and PHg concentration decreased from slightly positive to a little negative, and then rose up to around 0.6 as increasing of the particle size. Particles with a size at 355 nm showed the most positive correlation with PHg, and the correlation coefficient was 0.65. It can be seen from Figure **h** that the aerosol with this specific size showed a very similar trend with PHg when PHg concentration was rising up from the beginning, but the trend was not so similar then after PHg concentration rose up to around 250 ng m^{-3}.

3.6.3 PHg episode 3

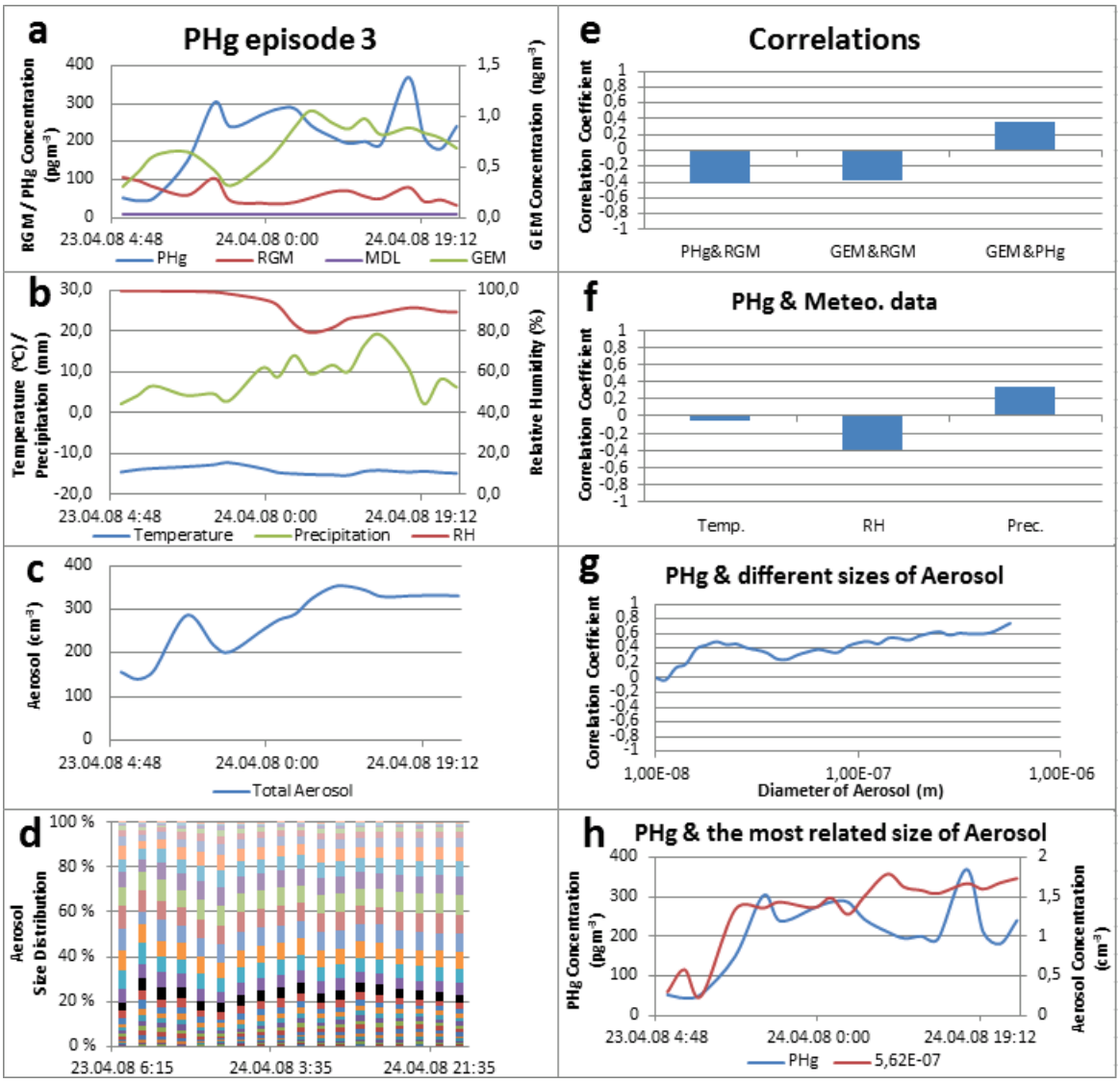

Figure 3.17: PHg episode 3. Figure **a**: Concentrations of GEM, RGM and PHg. Figure **b**: Temperature, relative humidity and 10-day accumulated precipitation. Figure **c**: Number concentration of total detected aerosol. Figure **d**: Aerosol size distribution along time, different size interval of aerosols are colored and small to large sizes are shown from bottom to top where the black color represents 100 nm as the middle size. Figure **e**: Correlations between PHg and RGM, GEM and RGM, GEM and PHg. Figure **f**: Correlations between Temperature and PHg, RH and PHg, precipitation and PHg. Figure **g**: Correlations between aerosols and PHg as a function of particle size. Figure **h**: Concentrations of PHg and aerosols that correlate to PHg the most.

In Figure 3.17, PHg concentration rose quickly from around 50 to 300 pg m^{-3} in a few hours, and then it kept a relatively high level (above 200 pg m^{-3}) ending up with about 240 pg m^{-3}. RGM decreased gradually from above 100 to only 30 pg m^{-3}. GEM started rising from 0.3 ng m^{-3} and vibrated a few times before ending with 0.7 ng m^{-3}. It was a time period short after episode 2, and GEM concentration was recovering from the lowest point. RGM concentration was slightly anti-correlated with both GEM and PHg, while GEM and PHg had a very small positive correlation.

Temperature was very stable and was not changed very much during episode 3, and it did not show any correlation with PHg concentration. Relative humidity decreased from a very high level (nearly 100%) to 80% and then increased to 90%, and It showed a very small negative correlation with PHg concentration. Precipitation showed a very small positive correlation with PHg.

Total aerosol concentration had a trend to increase during this episode, and accumulation mode particles contributed most of the aerosols. It had a positive correlation between the concentration of aerosols and PHg, and the correlation showed an increasing trend with the increasing sizes. The largest particles with the diameter of 562 nm were correlated with PHg concentration the most, and it had a correlation coefficient of 0.74.

The first three PHg episodes were all under AMDEs in springtime of 2008, but the correlation pattern between mercury species in episode 3 was quite different from episode 1 and episode 2. Meteorological data did not show very clear correlation trends with PHg within these three episodes. Aerosol particles were dominated by accumulation mode particles in all of these three episodes, and larger detected aerosols generally had high positive correlations with PHg concentration.

3.6.4 PHg episode 4

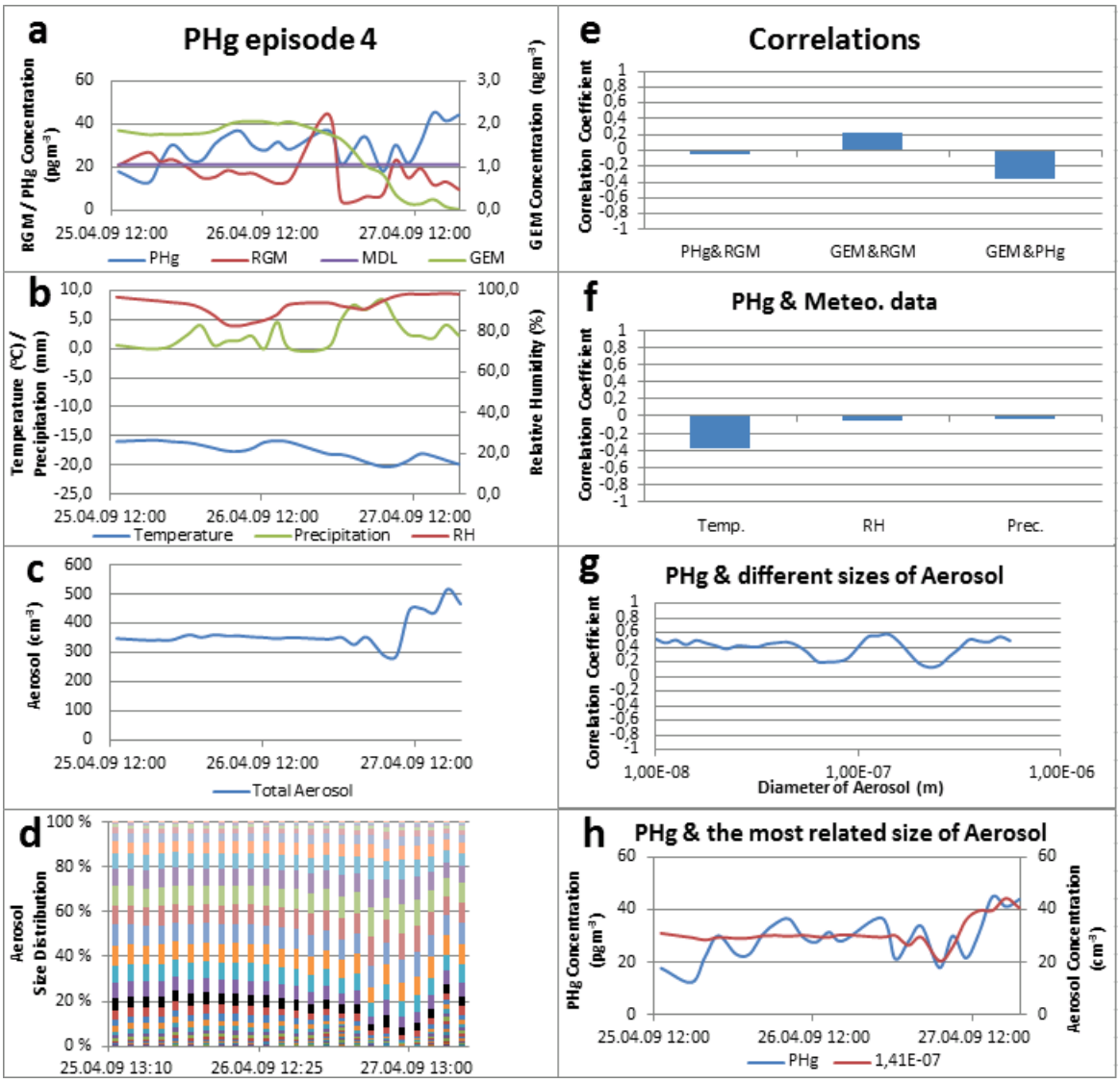

Figure 3.18: PHg episode 4. Figure **a**: Concentrations of GEM, RGM and PHg. Figure **b**: Temperature, relative humidity and 10-day accumulated precipitation. Figure **c**: Number concentration of total detected aerosol. Figure **d**: Aerosol size distribution along time, different size interval of aerosols are colored and small to large sizes are shown from bottom to top where the black color represents 100 nm as the middle size. Figure **e**: Correlations between PHg and RGM, GEM and RGM, GEM and PHg. Figure **f**: Correlations between Temperature and PHg, RH and PHg, precipitation and PHg. Figure **g**: Correlations between aerosols and PHg as a function of particle size. Figure **h**: Concentrations of PHg and aerosols that correlate to PHg the most.

Figure 3.18 shows that PHg concentration started from below the MDL, fluctuated in most of the time during this episode and finally kept relatively stable at above 40 pg m^{-3}. The concentration of RGM also fluctuated many times, and it started at around the MDL and ended at below the MDL. GEM concentration was above background level (at around 1.9 ng m^{-3}) in the beginning, and it gradually decreased to below the MDL at the end of this episode. The three species of mercury did not show any strong correlations between each other in this case.

Temperature had a slightly decreasing trend, and it had a range between -15 to $-20\,^{\circ}$C. Relative humidity and precipitation did not show any correlation with PHg at all, and temperature had a very small anti-correlation with PHg. Neither mercury data nor meteorological data had strong correlations with PHg data during this episode.

Total aerosol was in a relatively high level (generally above 300 cm^{-3}), and large particles dominated the total concentration of aerosol. All the different sizes of particles showed positive correlations with PHg concentration, and the most correlative diameter of the particles was around 141 nm. The correlation coefficient between particles with this specific size interval and PHg concentrations was 0.58.

3.6.5 PHg episode 5

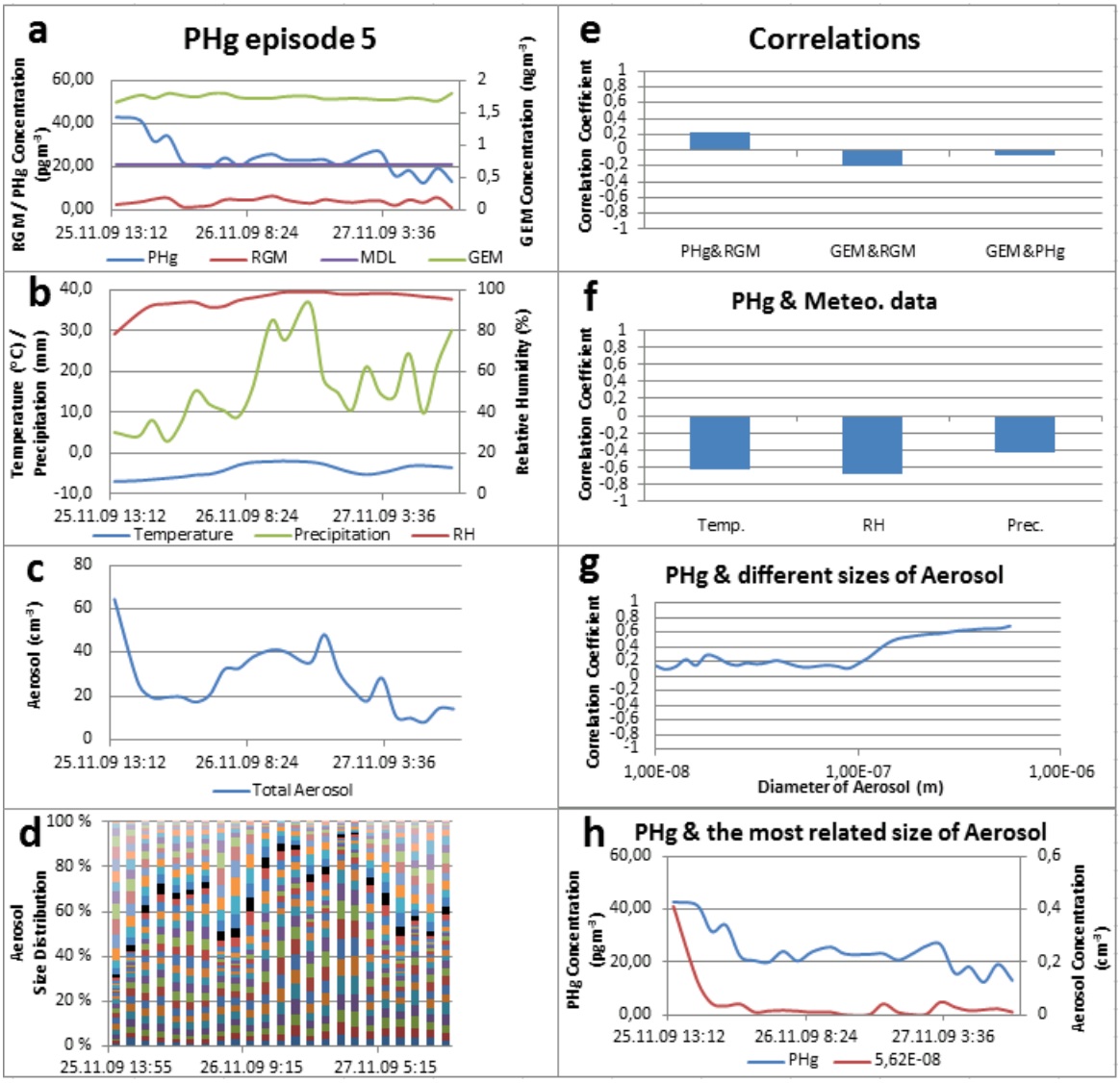

Figure 3.19: PHg episode 5. Figure **a**: Concentrations of GEM, RGM and PHg. Figure **b**: Temperature, relative humidity and 10-day accumulated precipitation. Figure **c**: Number concentration of total detected aerosol. Figure **d**: Aerosol size distribution along time, different size interval of aerosols are colored and small to large sizes are shown from bottom to top where the black color represents 100 nm as the middle size. Figure **e**: Correlations between PHg and RGM, GEM and RGM, GEM and PHg. Figure **f**: Correlations between Temperature and PHg, RH and PHg, precipitation and PHg. Figure **g**: Correlations between aerosols and PHg as a function of particle size. Figure **h**: Concentrations of PHg and aerosols that correlate to PHg the most.

In Figure 3.19, PHg concentration decreased gradually from above 40 pg m^{-3} to below the MDL. RGM concentration kept below the MDL level during the whole episode. And GEM concentration was very stable at a background level (around 1.7 ng^{-3}). Concentrations of all the three mercury species were not correlated with each other during this episode.

Temperature had a general increasing trend from -7 to $-4\,^{\circ}$C, and it had an anti-correlation with PHg concentration as the correlation coefficient was -0.63. Relative humidity also rose from below 80% to a high level (nearly 100%), and it had a negative correlation coefficient of -0.68 with PHg. Precipitation fluctuated a lot, and it had a high level (around 30 mm) in the middle of this episode. A small negative correlation appeared between precipitation and PHg.

Total aerosol had a decreasing trend, and the concentration was generally very low (below 65 cm^{-3}). Accumulation mode particles are a bit more than Aitken mode ones, and the concentrations of larger particles were more positively correlated with PHg concentrations. The largest detected particles which had a diameter of 562 nm were correlated with PHg concentration the most, and the correlation coefficient was 0.69.

3.6.6 PHg episode 6

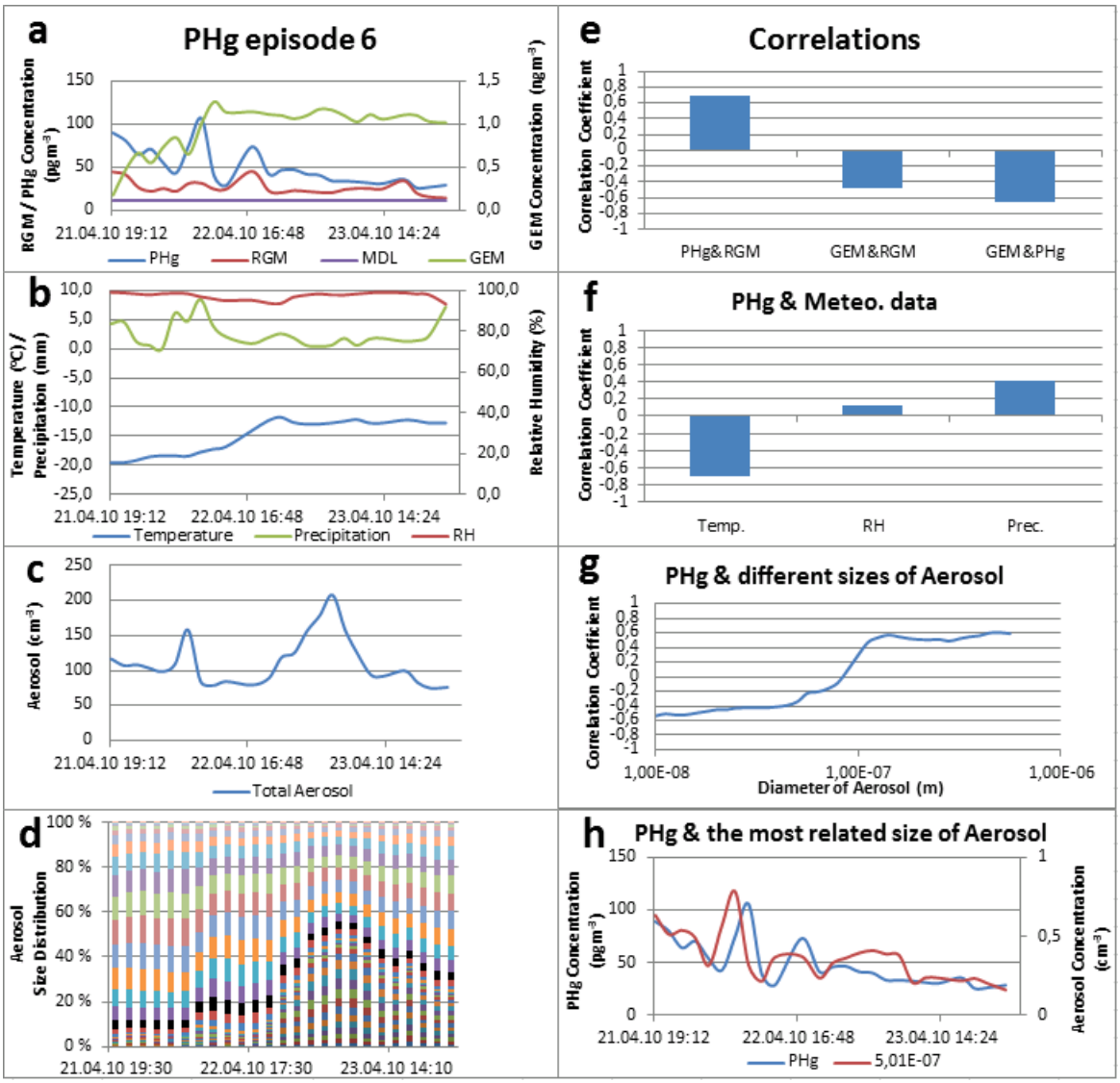

Figure 3.20: PHg episode 6. Figure **a**: Concentrations of GEM, RGM and PHg. Figure **b**: Temperature, relative humidity and 10-day accumulated precipitation. Figure **c**: Number concentration of total detected aerosol. Figure **d**: Aerosol size distribution along time, different size interval of aerosols are colored and small to large sizes are shown from bottom to top where the black color represents 100 nm as the middle size. Figure **e**: Correlations between PHg and RGM, GEM and RGM, GEM and PHg. Figure **f**: Correlations between Temperature and PHg, RH and PHg, precipitation and PHg. Figure **g**: Correlations between aerosols and PHg as a function of particle size. Figure **h**: Concentrations of PHg and aerosols that correlate to PHg the most.

Figure 3.20 shows that PHg concentration decreased from about 90 to 30 pg m^{-3} within 2 days. RGM also had a decreasing trend, and the concentration was from 44 to 14 pg m^{-3}. The concentrations of RGM and PHg were positively correlated with each other, and the correlation coefficient was 0.69. GEM showed an increasing trend from around 0.2 to more than 1 ng m^{-3}, and it had negative correlations with both RGM and PHg. The correlation coefficient between GEM and PHg was -0.65 which was stronger than that of GEM and RGM. This episode happened in the post period of a mercury depletion event, and it showed GEM concentration was recovering back from a very low value.

Temperature in this episode was gradually increasing, and it increased from -20 to around $-13\,^{\circ}$C. Temperature showed an anti-correlation with PHg concentration, and the correlation coefficient was -0.70. Relative humidity kept above 90% during the whole episode, and it did not have any correlation with PHg concentration. Precipitation had a small positive correlation with PHg concentration, but it was not very much.

Total aerosol was around the yearly median value, and the concentration fluctuated a few times. Accumulation mode particles dominated the total concentration during the first half stage of this episode, while large and small particles were more equally distributed during the post stage of this period. The concentrations of small particles were anti-correlated with PHg concentrations, and the concentrations of larger particles were positively correlated with PHg concentrations. The size point that changed the correlation from negative to positive was around 79 nm in diameter. Aerosols that had a diameter of 10 nm showed the strongest anti-correlation with PHg, and the correlation coefficient was -0.54. Aerosols that have a diameter of around 501 nm had a positive correlation coefficient of 0.60.

3.6.7 PHg episode 7

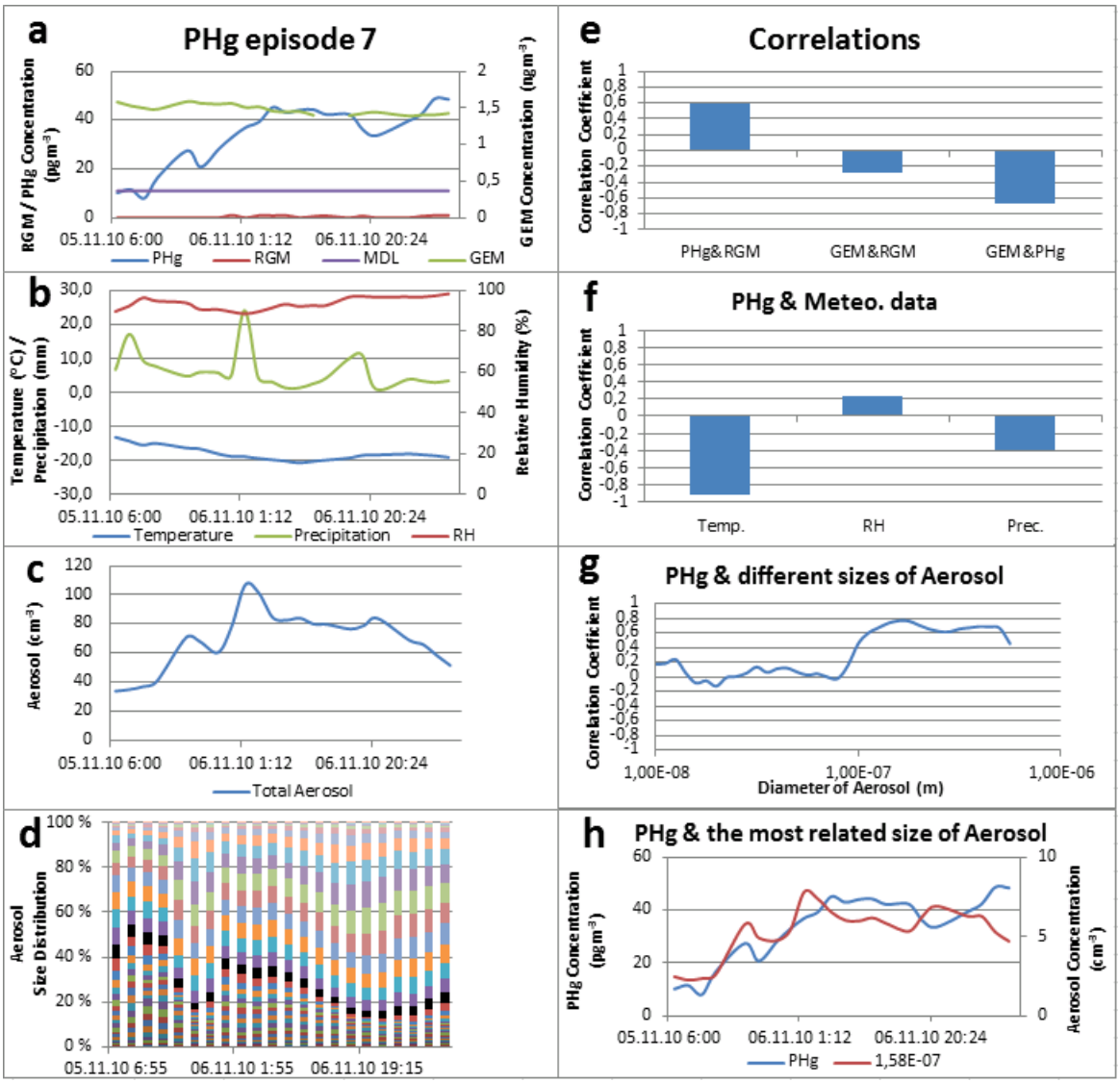

Figure 3.21: PHg episode 7. Figure **a**: Concentrations of GEM, RGM and PHg. Figure **b**: Temperature, relative humidity and 10-day accumulated precipitation. Figure **c**: Number concentration of total detected aerosol. Figure **d**: Aerosol size distribution along time, different size interval of aerosols are colored and small to large sizes are shown from bottom to top where the black color represents 100 nm as the middle size. Figure **e**: Correlations between PHg and RGM, GEM and RGM, GEM and PHg. Figure **f**: Correlations between Temperature and PHg, RH and PHg, precipitation and PHg. Figure **g**: Correlations between aerosols and PHg as a function of particle size. Figure **h**: Concentrations of PHg and aerosols that correlate to PHg the most.

In Figure 3.21, PHg gradually rose from below the MDL to 49 pg m^{-3} in 2 days. RGM concentration was all below the MDL through the whole episode. GEM concentration had a very small decreasing trend, and it decreased from around 1.6 to 1.4 ng m^{-3}. GEM concentration was more negatively correlated with PHg than with GEM, and the correlation coefficient between GEM and PHg was -0.68.

Temperature gradually decreased from -13 to $-19\,^{\circ}$C, and it had a strongly negative correlation with PHg concentration as the correlation coefficient equaled to -0.91. Relative humidity was fairly stable between 85 to 100%, and it did not show much correlation with PHg concentration. Precipitation fluctuated a few times, and it had a very small anti-correlation with PHg concentration.

Total aerosol concentration had a range between around 30 to 110 cm^{-3}, and accumulation mode particles contributed more to the total concentration. Most of the particles had positive correlations with PHg, and especially very large particles detected. The highest correlation coefficient was 0.77 where the particles had a size of 158 nm in diameter.

PHg episode 6 and 7 were in the period of 2010, and episode 6 happened during AMDEs while episode 7 did not. The correlations between mercury species showed a very similar pattern, in which PHg was positively correlated with RGM, and GEM was negatively correlated with both RGM and PHg. Temperature in both episodes show an anti-correlation with PHg concentration, while RH and precipitation did not show very clear correlations with PHg. Accumulation mode particles in both episodes were relatively more than Aitken mode particles in number, and they were positively correlated with PHg concentration.

3.6.8 PHg episode 8

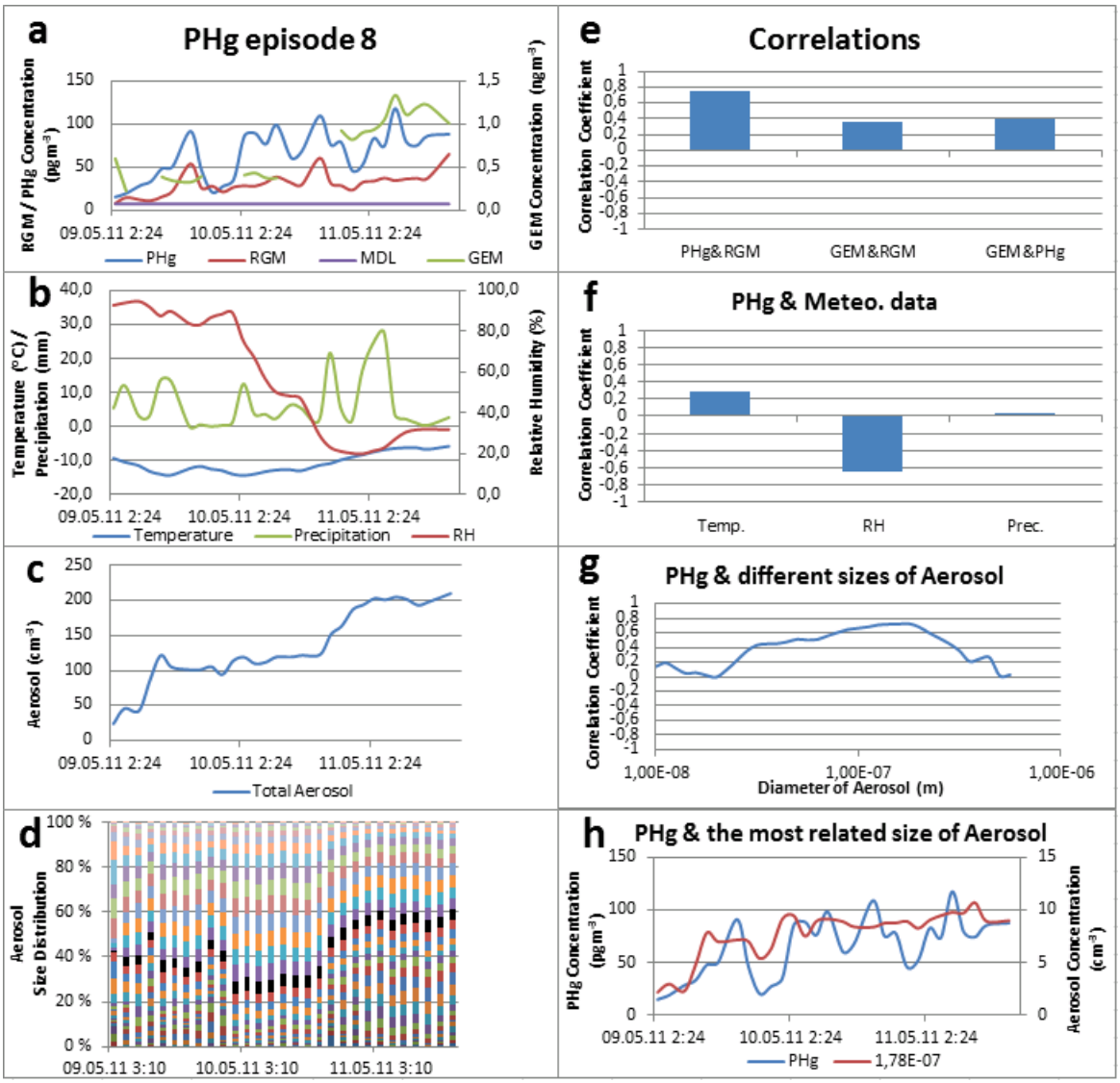

Figure 3.22: PHg episode 8. Figure **a**: Concentrations of GEM, RGM and PHg. Figure **b**: Temperature, relative humidity and 10-day accumulated precipitation. Figure **c**: Number concentration of total detected aerosol. Figure **d**: Aerosol size distribution along time, different size interval of aerosols are colored and small to large sizes are shown from bottom to top where the black color represents 100 nm as the middle size. Figure **e**: Correlations between PHg and RGM, GEM and RGM, GEM and PHg. Figure **f**: Correlations between Temperature and PHg, RH and PHg, precipitation and PHg. Figure **g**: Correlations between aerosols and PHg as a function of particle size. Figure **h**: Concentrations of PHg and aerosols that correlate to PHg the most.

In the Figure 3.22, PHg concentration increased from 15 to 88 pg m^{-3} in 3 days, and it fluctuated many times before keeping relatively stable. RGM concentration also showed an increasing trend, and it was from 8 to around 65 pg m^{-3}. RGM showed a positive correlation with PHg, and the correlation coefficient was 0.75. GEM concentration decreased a little in the beginning from 0.6 to 0.2 ng m^{-3}, and then rose gradually to above 1 ng m^{-3}. During this episode, the data of GEM concentration was not complete, and GEM concentration showed slightly positive correlations with both RGM and PHg.

Temperature was relatively stable, and it decreased from -9 to $-14\,^{\circ}$C then rose up to $-6\,^{\circ}$C. It showed a slightly positive correlation with PHg. Relative humidity had a significant decreasing trend, ant it decreased from more than 90 to around 32%. Relative humidity showed a negative correlation with PHg concentration, and the correlation coefficient was around -0.65. Precipitation fluctuated a lot, and it did not show any correlation with PHg concentration.

Total aerosol gradually rose from a low level (around 30 cm^{-3}) to above 200 cm^{-3}, and both accumulation mode and Aitken mode particles had relatively equal contribution to the total concentration. Most of the aerosols in different size intervals showed positive correlation with PHg concentration, and the highest correlation coefficient was 0.73 where the particles had a size of 178 nm in diameter.

3.6.9 PHg episode 9

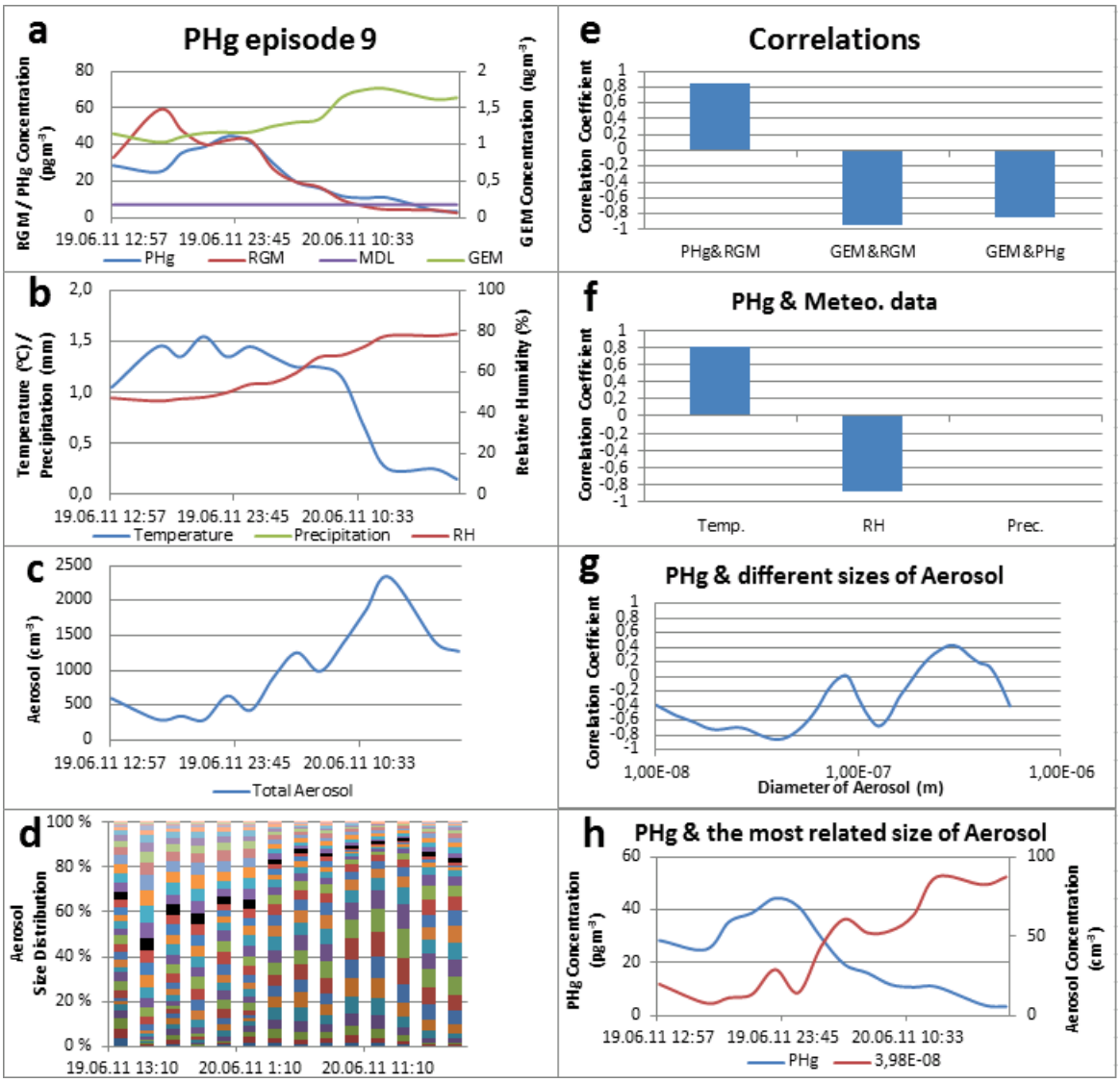

Figure 3.23: PHg episode 9. Figure **a**: Concentrations of GEM, RGM and PHg. Figure **b**: Temperature, relative humidity and 10-day accumulated precipitation. Figure **c**: Number concentration of total detected aerosol. Figure **d**: Aerosol size distribution along time, different size interval of aerosols are colored and small to large sizes are shown from bottom to top where the black color represents 100 nm as the middle size. Figure **e**: Correlations between PHg and RGM, GEM and RGM, GEM and PHg. Figure **f**: Correlations between Temperature and PHg, RH and PHg, precipitation and PHg. Figure **g**: Correlations between aerosols and PHg as a function of particle size. Figure **h**: Concentrations of PHg and aerosols that correlate to PHg the most.

In Figure 3.23, PHg first increased from 29 to 45 pg m^{-3}, and then decreased gradually to a very low level. RGM showed a similar trend which first increased from 33 to 60 pg m^{-3}, and then decreased gradually to a very low level. RGM and PHg concentrations had a strongly positive correlation, and the correlation coefficient was around 0.85. GEM concentration had an increasing trend, and it increased from about 1.1 to 1.6 ng m^{-3}. GEM concentration showed strongly negative correlations with both RGM and PHg, and its correlation coefficients with RGM and PHg were -0.93, -0.84 respectively.

Temperature rose up and down within a range of 0 to 1.5 °C, and it showed a positive correlation with PHg concentration and the correlation coefficient equaled to 0.81. Relative humidity rose from 47 to 79%, and it had a strongly negative correlation with PHg concentration and the correlation coefficient equaled to -0.88. The precipitation data was all 0 during the whole episode, so it did not have any correlation with PHg concentration.

Total aerosol had a very high concentration during this episode, and Aitken mode particles contributed most of the total concentration. The concentration of total aerosol had an increasing trend, and the correlations between particles and PHg varied a lot at different aerosol sizes. Both negative and positive correlations were shown in figure **g**, and the aerosol with a diameter at 39.8 nm had the most negative correlation with PHg and the correlation coefficient equaled to -0.86. Although most of the particles had anti-correlations with PHg in general, there were a small size interval of accumulation mode particles that showed positive correlation with PHg.

3.6.10 PHg episode 10

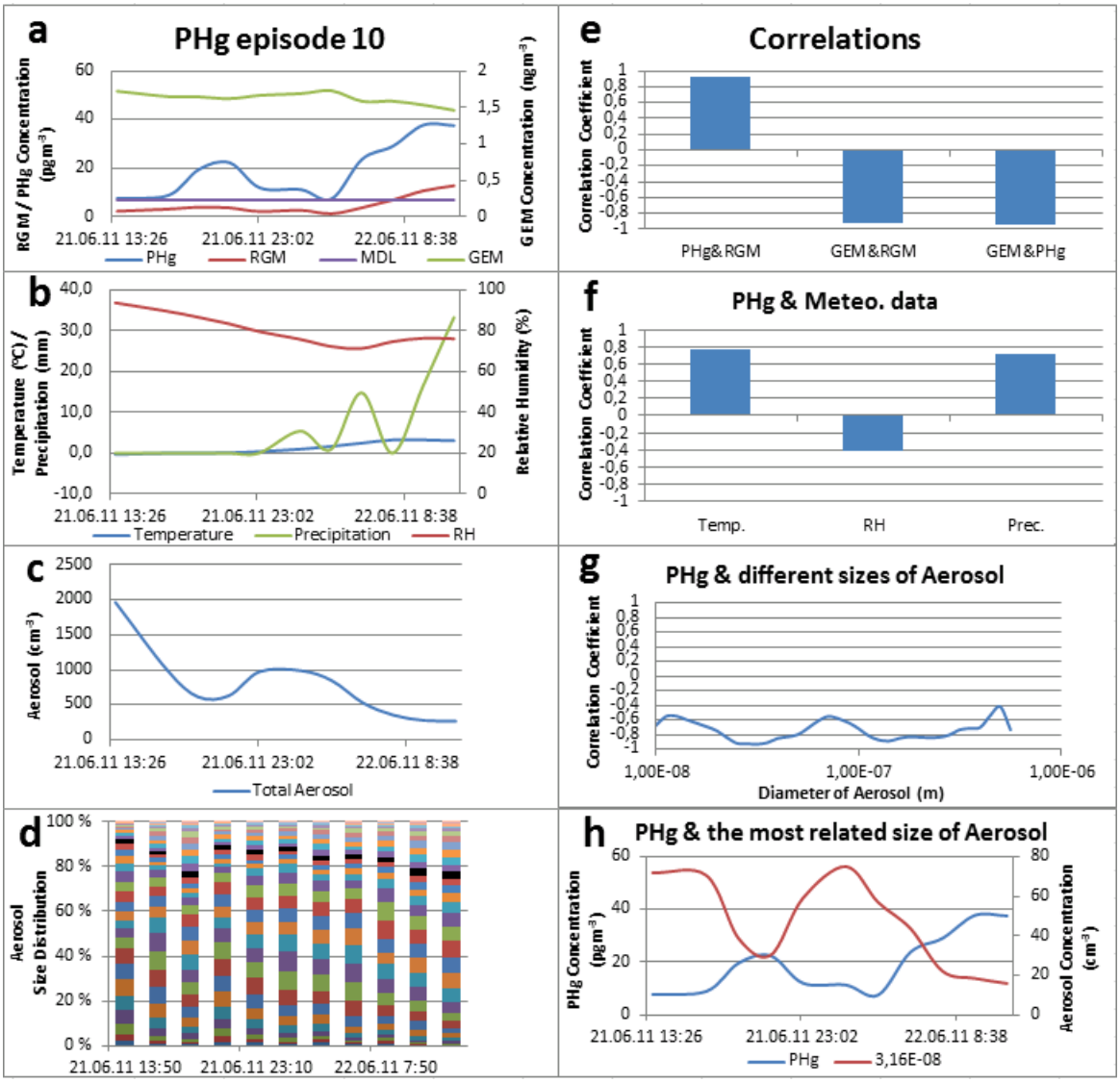

Figure 3.24: PHg episode 10. Figure **a**: Concentrations of GEM, RGM and PHg. Figure **b**: Temperature, relative humidity and 10-day accumulated precipitation. Figure **c**: Number concentration of total detected aerosol. Figure **d**: Aerosol size distribution along time, different size interval of aerosols are colored and small to large sizes are shown from bottom to top where the black color represents 100 nm as the middle size. Figure **e**: Correlations between PHg and RGM, GEM and RGM, GEM and PHg. Figure **f**: Correlations between Temperature and PHg, RH and PHg, precipitation and PHg. Figure **g**: Correlations between aerosols and PHg as a function of particle size. Figure **h**: Concentrations of PHg and aerosols that correlate to PHg the most.

Figure 3.24 showed an episode which happened right after episode 9. PHg concentration increased from 8 to 38 pg m^{-3} within one day. RGM concentration also gradually increased a little from below the MDL to around 13 pg m^{-3}. RGM had a very strongly positive correlation with PHg concentration and the correlation coefficient equaled to 0.92. GEM concentration decreased from background level to 1.5 ng m^{-3}, and it had very high anti-correlations with both RGM and PHg. The correlations between every two of the three mercury species were very similar to that of the episode 9.

Temperature rose from 0 to 3 °C, and it was positively correlated with PHg concentration. Relative humidity decreased from above 90 to under 80%, and it showed a slight anti-correlation with PHg concentration. Precipitation increased a lot during the last period of the episode, and it showed a positive correlation with PHg concentration.

Total aerosol concentration decreased from a very high level (around 2000 cm^{-3}) to around 270 particles cm^{-3}, and Aitken mode particles dominated the total concentration. Particles in every size intervals showed negative correlations with PHg concentration, and the highest level of the correlation coefficient was -0.93 where particles had a size of 31.6 nm in diameter. This was the only episode found which had only negative correlations between aerosol concentrations and PHg concentrations within the total 10 episodes.

In general, most of the episodes showed that the change of PHg concentration was positively correlated with RGM concentration except episode 3 and 4. Lindberg et al. (2002) reported that RGM and PHg were anti-correlated with each other during AMDE period between the sunrise and polar day, and they were positively correlated in summertime in Barrow, Alaska. The correlations of RGM and PHg did not correspond to this trend very well as they were positively correlated in most cases, but it corresponded to Moen (2012) where RGM and PHg also had a positive correlation in general. GEM concentration was negatively correlated with both RGM and PHg concentration in general, but it did not show very clear correlations with RGM and PHg during episode 3, 4, 5, and 8. It might be due to the increasing and decreasing trends of PHg were relatively very small in episode 4 and 5 compared with the rests, and GEM data was not so complete in episode 8.

Temperature showed very different correlations with PHg concentration in different episodes. In episode 1, 9 and 10, temperature showed a clear positive correlation with PHg, while they

were anti-correlated in episode 5, 6 and 7. It corresponded to Moen (2012) in which temperature also alternated between positive and negative correlations with PHg at Zeppelin station. However, it did not correspond well with Cobbett et al. (2007) in which temperature showed an anti-correlation with PHg and high PHg concentrations typically occurred at a temperature below −20 °C at Alert, Canada.

Relative humidity in half of the 10 episodes showed an anti-correlation with PHg concentration, and the similar trend was also reported by Moen (2012). 10-day accumulated precipitation in most episodes did not show clear correlations with PHg concentration. The unclear correlation trend between precipitation and PHg concentration did not correspond to Cole et al. (2014), in which low precipitation might lead to a high PHg concentration in the air.

The aerosol concentrations had very clear correlations with PHg concentrations, and in most cases there were generally positive correlations between aerosols and PHg. There was a trend that PHg concentrations are more positively correlated with accumulation mode particles which are larger than 100 nm in diameter. Keeler et al. (1995) reported that the average particle size of PHg measured in fin mode was 680 nm. Kim et al. (2012) also reported that the size distribution of PHg had 70% in 680 nm. In this thesis, the correlations varied in different episodes, and it was difficult to summarize that under which size interval would aerosol concentrations correlate with PHg concentrations the most. In some episodes, it showed a high relative humidity and relatively low precipitation, which was a typical condition for clouds forming. And PHg concentrations generally showed positive correlations with accumulation mode particles which were considered as important cloud condensation nucleus (Pandis and Seinfeld, 2006). This indicated that PHg might consisted of much cloud associated mercury in many of the episodes.

3.7 The influence of meteorological conditions on PHg concentration

Moen (2012) reported that temperature and relative humidity generally had negative correlations with PHg concentration. In this thesis, RH showed a general anti-correlation with PHg, but the relations between the other meteorological conditions and PHg remained not very clear as discussed in Section 3.6. Especially the 10-day accumulated precipitation did not show very

clear correlation with PHg in most cases. Theoretically, mercury in precipitation results from the scavenging of PHg and RGM (Guentzel et al., 2001). Low precipitation amounts can lead to high concentrations of PHg and RGM which can build up in the air or on could droplets (Cole et al., 2014). However, the correlations between precipitation and PHg did not correspond to these studies. The unclear correlation might indicated that the data should be looked in a different aspect instead of only be judged by the correlation coefficient. In most of the PHg episodes, 10-day accumulated precipitation varied a lot from time to time, but the changes of temperature and relative humidity were relatively smoother. Hence, accumulated precipitation in shorter terms had been taken into consideration. The comparisons are shown from Table 3.8 to Table 3.17 corresponding to the 10 PHg episodes.

3.7.1 Detailed meteorological conditions in PHg episode 1

Time	PHg ($pg\,m^{-3}$)	Temp. (°C)	RH (%)	Prec. 1h	Prec. 3h	Prec. 6h	Prec. 12h	Prec. 1d	Prec. 3d	Prec. 10d
23.03.08 19:30	4	-22.7	98.8	0	0.2	0.4	0.4	0.4	0.4	0.4
23.03.08 21:30	7	-23.3	98.7	0	0.3	0.5	0.5	0.5	0.5	0.5
23.03.08 23:30	13	-23.6	99.1	0.1	0.5	0.8	0.8	0.8	0.8	2.0
24.03.08 03:30	35	-23.6	99.9	0.1	0.5	0.5	0.5	0.5	0.5	1.9
24.03.08 05:30	49	-23.6	99.9	0.1	0.5	0.7	0.8	1.0	1.0	2.5
24.03.08 10:10	76	-22.7	100	0	0.6	1.0	1.0	2.0	2.0	2.0
24.03.08 12:10	120	-22.3	99.6	0	0	0.6	1.2	2.1	2.1	2.1
24.03.08 14:10	154	-22.1	99.4	0	0	0.2	0.6	2.1	2.1	2.1
24.03.08 17:30	234	-21.6	99.4	0.2	0.4	0.4	0.7	2.4	2.5	2.5
24.03.08 19:30	165	-21.6	99.4	0.2	0.4	0.5	0.8	2.0	2.4	2.4
24.03.08 21:30	176	-21.4	98.0	0.2	0.4	0.7	0.7	1.1	2.2	2.2
25.03.08 01:30	145	-21.2	96.5	0	0.1	0.4	0.9	1.6	3.1	3.1
25.03.08 03:30	132	-21.5	97.3	0	0.1	0.2	0.7	0.8	2.3	2.3
25.03.08 07:30	106	-21.9	97.7	0	0	0.3	0.4	0.7	2.2	2.2
25.03.08 09:30	70	-22.1	97.7	0	0.1	0.1	0.1	0.1	2.0	2.0
25.03.08 14:10	94	-21.7	97.3	0	0	0.1	0.1	0.1	2.9	2.9
25.03.08 17:30	156	-20.9	97.8	0	0.1	0.3	0.3	0.3	2.9	2.9
25.03.08 21:30	66	-20.0	97.8	0	0	0	0	0	1.8	1.8
25.03.08 23:30	52	-19.7	99.1	0	0.1	0.1	0.1	0.1	1.6	2.1

Table 3.8: PHg episode 1. Accumulated precipitation data is separated into the recent historical 1 hour, 3 hours, 6 hours, 12 hours, 1 day, 3 days and up to 10 days. It is counted backwards from the air parcel reaching at Zeppelin station. The unit of precipitation is in mm.

It can be seen from Table 3.8 that relative humidity was very high (above 96.5%) through the whole period, and precipitation during the last 1 hour was generally very low (most were 0). Thus it provided a good condition for forming clouds with only a little precipitation during this one hour (Wang, 2013). Although the highest PHg concentration (234 $pg\,m^{-3}$) appeared when there was some precipitation (0.2 mm during the last 1 hour, and even more for a longer period), the high relative humidity (99.4%) might be sufficient enough to form clouds that mercury can fast associate with (Lindberg et al., 2007).

3.7.2 Detailed meteorological conditions in PHg episode 2

Time	PHg ($pg\,m^{-3}$)	Temp. (°C)	RH (%)	Prec. 1h	Prec. 3h	Prec. 6h	Prec. 12h	Prec. 1d	Prec. 3d	Prec. 10d
16.04.08 13:30	4	-12.8	96.6	0	0	0	0	0	0.9	1.9
16.04.08 20:10	21	-17.2	99.7	0.2	0.5	0.5	0.6	0.6	0.6	0.6
16.04.08 22:10	55	-18.8	99.7	0.2	0.4	0.4	0.5	0.5	0.5	10.4
17.04.08 02:10	75	-19.8	99.7	0.3	0.5	0.5	0.5	0.5	0.5	0.5
17.04.08 04:10	108	-20.5	99.7	0.1	0.3	0.3	0.4	0.5	0.5	1.2
17.04.08 06:10	183	-20.5	99.7	0.1	0.2	0.2	0.5	0.5	0.5	0.5
17.04.08 08:10	258	-20.3	99.8	0.2	0.4	0.4	0.5	0.6	0.6	2.3
17.04.08 10:10	340	-20.0	99.8	0.1	0.2	0.2	0.2	0.3	2.0	3.3
17.04.08 12:10	199	-19.9	99.8	0.1	0.2	0.2	0.2	0.2	1.1	2.1
17.04.08 17:30	369	-19.1	100	0.3	0.6	0.6	0.6	0.6	0.7	0.7
17.04.08 21:30	186	-16.6	100	0.5	1.4	2.0	2.0	2.0	2.0	2.0
18.04.08 00:10	252	-17.2	99.8	0.2	0.5	1.4	1.9	1.9	5.6	5.6
18.04.08 04:10	211	-17.0	99.7	0.1	0.5	0.5	1.1	1.1	4.0	4.7

Table 3.9: PHg episode 2. Accumulated precipitation data is separated into the recent historical 1 hour, 3 hours, 6 hours, 12 hours, 1 day, 3 days and up to 10 days. It is counted backwards from the air parcel reaching at Zeppelin station. The unit of precipitation is in mm.

In Table 3.9, RH similarly kept a very high level (above 96.6%) through the whole period as episode 1. In this case, the accumulated precipitation for any time interval seemed not able to explain PHg concentration change. In both episode 1 and 2, PHg concentration reached a very high level (above 200 $pg\,m^{-3}$) under precipitation in recent hours and a temperature between -17.0 to −21.6 °C.

3.7.3 Detailed meteorological conditions in PHg episode 3

Time	PHg ($pg\,m^{-3}$)	Temp. (°C)	RH (%)	Prec. 1h	Prec. 3h	Prec. 6h	Prec. 12h	Prec. 1d	Prec. 3d	Prec. 10d
23.04.08 06:15	52	-14.6	99.9	0.1	0.3	0.6	0.6	0.6	2.2	2.2
23.04.08 08:15	44	-14.0	99.9	0.1	0.5	0.7	1.4	1.4	1.4	4.2
23.04.08 10:15	54	-13.7	99.8	0.1	0.7	1.1	2.6	3.0	6.2	6.6
23.04.08 14:15	149	-13.3	99.7	0.3	0.7	1.0	1.7	4.1	4.3	4.3
23.04.08 17:35	303	-12.8	99.3	0	0.3	0.9	1.0	2.3	2.7	4.7
23.04.08 19:35	239	-12.3	98.4	0	0.2	1.0	1.5	2.1	3.0	3.0
23.04.08 23:35	272	-13.7	95.8	0	0.2	1.0	2.4	5.3	11.0	11.0
24.04.08 01:35	287	-14.7	92.7	0	0	0.6	1.8	3.6	4.5	8.8
24.04.08 03:35	283	-15.0	83.6	0	0	0	0.7	1.9	7.5	9.5
24.04.08 05:35	243	-15.2	79.4	0	0	0	0.3	0.9	7.9	9.5
24.04.08 08:15	212	-15.3	81.7	0	0	0	0.1	0.6	5.9	11.7
24.04.08 10:15	195	-15.4	86.2	0	0	0	0	0.2	5.5	10.1
24.04.08 12:15	201	-14.4	87.4	0	0	0	0	0.1	5.7	16.7
24.04.08 14:15	194	-14.2	89.0	0	0	0	0	0	4.1	19.1
24.04.08 17:35	370	-14.6	91.5	0	0	0	0	0	4.3	11.2
24.04.08 19:35	211	-14.4	91.2	0	0	0	0	0	1.2	2.2
24.04.08 21:35	181	-14.7	89.8	0	0	0	0	0	3.8	8.2
24.04.08 23:35	241	-14.9	89.5	0	0	0	0	0	4.5	6.3

Table 3.10: PHg episode 3. Accumulated precipitation data is separated into the recent historical 1 hour, 3 hours, 6 hours, 12 hours, 1 day, 3 days and up to 10 days. It is counted backwards from the air parcel reaching at Zeppelin station. The unit of precipitation is in mm.

Table 3.10 showed a different condition compared with the first two episodes. Relative humidity in the beginning was very high, and then it decreased to below 80% in the middle of the episode. PHg concentration kept a very high level (above 200 $pg\,m^{-3}$ at many times) after a quick rising in the beginning. If looking at the precipitation at the same time, it can be seen that the precipitation was also decreasing in short periods following the relative humidity. There was no precipitation during the recent 1 hour when relative humidity was below 99.7%, and no precipitation during the last 3 hours when relative humidity was below 95.8%. The highest PHg concentration (370 $pg\,m^{-3}$) appeared at a temperature of $-14.6\,°C$ and no precipitation during the recent one day.

3.7.4 Detailed meteorological conditions in PHg episode 4

Time	PHg ($pg\,m^{-3}$)	Temp. (°C)	RH (%)	Prec. 1h	Prec. 3h	Prec. 6h	Prec. 12h	Prec. 1d	Prec. 3d	Prec. 10d
25.04.09 13:10	10	-16.0	96.8	0	0	0	0	0	0	0.6
25.04.09 17:45	10	-15.8	95.4	0	0	0	0	0	0	0
25.04.09 19:45	22	-15.8	94.9	0	0	0	0	0	0	0
25.04.09 21:45	30	-16.0	94.2	0	0	0	0	0	0	0.5
26.04.09 00:25	23	-16.2	93.4	0	0	0	0	0	0	2.5
26.04.09 02:25	23	-16.6	91.5	0	0	0	0	0	0	4.0
26.04.09 04:25	31	-17.1	87.9	0	0	0	0	0	0	0.6
26.04.09 06:25	35	-17.6	83.3	0	0	0	0	0	0	1.3
26.04.09 08:25	37	-17.7	82.6	0	0	0	0	0	0	1.4
26.04.09 10:25	30	-17.2	84.0	0	0	0	0	0	0	2.2
26.04.09 12:25	28	-16.1	85.4	0	0	0	0	0	0	0
26.04.09 14:25	32	-16.9	88.2	0	0	0	0	0	0	4.6
26.04.09 16:25	28	-16.1	93.2	0	0	0	0	0	0	0
26.04.09 22:20	37	-18.1	94.0	0	0	0	0	0	0	0.2
27.04.09 00:20	21	-18.2	92.5	0	0	0	0	0	0.6	4.7
27.04.09 02:20	28	-18.7	91.5	0	0	0	0	0	0	7.5
27.04.09 04:20	34	-19.5	91.0	0	0	0	0	0	0	6.7
27.04.09 07:00	10	-20.3	94.8	0	0	0	0	0	0	8.5
27.04.09 09:00	30	-20.2	97.2	0	0	0	0	0	0	5.1
27.04.09 11:00	22	-19.3	98.3	0	0	0	0	0	0	2.5
27.04.09 13:00	32	-18.1	98.1	0	0	0	0	0	0	2.2
27.04.09 15:00	45	-18.5	98.3	0	0	0	0	0	0	1.8
27.04.09 17:00	41	-19.2	98.6	0	0	0	0	0	0	4.1
27.04.09 19:00	44	-19.9	98.2	0	0	0	0	0	0	2.3

Table 3.11: PHg episode 4. Accumulated precipitation data is separated into the recent historical 1 hour, 3 hours, 6 hours, 12 hours, 1 day, 3 days and up to 10 days. It is counted backwards from the air parcel reaching at Zeppelin station. The unit of precipitation is in mm.

Table 3.11 showed a slightly increasing trend of PHg which was from 10 to 44 $pg\,m^{-3}$. Relative humidity in this episode had a range of 82.6-98.6%, and precipitation were almost nothing during the last 3 days throughout the whole episode. So PHg in this episode might be able to build up in the air or on cloud droplets under the low precipitation (Cole et al., 2014).

3.7.5 Detailed meteorological conditions in PHg episode 5

Time	PHg ($pg\,m^{-3}$)	Temp. (°C)	RH (%)	Prec. 1h	Prec. 3h	Prec. 6h	Prec. 12h	Prec. 1d	Prec. 3d	Prec. 10d
25.11.09 13:55	43	-7.0	78.5	0	0	0	0	2.2	2.2	5.1
25.11.09 17:15	42	-6.8	88.5	0	0	0	0	0	0	4.1
25.11.09 19:15	32	-6.5	92.6	0	0	0.5	0.5	0.5	1.2	8.1
25.11.09 21:15	34	-6.2	93.3	0	0.3	1.6	1.6	1.6	1.6	2.9
25.11.09 23:15	22	-5.9	94.0	0.3	0.9	2.2	2.6	2.6	2.6	7.4
26.11.09 01:15	10	-5.4	94.1	0.7	1.3	2.1	3.0	3.0	3.0	15.3
26.11.09 03:15	10	-5.2	91.7	0.7	2.1	3.0	4.4	4.4	4.4	12.0
26.11.09 05:15	24	-4.3	92.1	0	0.7	1.7	3.5	4.3	4.3	10.5
26.11.09 07:15	10	-3.0	95.0	0	1.3	2.6	4.0	5.8	5.8	8.9
26.11.09 09:15	24	-2.3	96.3	0	1.0	4.9	5.8	10.1	10.1	15.7
26.11.09 11:15	26	-2.1	97.9	0.7	2.4	6.3	10.3	14.0	17.9	32.4
26.11.09 13:15	23	-2.0	99.1	1.0	2.7	5.7	9.9	13.2	20.0	27.8
26.11.09 17:15	23	-2.2	99.2	0.3	1.9	6.1	11.0	18.4	29.3	37.0
26.11.09 19:15	23	-2.7	99.2	0.5	0.5	3.7	10.0	14.6	15.5	18.2
26.11.09 21:15	21	-3.8	98.2	0.5	0.5	0.5	5.8	10.3	11.6	14.9
26.11.09 23:15	23	-4.8	98.0	0.3	0.3	0.3	3.6	5.9	7.8	10.6
27.11.09 01:15	26	-5.3	98.3	0.3	0.3	1.7	2.0	3.5	6.3	10.6
27.11.09 03:15	27	-4.9	98.5	0.3	0.6	1.8	2.4	8.9	13.1	14.6
27.11.09 05:15	10	-4.1	98.3	0.3	0.6	2.7	5.2	5.2	9.6	14.0
27.11.09 07:15	10	-3.2	97.7	0.3	1.3	3.0	4.3	5.1	8.9	24.5
27.11.09 09:15	10	-3.1	96.9	0.3	1.3	3.0	4.0	4.9	4.9	9.8
27.11.09 11:15	10	-3.3	96.4	0.3	1.3	3.0	4.5	5.3	5.3	21.8
27.11.09 13:15	10	-3.3	95.6	0.7	2.1	3.1	6.4	7.1	7.1	30.2

Table 3.12: PHg episode 5. Accumulated precipitation data is separated into the recent historical 1 hour, 3 hours, 6 hours, 12 hours, 1 day, 3 days and up to 10 days. It is counted backwards from the air parcel reaching at Zeppelin station. The unit of precipitation is in mm.

Table 3.12 shows that PHg decreased from 43 $pg\,m^{-3}$ to below MDL. Relative humidity was below 80% and no precipitation during recent 12 hours in the beginning. PHg concentration decreased to 22 $pg\,m^{-3}$ when there was 0.3 mm precipitation during the last 1 hour. Precipitation then kept at above 3 mm during the last 1 hour in most of the time, and resulted in a relatively low PHg level compared with that in the beginning.

3.7.6 Detailed meteorological conditions in PHg episode 6

Time	PHg ($pg\,m^{-3}$)	Temp. (°C)	RH (%)	Prec. 1h	Prec. 3h	Prec. 6h	Prec. 12h	Prec. 1d	Prec. 3d	Prec. 10d
21.04.10 19:30	89	-19.6	99.2	0	0	0	0	0	2.1	4.3
21.04.10 21:30	80	-19.6	98.9	0	0	0	0	0	0.9	4.6
21.04.10 23:30	64	-19.2	98.4	0	0	0	0	0	0	1.2
22.04.10 01:30	71	-18.6	97.9	0	0	0	0	0	0	0.6
22.04.10 03:30	54	-18.4	98.5	0	0	0	0	0	0	0
22.04.10 05:30	43	-18.4	98.7	0	0	0	0	0	0	6.1
22.04.10 07:30	75	-18.5	98.5	0	0	0	0	0	0	4.7
22.04.10 09:30	106	-17.8	97.0	0	0	0	0	0	0	8.5
22.04.10 11:30	39	-17.3	96.0	0	0	0	0	0	0	4.0
22.04.10 13:30	29	-16.9	95.1	0	0	0	0	0	0	2.1
22.04.10 17:30	73	-14.2	95.3	0	0	0	0	0	0	0.9
22.04.10 20:10	42	-12.4	93.9	0	0	0	0	0	0	1.9
22.04.10 22:10	46	-11.8	93.7	0.2	0.2	0.2	0.2	0.2	0.2	2.6
23.04.10 00:10	47	-12.7	96.8	0.2	0.4	0.4	0.4	0.4	0.4	1.9
23.04.10 02:10	42	-13.0	97.8	0.2	0.6	0.6	0.6	0.6	0.6	0.6
23.04.10 04:10	40	-13.0	98.4	0.2	0.4	0.4	0.4	0.4	0.4	0.4
23.04.10 06:10	34	-12.8	97.9	0.2	0.6	0.6	0.6	0.6	0.6	0.6
23.04.10 08:10	34	-12.5	97.8	0.3	0.8	0.8	0.8	0.8	0.8	1.8
23.04.10 10:10	33	-12.2	98.4	0.3	0.6	0.6	0.6	0.6	0.6	0.6
23.04.10 12:10	31	-12.8	98.9	0.3	0.9	0.9	0.9	0.9	0.9	1.7
23.04.10 14:10	31	-12.8	99.2	0.3	0.9	1.2	1.2	1.2	1.2	1.8
23.04.10 17:30	36	-12.3	98.9	0	0.3	1.3	1.3	1.3	1.3	1.3
23.04.10 19:30	26	-12.4	98.4	0	0	0.6	1.4	1.4	1.4	1.4
23.04.10 21:30	27	-12.8	98.0	0	0	0	1.2	1.2	1.2	2.2
24.04.10 00:10	29	-12.8	93.4	0	0	0	0.9	3.0	3.6	7.2

Table 3.13: PHg episode 6. Accumulated precipitation data is separated into the recent historical 1 hour, 3 hours, 6 hours, 12 hours, 1 day, 3 days and up to 10 days. It is counted backwards from the air parcel reaching at Zeppelin station. The unit of precipitation is in mm.

Table 3.13 showed a decreasing trend of PHg concentration which was from 89 to 29 $pg\,m^{-3}$. The highest PHg concentration (106 $pg\,m^{-3}$) appeared when RH was 97.0% and there was no precipitation during the recent 3 days. And then PHg concentration suddenly decreased to 39 $pg\,m^{-3}$ within 2 hours, and it kept a relatively lower level compared with before. Relative humidity de-

creased from 97 to 96% at the same period as the drop of PHg, which might be an important reason for the decreasing of PHg because neither temperature or precipitation showed a sudden change within this 2 hours.

3.7.7 Detailed meteorological conditions in PHg episode 7

Time	PHg ($pg\,m^{-3}$)	Temp. (°C)	RH (%)	Prec. 1h	Prec. 3h	Prec. 6h	Prec. 12h	Prec. 1d	Prec. 3d	Prec. 10d
05.11.10 06:55	5	-13.2	89.9	0.3	1.1	2.7	4.8	4.8	6.8	6.8
05.11.10 08:55	12	-14.3	92.5	0.3	1.1	3.1	4.0	4.0	6.1	17.2
05.11.10 10:55	5	-15.5	96.5	0	2.0	5.7	7.0	9.0	9.6	9.6
05.11.10 12:55	17	-15.0	95.0	0	0	4.8	6.9	7.7	7.7	7.7
05.11.10 17:15	28	-16.3	94.1	0.3	0.8	1.2	4.5	4.7	4.9	4.9
05.11.10 19:15	21	-16.6	90.9	0.3	0.9	1.5	2.1	2.4	2.4	6.0
05.11.10 21:55	28	-18.0	90.8	0.3	0.9	1.6	1.9	2.5	4.9	5.9
05.11.10 23:55	33	-18.8	89.7	0	0.3	0.9	1.2	1.2	3.8	4.9
06.11.10 01:55	37	-18.9	88.7	0	0	0.4	1.4	1.7	1.7	24.2
06.11.10 03:55	39	-19.4	89.7	0	0	0.4	1.2	1.2	1.2	4.4
06.11.10 05:55	45	-19.8	91.6	0	0	0.4	1.4	1.4	1.4	3.2
06.11.10 07:55	43	-20.2	93.4	0	0	0.4	1.4	1.4	1.4	1.4
06.11.10 09:55	44	-20.7	92.3	0	0	0.4	1.4	1.4	1.4	1.4
06.11.10 11:55	44	-20.3	92.8	0	0	0.4	1.2	1.2	1.2	2.6
06.11.10 13:55	42	-19.9	92.8	0	0	0.6	1.4	1.4	1.4	4.3
06.11.10 17:15	42	-19.3	96.9	0	0.3	1.1	1.1	1.1	1.1	10.0
06.11.10 19:15	36	-18.5	97.3	0	0	0.6	0.9	0.9	0.9	11.0
06.11.10 21:15	34	-18.4	96.9	0	0.2	0.2	0.5	0.5	0.5	1.0
07.11.10 01:55	40	-18.1	97.0	0	0.2	0.8	1.1	1.1	1.1	3.9
07.11.10 03:55	43	-18.3	96.9	0	0	0.6	0.9	0.9	0.9	3.5
07.11.10 05:55	49	-18.6	97.5	0	0	0.8	1.0	1.0	1.0	3.0
07.11.10 07:55	49	-19.1	98.5	0	0	0.6	0.9	0.9	0.9	3.5

Table 3.14: PHg episode 7. Accumulated precipitation data is separated into the recent historical 1 hour, 3 hours, 6 hours, 12 hours, 1 day, 3 days and up to 10 days. It is counted backwards from the air parcel reaching at Zeppelin station. The unit of precipitation is in mm.

In Table 3.14, it can be seen that PHg concentration gradually increased from below MDL to a relatively higher level (49 $pg\,m^{-3}$). RH in the beginning was 90%, and there was some precipita-

tion during the most recent 1 hour at the beginning. PHg started increasing gradually when then recent 1-hour precipitation stopped. In this case, it might be explained by the low precipitation could provide a condition for PHg to build up in the air or on cloud droplets (Cole et al., 2014). And it might also be speculated that accumulated precipitation in the most recent hours might effect more on PHg concentration compared with the 10-day accumulated precipitation.

3.7.8 Detailed meteorological conditions in PHg episode 8

Time	PHg ($pg\,m^{-3}$)	Temp. (°C)	RH (%)	Prec. 1h	Prec. 3h	Prec. 6h	Prec. 12h	Prec. 1d	Prec. 3d	Prec. 10d
09.05.11 03:10	15	-9.4	92.8	0.2	0.6	1.3	2.5	2.5	2.5	5.4
09.05.11 05:10	19	-10.5	93.9	0.1	0.7	1.8	3.0	3.0	3.0	12.1
09.05.11 07:50	29	-11.6	94.7	0.2	0.8	1.7	2.7	2.7	2.9	3.1
09.05.11 09:50	33	-13.3	92.0	0.1	1.0	1.1	1.8	1.8	1.8	3.1
09.05.11 11:50	48	-14.1	87.6	0	0.1	0.1	0.1	0.1	1.0	13.6
09.05.11 13:50	51	-14.4	89.8	0	0	0	0	0	0.6	13.3
09.05.11 17:10	91	-12.5	83.8	0	0	0	0	0	0	0
09.05.11 19:10	47	-11.8	83.2	0	0	0	0	0	0	0.5
09.05.11 21:10	21	-12.6	86.8	0	0	0	0	0	0	0
09.05.11 23:10	28	-13.0	88.4	0	0	0	0	0	0.3	0.3
10.05.11 01:10	36	-14.1	89.1	0	0	0	0	0	0.6	1.2
10.05.11 03:10	86	-14.5	75.2	0	0	0	0	0	0.6	12.5
10.05.11 05:10	89	-14.1	67.2	0	0	0	0	0	1.5	3.7
10.05.11 07:10	76	-13.4	56.9	0	0	0	0	0	0.9	3.6
10.05.11 09:10	99	-12.9	50.2	0	0	0	0	0	0.6	2.3
10.05.11 11:50	61	-12.8	48.2	0	0	0	0	0	1.3	6.3
10.05.11 13:50	68	-13.1	46.8	0	0	0	0	0	1.4	5.4
10.05.11 17:10	109	-11.5	29.4	0	0	0	0	0	0	1.8
10.05.11 19:10	76	-11.0	23.2	0	0	0	0	0	0.2	21.6
10.05.11 21:10	78	-9.9	21.1	0	0	0	0	0	0.3	5.4
10.05.11 23:10	46	-9.1	20.2	0	0	0	0	0	0.4	1.5
11.05.11 01:10	53	-8.4	19.8	0	0	0	0	0	1.8	16.5
11.05.11 03:10	83	-7.6	21.3	0	0	0	0	0	0.3	24.5
11.05.11 05:10	74	-6.9	22.8	0	0	0	0	0	0	27.7
11.05.11 07:10	118	-6.5	27.0	0	0	0	0	0	0.4	3.5
11.05.11 09:10	80	-6.3	30.5	0	0	0	0	0	0	2.2
11.05.11 11:10	75	-6.3	31.7	0	0	0	0	0	0	1.0
11.05.11 13:10	86	-6.8	31.9	0	0	0	0	0	0	0.3
11.05.11 17:10	88	-5.9	31.8	0	0	0	0	0	0	2.6

Table 3.15: PHg episode 8. Accumulated precipitation data is separated into the recent historical 1 hour, 3 hours, 6 hours, 12 hours, 1 day, 3 days and up to 10 days. It is counted backwards from the air parcel reaching at Zeppelin station. The unit of precipitation is in mm.

Table 3.15 showed an increasing trend of PHg concentration (from 15 to 88 pg m^{-3}) with a decreasing trend of relative humidity (from 93 to 32%). PHg concentration was relatively low in the beginning when there was some precipitation during the recent 1 day. And when the recent 1-day precipitation suddenly stopped, PHg started to build up. The highest PHg concentration (118 pg m^{-3} appeared when temperature was −6.5 °C which was not very low, RH was 27.0% and there was no precipitation during the recent 1 day. Although PHg concentration fluctuated a lot from time to time, it might be speculated that low precipitation could only provide a condition for the appearing of high PHg concentrations (Cole et al., 2014).

3.7.9 Detailed meteorological conditions in PHg episode 9 and 10

Time	PHg (pg m^{-3})	Temp. (C)	RH (%)	Prec. 1h	Prec. 3h	Prec. 6h	Prec. 12h	Prec. 1d	Prec. 3d	Prec. 10d
19.06.11 13:10	29	1.1	47.3	0	0	0	0	0	0	0
19.06.11 17:10	25	1.5	45.8	0	0	0	0	0	0	0
19.06.11 19:10	36	1.4	46.9	0	0	0	0	0	0	0
19.06.11 21:10	39	1.6	47.6	0	0	0	0	0	0	0
19.06.11 23:10	45	1.4	49.9	0	0	0	0	0	0	0
20.06.11 1:10	41	1.5	54.0	0	0	0	0	0	0	0
20.06.11 3:10	30	1.4	54.8	0	0	0	0	0	0	0
20.06.11 5:10	19	1.3	59.5	0	0	0	0	0	0	0
20.06.11 7:10	16	1.3	67.3	0	0	0	0	0	0	0
20.06.11 9:10	12	1.2	68.3	0	0	0	0	0	0	0
20.06.11 11:10	11	0.7	72.6	0	0	0	0	0	0	0
20.06.11 13:10	11	0.3	77.9	0	0	0	0	0	0	0
20.06.11 17:10	4	0.3	77.8	0	0	0	0	0	0	0
20.06.11 19:10	4	0.2	78.8	0	0	0	0	0	0	0

Table 3.16: PHg episode 9. Accumulated precipitation data is separated into the recent historical 1 hour, 3 hours, 6 hours, 12 hours, 1 day, 3 days and up to 10 days. It is counted backwards from the air parcel reaching at Zeppelin station. The unit of precipitation is in mm.

Time	PHg ($pg\,m^{-3}$)	Temp. (°C)	RH (%)	Prec. 1h	Prec. 3h	Prec. 6h	Prec. 12h	Prec. 1d	Prec. 3d	Prec. 10d
21.06.11 13:50	8	-0.4	93.8	0	0	0	0	0	0	0
21.06.11 17:10	9	-0.1	89.7	0	0	0	0	0	0	0
21.06.11 19:10	20	-0.1	86.8	0	0	0	0	0	0	0
21.06.11 21:10	22	0.1	83.6	0	0	0	0	0	0	0
21.06.11 23:10	12	0.4	79.7	0	0	0	0	0	0	0
22.06.11 01:50	11	1.0	75.9	0	0	0	0	0	0	5.4
22.06.11 03:50	8	1.7	72.4	0	0	0	0	0	0	0.9
22.06.11 05:50	24	2.5	71.4	0	0	0	0	0	0	14.8
22.06.11 07:50	29	3.3	74.7	0	0	0	0	0	0	0
22.06.11 09:50	38	3.3	76.4	0	0	0	0	0.6	1.0	16.5
22.06.11 11:50	38	3.1	76.1	0	0	0	0	0.7	21.4	33.3

Table 3.17: PHg episode 10. Accumulated precipitation data is separated into the recent historical 1 hour, 3 hours, 6 hours, 12 hours, 1 day, 3 days and up to 10 days. It is counted backwards from the air parcel reaching at Zeppelin station. The unit of precipitation is in mm.

Table 3.16 and Table 3.17 showed the decreasing and increasing trends of PHg concentrations in a continuous time period. Through the two episodes, precipitation for the recent 12 hours period backwards was all 0. It indicated that PHg concentration changes were independent on precipitation in these two episodes, and there was an anti-correlation between RH and PHg concentration.

Although the correlation coefficients were not so high between meteorological data and PHg concentrations, it showed some regulation trends by looking into the detailed meteorological data in each PHg episode. 10-day accumulated precipitation did not show clear correlations with PHg concentration as discussed in Section 3.6. However, no or very low accumulated precipitation showing in recent hours would provide a condition for high PHg concentration to occur. This regulation corresponded to Cole et al. (2014) very well which indicated that low precipitation would provide a condition for PHg to build up in the air or on cloud droplets.

Steffen et al. (2013) reported that high levels of PHg associated with low air temperature and RH below 75% in Barrow, Alaska. Cobbett et al. (2007) also reported that elevated concentrations of PHg occurred preferably at a low humidity. However, in this study, high PHg concentrations occurred under a high RH many times, which did not correspond to the previous study well.

PHg could also reach a high level when there was some recently accumulated precipitation, as long as RH was also very high (above 98% or so). It was reported by Pirrone et al. (1996) that PHg concentration was highly correlated with RH, and it was probably due to the effect of water adsorbed on the suspended particulate matter which might play an important role in the exchange of gaseous mercury at the air-particle interface.

To sum up, it was found in this study that either no or very low recently accumulated precipitation or a high relative humidity would provide a good condition for the high PHg concentrations to occur.

3.8 AMDE episodes

Moen (2012) reported that meteorological conditions and aerosol concentrations also had some correlation trends with GEM. So to investigate those relations and to have a better understanding of AMDEs, 10 typical GEM depletion episodes have been chosen for further analysis as shown in Table 3.18.

AMDE episode	Start time	End time	Duration	Start Conc.	End Conc.	Lowest Conc.	Median Conc.
1	25.05.2007 14:00	29.05.2007 07:00	3d 17h	1.79	1.74	0.26	0.82
2	23.03.2008 18:00	27.03.2008 09:00	3d 15h	1.53	1.40	0.37	0.80
3	27.03.2008 10:00	28.03.2008 10:00	1d	1.24	1.32	0.59	1.04
4	16.04.2008 14:00	19.04.2008 09:00	2d 19h	1.41	1.67	0.23	0.68
5	20.04.2008 09:00	26.04.2008 09:00	6d	1.30	1.51	<MDL	0.82
6	17.03.2009 04:00	19.03.2009 11:00	2d 7h	1.64	1.52	0.33	0.94
7	27.04.2009 00:00	29.04.2009 12:00	2d 12h	1.66	1.77	<MDL	0.58
8	16.05.2009 13:00	18.05.2009 09:00	1d 20h	1.72	1.46	0.23	1.11
9	02.06.2009 18:00	05.06.2009 10:00	2d 16h	1.46	1.51	0.38	0.93
10	21.04.2010 02:00	22.04.2010 12:00	1d 10h	1.46	1.26	0.16	0.70

Table 3.18: AMDE episodes chosen during 2007-2011. The unit of concentration is in $ng\,m^{-3}$

The episodes during AMDEs were selected with a duration from one to six days which were a bit longer than PBM episodes. The episodes were selected according to GEM concentrations change compared with the criteria of PHg concentrations in PHg episodes. GEM concentration

started and ended at a relatively stable and high level, and it had one or more decreasing trends in between. The start and end concentrations were at least higher than 1.2 ng m^{-3}, and the lowest concentrations during the episodes were lower than 0.6 ng m^{-3}.

The figures for each episode are shown in Figure 3.25 to Figure 3.34, and they include the similar subparts as PHg episodes discussed.

3.8.1 AMDE episode 1

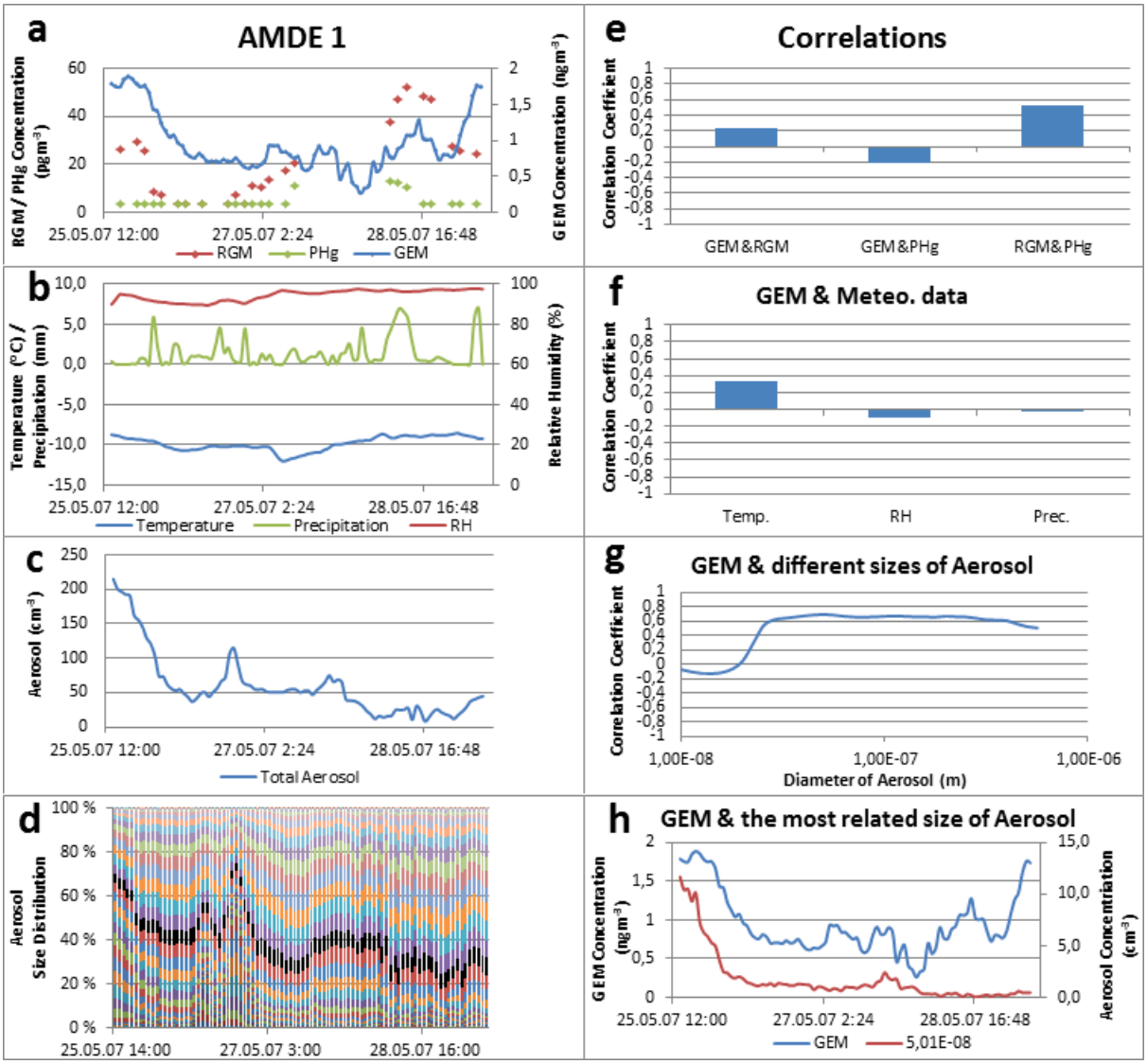

Figure 3.25: AMDE episode 1. Figure **a**: Concentrations of GEM, RGM and PHg. Figure **b**: Temperature, relative humidity and 10-day accumulated precipitation. Figure **c**: Number concentration of total detected aerosol. Figure **d**: Aerosol size distribution along time, different size interval of aerosols are colored and small to large sizes are shown from bottom to top where the black color represents 100 nm as the middle size. Figure **e**: Correlations between GEM and RGM, GEM and PHg, RGM and PHg. Figure **f**: Correlations between Temperature and GEM, RH and GEM, precipitation and GEM. Figure **g**: Correlations between aerosols and GEM as a function of particle size. Figure **h**: Concentrations of PHg and aerosols that correlate to GEM the most.

Figure 3.25 describes the conditions during AMDE episode 1. It shows that GEM concentration gradually decreased from the background level to around 0.5 ng m^{-3}, and then vibrated several times before decreasing to the lowest value of 0.26 ng m^{-3}. It rose back to background level again after some vibrations, and the whole episode kept for more than 3 and half days. RGM concentration decreased in the beginning, and then showed an increasing trend as the decreasing of GEM concentration. PHg stayed in a low level and rose a bit when GEM getting to around the lowest concentration. Both RGM and PHg in this episode did not show clear correlations, but RGM and PHg had a positive correlation.

Temperature kept at around −10 °C and did not change a lot. Relative humidity were generally above 90% during the whole period. 10-day accumulated precipitation had a range between 0 and 7 mm. None of the meteorological data showed clear correlations with GEM concentration during this episode.

Total aerosol concentration showed a decreasing trend through the episode. Aitken mode particles contributed more in the beginning, and accumulation mode particles contributed relatively more after a while. Most of the aerosols showed positive correlations with GEM concentrations, and all the particles that larger than 25 nm in diameter had correlation coefficients between 0.5 and 0.7. Particles with a diameter of 50.1 nm had the highest correlation coefficient with GEM which was 0.69.

3.8.2 AMDE episode 2

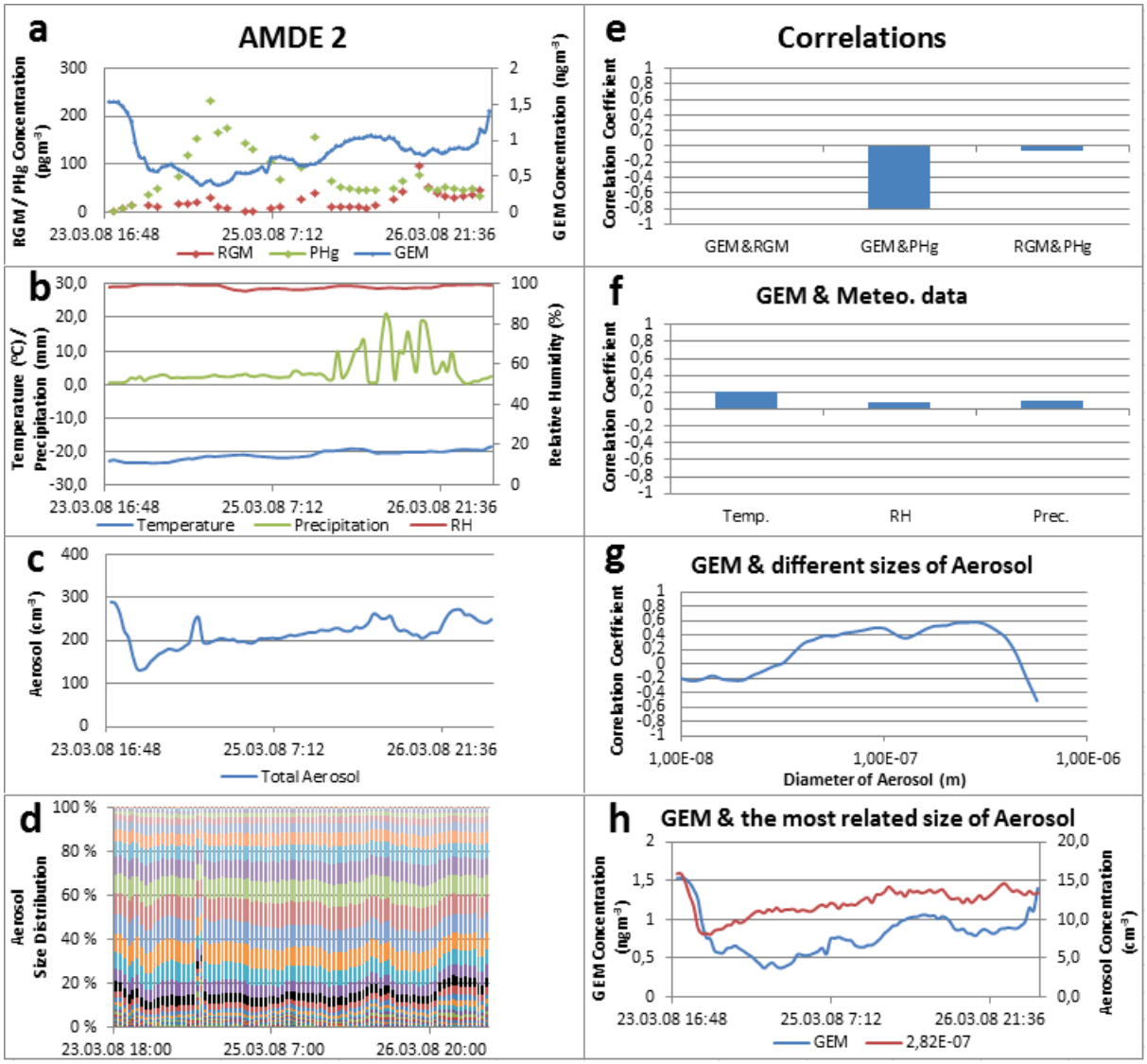

Figure 3.26: AMDE episode 2. Figure **a**: Concentrations of GEM, RGM and PHg. Figure **b**: Temperature, relative humidity and 10-day accumulated precipitation. Figure **c**: Number concentration of total detected aerosol. Figure **d**: Aerosol size distribution along time, different size interval of aerosols are colored and small to large sizes are shown from bottom to top where the black color represents 100 nm as the middle size. Figure **e**: Correlations between GEM and RGM, GEM and PHg, RGM and PHg. Figure **f**: Correlations between Temperature and GEM, RH and GEM, precipitation and GEM. Figure **g**: Correlations between aerosols and GEM as a function of particle size. Figure **h**: Concentrations of PHg and aerosols that correlate to GEM the most.

In Figure 3.26, GEM concentration decreased quickly from around 1.5 ng m^{-3} to the lowest point at 0.37 ng m^{-3} within one day, and then it slowly rose up and back to 1.4 ng m^{-3} at the end. RGM concentration was relatively stable in a low level, and rose up to around 100 pg m^{-3} at the end of the episode, and then decreased down. PHg concentration increased in the beginning as the decreasing of GEM concentration, and reached a peak value at more than 200 pg m^{-3}. And then PHg concentration gradually decreased, and ended by around 30 pg m^{-3}. During this episode, PHg and GEM showed a high negative correlation coefficient which was -0.80. However, RGM did not show any correlation with either GEM or PHg.

Temperature gradually increased from -23 to $-19\,^{\circ}$C, and relative humidity kept a high level which is nearly 100%. Precipitation was relatively stable in the first half stage, and then it fluctuated several times. Again, none of the meteorological parameter showed clear correlation with GEM concentrations.

Total aerosol concentration first dropped from 290 to 130 particles cm^{-3}, and then it gradually rose up. Accumulation mode particles were dominant during the whole episode, and most of the aerosols at different size intervals showed positive correlations with GEM concentration. Particles with a size of 282 nm in diameter had the highest correlation coefficient with GEM which was 0.58.

3.8.3 AMDE episode 3

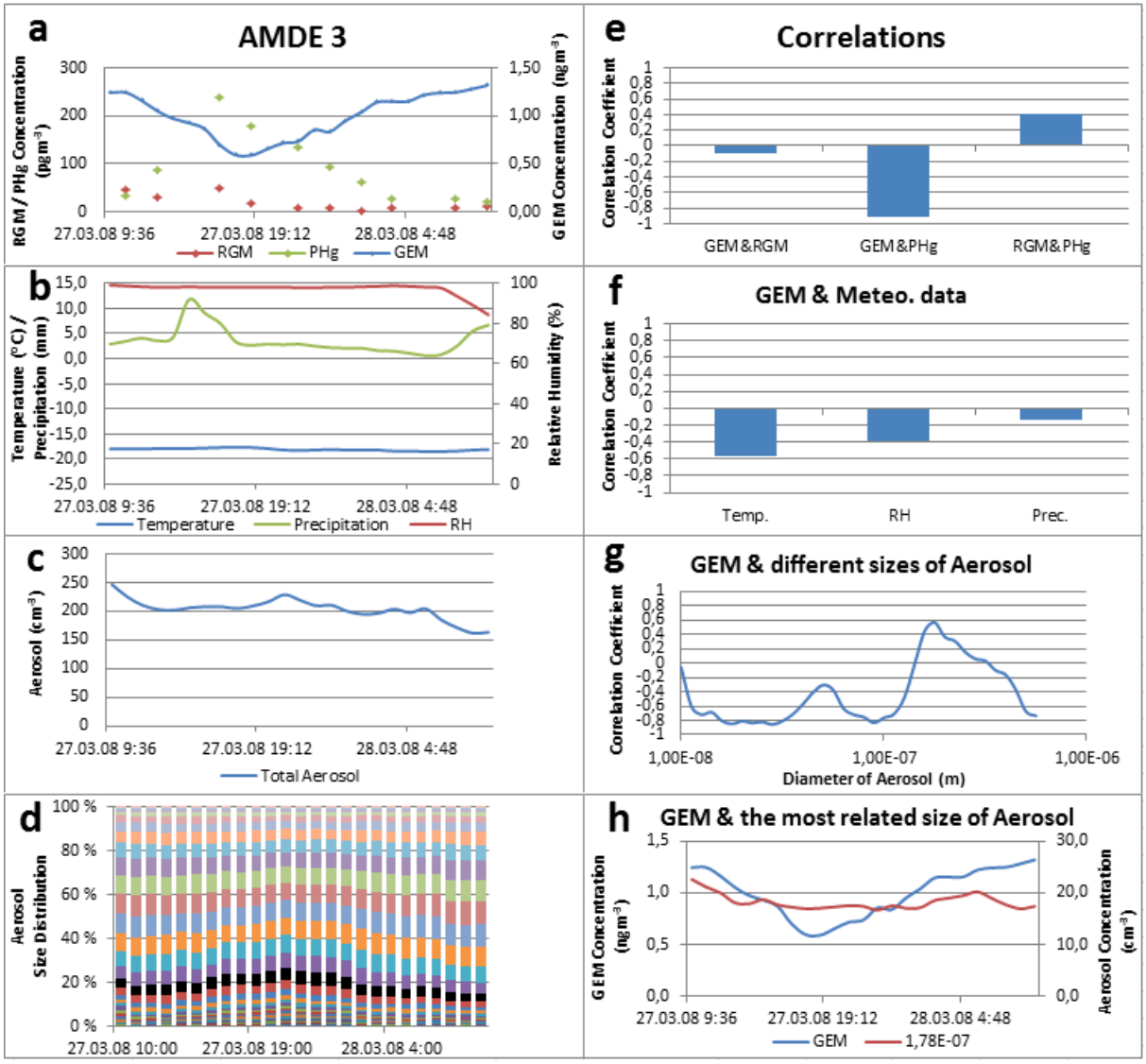

Figure 3.27: AMDE episode 3. Figure **a**: Concentrations of GEM, RGM and PHg. Figure **b**: Temperature, relative humidity and 10-day accumulated precipitation. Figure **c**: Number concentration of total detected aerosol. Figure **d**: Aerosol size distribution along time, different size interval of aerosols are colored and small to large sizes are shown from bottom to top where the black color represents 100 nm as the middle size. Figure **e**: Correlations between GEM and RGM, GEM and PHg, RGM and PHg. Figure **f**: Correlations between Temperature and GEM, RH and GEM, precipitation and GEM. Figure **g**: Correlations between aerosols and GEM as a function of particle size. Figure **h**: Concentrations of PHg and aerosols that correlate to GEM the most.

Figure 3.27 shows that GEM concentration decreased from a little higher than 1.2 to around 0.6 ng m^{-3} in half a day, and then gradually rose back to about 1.3 ng m^{-3}. RGM concentration had a decreasing trend, and it did not show much correlation with either GEM or PHg. PHg concentration rose significantly corresponding to the decreasing concentration of GEM, and it decreased after reaching peak point at more than 200 pg m^{-3}. The concentrations of PHg and GEM had a highly negative correlation, and the correlation coefficient was -0.91.

Temperature was very stable at around $-18\,^{\circ}$C, and it showed some negative correlation with GEM concentration. Relative humidity keeps a high level, and it decreased to around 80% at the end of this episode. Precipitation was also relatively stable despite of 2 peaks, and both relative humidity and precipitation showed very little correlations with GEM concentration.

The total aerosol concentration had a small decreasing trend, and it was dominated by accumulation mode particles. Most of the particles actually showed negative correlation with GEM concentration, but the particles within a size range of around 150 to 230 nm showed positive correlation with GEM concentration. Some different ranges of the sizes contained large values of negative correlation coefficients, which were around -0.8. There was a peak value of positive correlation coefficient where the size of aerosols was 178 nm in diameter, and the correlation coefficient was 0.57.

3.8.4 AMDE episode 4

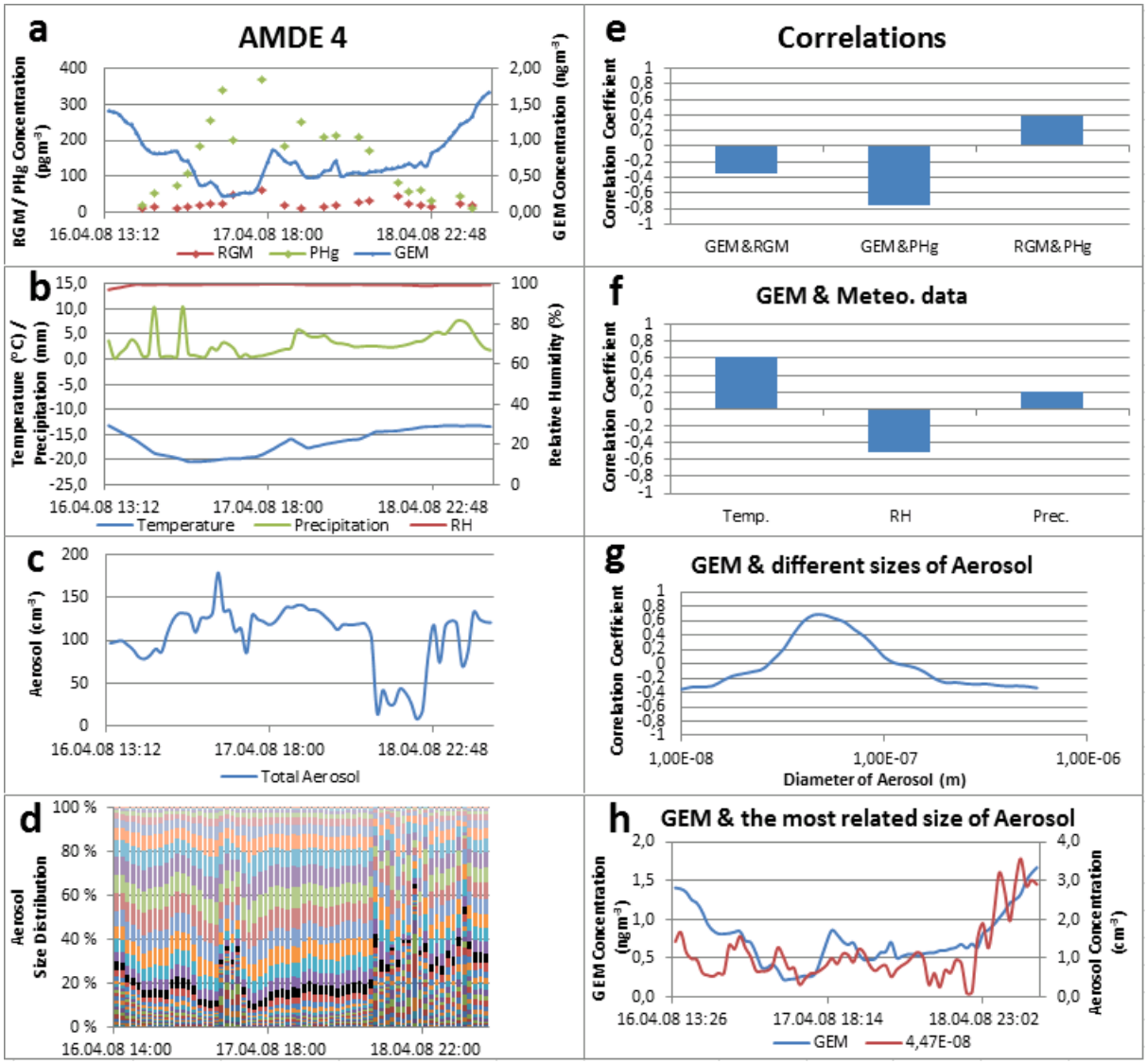

Figure 3.28: AMDE episode 4. Figure **a**: Concentrations of GEM, RGM and PHg. Figure **b**: Temperature, relative humidity and 10-day accumulated precipitation. Figure **c**: Number concentration of total detected aerosol. Figure **d**: Aerosol size distribution along time, different size interval of aerosols are colored and small to large sizes are shown from bottom to top where the black color represents 100 nm as the middle size. Figure **e**: Correlations between GEM and RGM, GEM and PHg, RGM and PHg. Figure **f**: Correlations between Temperature and GEM, RH and GEM, precipitation and GEM. Figure **g**: Correlations between aerosols and GEM as a function of particle size. Figure **h**: Concentrations of PHg and aerosols that correlate to GEM the most.

In Figure 3.28, GEM concentration decreased from around 1.4 ng m^{-3} to the lowest value at 0.23 ng m^{-3}, and then gradually rose back to background level. RGM showed an increasing trend as the decreasing of GEM, and after reaching around 60 pg m^{-3}, it decreased down and vibrates a bit before getting stable. PHg concentration showed a dramatic increasing trend from about only 20 to above 300 pg m^{-3} as the decreasing of GEM concentration, and then it gradually decreased down and back to 20 pg m^{-3} at the end. PHg concentration had a negative correlation with GEM concentration, and the correlation coefficient was -0.75. However, RGM did not show very clear correlation with either PHg or GEM.

Temperature showed a similar trend with GEM concentration, and it first decreased from -13 to $-20\,^{\circ}$C and then gradually increased back. Temperature and GEM concentration had a correlation coefficient of 0.61. Relative humidity keeps a very high level of above 97%, and it showed a negative correlation with GEM concentration. Precipitation fluctuated a lot between 0 and 10 mm, and it did not show any correlation with GEM concentration.

The concentration of total aerosol vibrated a lot through this episode. Accumulation mode particles contributed the most of the total concentration, and particles at most of the size intervals did not show very clear correlation with GEM concentration. The correlation curve of Figure **g** showed an increasing trend for very small particles and a decreasing trend for the particles larger than around 45 nm in diameter. The highest correlation coefficient was 0.68 where the particles had a size of 44.7 nm in diameter. Figure **h** showed that the concentration of the particles at this specific size vibrated a lot, but it had a general trend correlated with GEM concentration.

3.8.5 AMDE episode 5

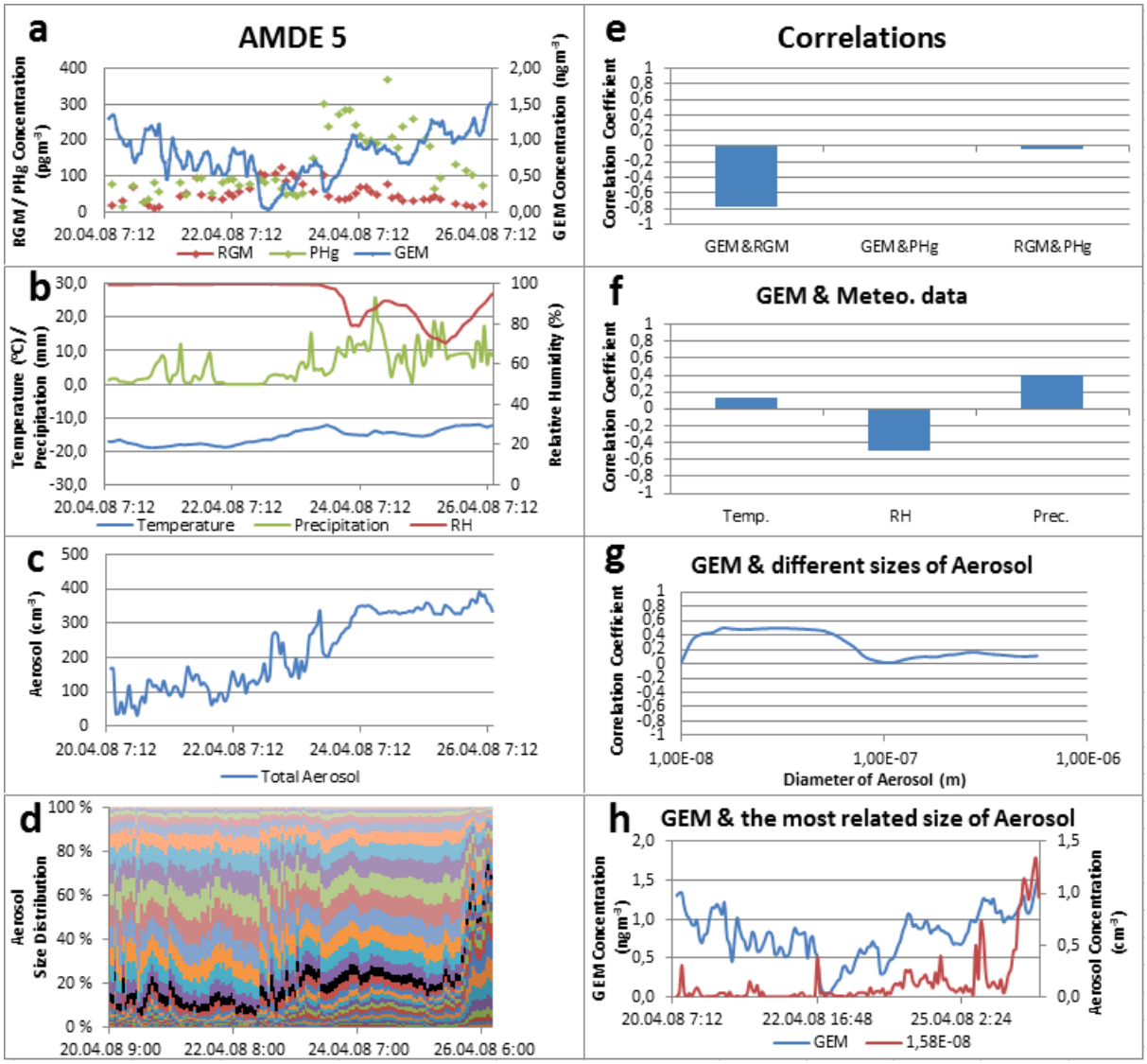

Figure 3.29: AMDE episode 5. Figure **a**: Concentrations of GEM, RGM and PHg. Figure **b**: Temperature, relative humidity and 10-day accumulated precipitation. Figure **c**: Number concentration of total detected aerosol. Figure **d**: Aerosol size distribution along time, different size interval of aerosols are colored and small to large sizes are shown from bottom to top where the black color represents 100 nm as the middle size. Figure **e**: Correlations between GEM and RGM, GEM and PHg, RGM and PHg. Figure **f**: Correlations between Temperature and GEM, RH and GEM, precipitation and GEM. Figure **g**: Correlations between aerosols and GEM as a function of particle size. Figure **h**: Concentrations of PHg and aerosols that correlate to GEM the most.

Figure 3.29 showed a long period of a mercury depletion event which had an duration for 6 days. GEM concentration started from 1.3 ng m^{-3}, and it vibrated many times but had a general decreasing trend in the beginning of this episode. It reached the lowest value which below MDL after two and half days, and then the concentration rose up together with many vibrations. RGM concentration was increasing gradually and reached the peak value of above 100 pg m^{-3} very near to the time where GEM concentration had the lowest value, and then RGM concentration gradually decreased. RGM concentration was very negatively correlated with GEM concentration, and the correlation coefficient equaled to -0.79. PHg concentration also showed an increasing trend, but the highest values appeared a few hours after the lowest concentration of GEM appearing. So PHg concentration did not show any clear correlations with either GEM or RGM.

Temperature had an increasing trend, and it was relatively stable between -20 to $-10\,^{\circ}$C. It did not show clear correlations with GEM concentration. Relative humidity was very high during the first half of this episode, and decreased to as low as 70% at the end. RH showed some negative correlation with GEM concentration. Precipitation had the highest value of above 20 mm when PHg had the highest concentrations, but it did not show a clear correlation with GEM concentration.

Total aerosol concentration showed a general increasing trend, and accumulation mode particles dominated most of the period except the last few hours. In general, most particles with different sizes showed some positive correlations with GEM concentrations. But due to the long duration of this episode, the correlations were not significantly high. Small particles had higher correlations with GEM, and the highest correlation coefficient was 0.50 where the particles had a size of 15.8 nm in diameter.

3.8.6 AMDE episode 6

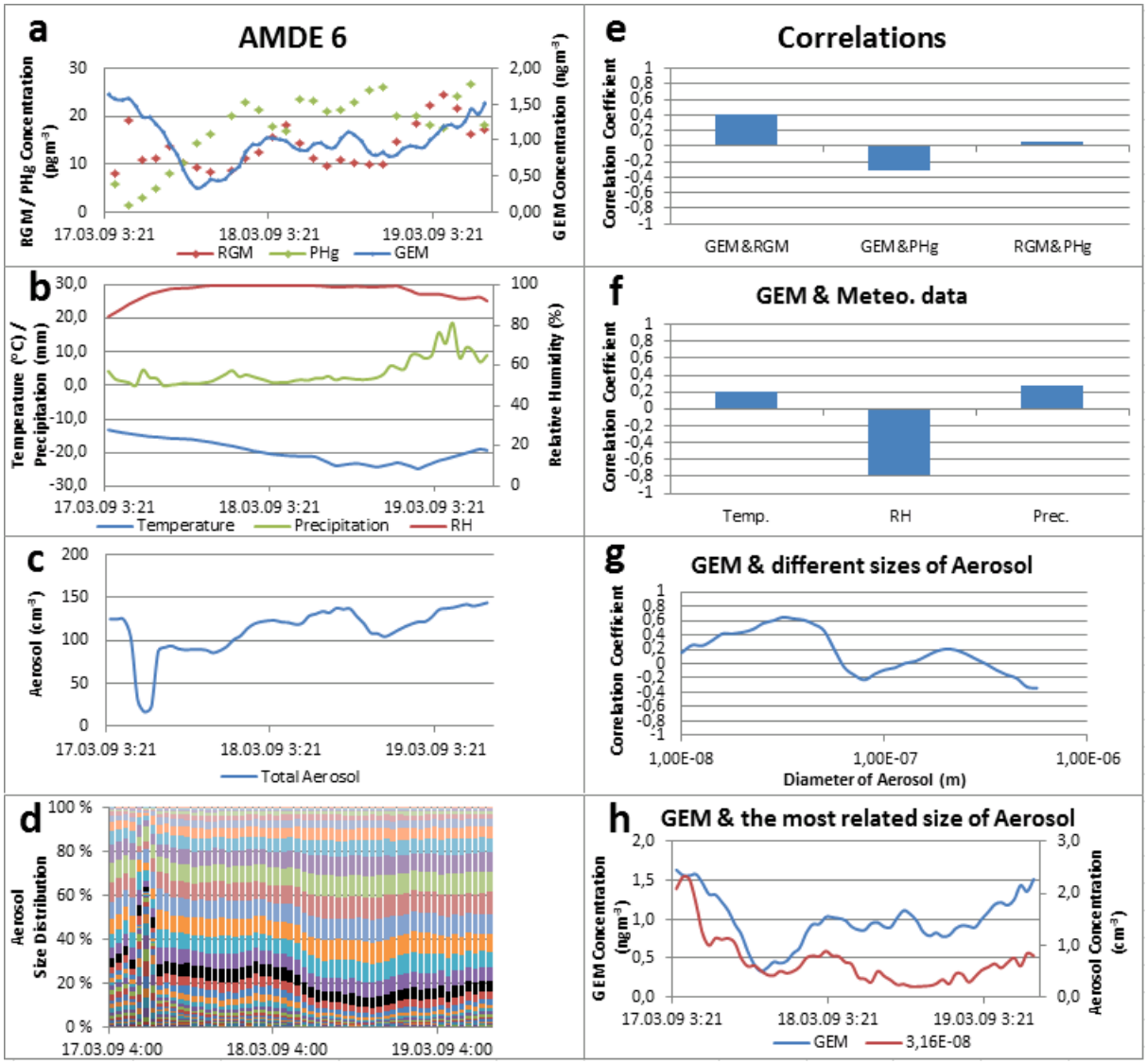

Figure 3.30: AMDE episode 6. Figure **a**: Concentrations of GEM, RGM and PHg. Figure **b**: Temperature, relative humidity and 10-day accumulated precipitation. Figure **c**: Number concentration of total detected aerosol. Figure **d**: Aerosol size distribution along time, different size interval of aerosols are colored and small to large sizes are shown from bottom to top where the black color represents 100 nm as the middle size. Figure **e**: Correlations between GEM and RGM, GEM and PHg, RGM and PHg. Figure **f**: Correlations between Temperature and GEM, RH and GEM, precipitation and GEM. Figure **g**: Correlations between aerosols and GEM as a function of particle size. Figure **h**: Concentrations of PHg and aerosols that correlate to GEM the most.

In Figure 3.30, GEM concentration decreased from 1.6 to around 0.4 ng m^{-3} quickly, and then it gradually rose back to 1.5 ng m^{-3}. RGM concentration vibrated from a range of 8 to 25 pg m^{-3}, and it did not show clear correlations with GEM concentration. PHg concentration showed an increasing trend, but it did not have any clear correlation with GEM or PHg either.

Temperature showed a decreasing trend, and it had an average of around −20 °C. Temperature did not show any correlation with GEM concentration. Relative humidity increased in the beginning, and then kept a high level for a long time before decreasing a bit at the end. And it showed a negative correlation with GEM concentration with a correlation coefficient at -0.79. Precipitation was relatively stable for a long time, and rose up at the end of the episode. It did not show much correlations with GEM concentration.

Total aerosol concentration kept a low level during this episode, and large particles dominated the total concentration. Most of the particles with different sizes did not show much correlation with GEM concentrations, but some small particles with a size range of around 15 nm to 50 nm showed positive correlations with GEM concentration. The highest correlation coefficient was 0.65 where particles had a size of 31.6 nm in diameter.

3.8.7 AMDE episode 7

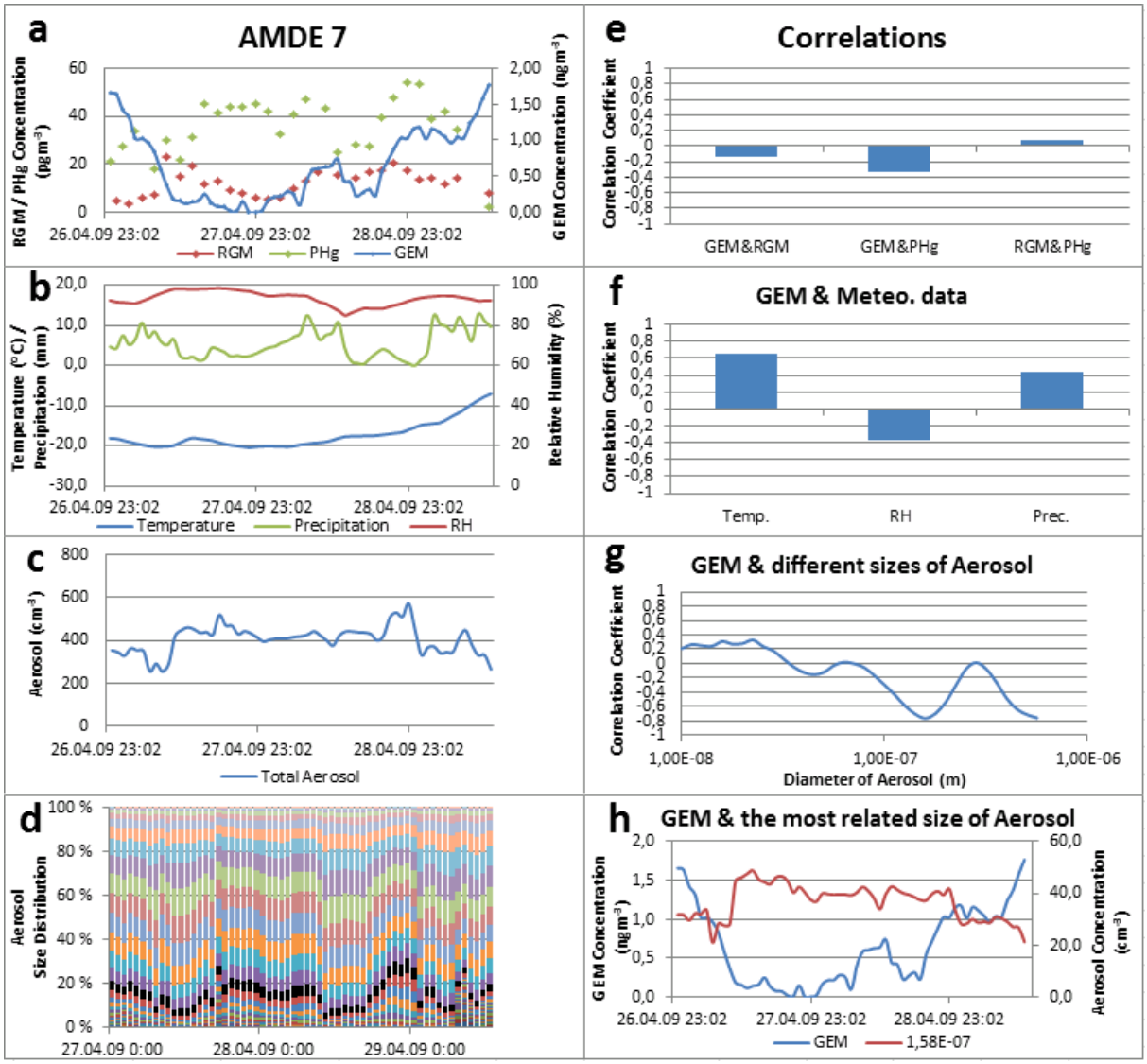

Figure 3.31: AMDE episode 7. Figure **a**: Concentrations of GEM, RGM and PHg. Figure **b**: Temperature, relative humidity and 10-day accumulated precipitation. Figure **c**: Number concentration of total detected aerosol. Figure **d**: Aerosol size distribution along time, different size interval of aerosols are colored and small to large sizes are shown from bottom to top where the black color represents 100 nm as the middle size. Figure **e**: Correlations between GEM and RGM, GEM and PHg, RGM and PHg. Figure **f**: Correlations between Temperature and GEM, RH and GEM, precipitation and GEM. Figure **g**: Correlations between aerosols and GEM as a function of particle size. Figure **h**: Concentrations of PHg and aerosols that correlate to GEM the most.

Figure 3.31 shows that GEM concentration decreased from background level to below MDL during only one day, and it kept at a low level for a few hours before gradually rising up to background level again. Most of the RGM concentration was below the MDL, and it did not show any correlation with either GEM or PHg. PHg concentration generally kept between the MDL and 60 pg m^{-3}, and it also showed no clear correlation with GEM.

Temperature had an increasing trend, and it rose from around -20 to $-7\,^{\circ}$C. It showed a positive correlation with GEM concentration, and the correlation coefficient was 0.65. Relative humidity was relatively stable, and it varied between 80 and 100%. It did not show clear correlation with GEM concentration. Precipitation vibrated between 0 and 13 mm, and It showed a small positive correlation with GEM concentration.

Total aerosol concentration was around 400 cm^{-3}, and accumulation mode particles dominated the total concentration. Most of the particles at different sizes did not show clear correlations with GEM concentration. But the particles with a size of around 160 and 500 nm in diameter had negative correlations with GEM concentration. The highest value of the correlation coefficient was -0.76 where particles had a size of 158 nm in diameter.

3.8.8 AMDE episode 8

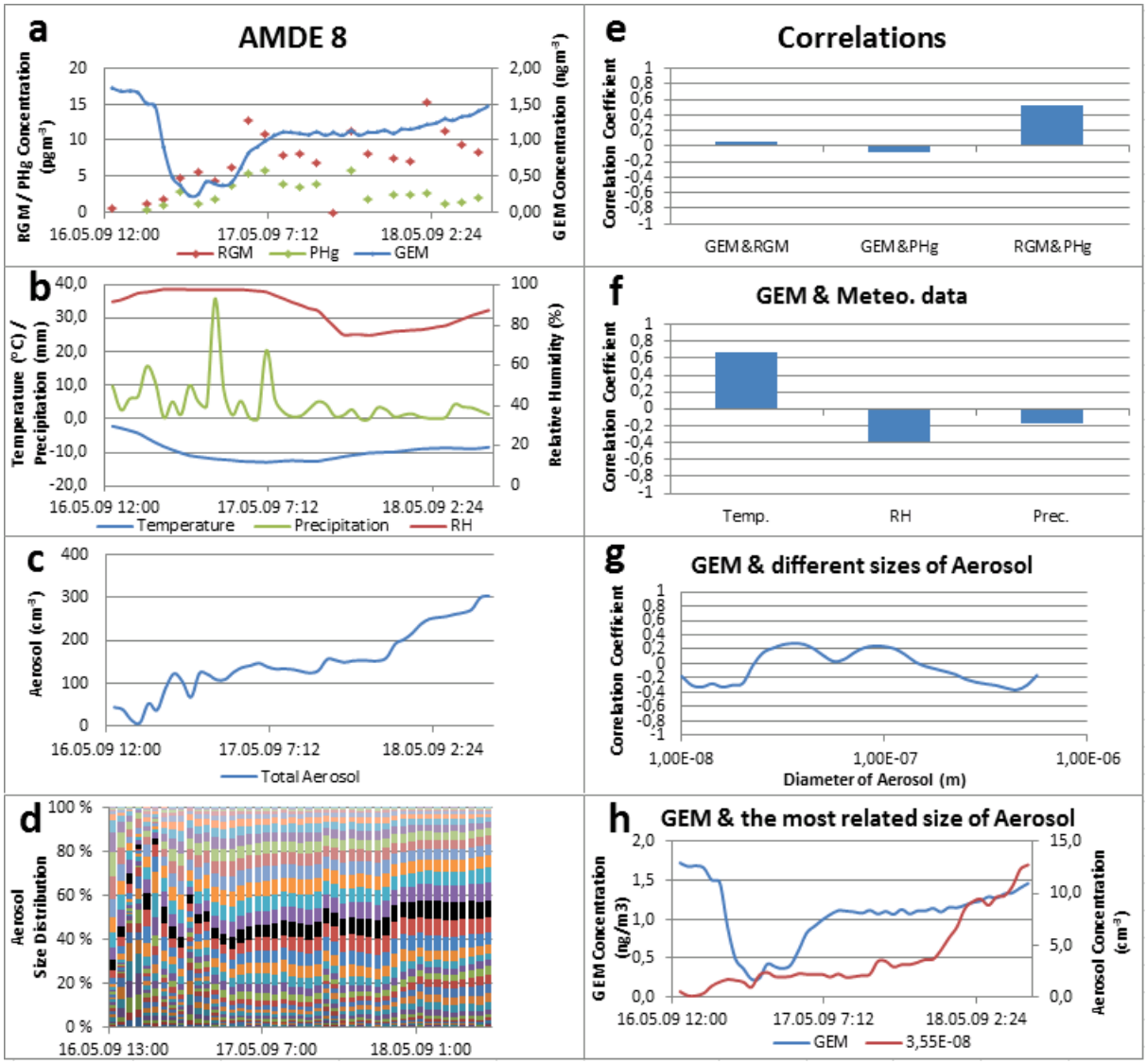

Figure 3.32: AMDE episode 8. Figure **a**: Concentrations of GEM, RGM and PHg. Figure **b**: Temperature, relative humidity and 10-day accumulated precipitation. Figure **c**: Number concentration of total detected aerosol. Figure **d**: Aerosol size distribution along time, different size interval of aerosols are colored and small to large sizes are shown from bottom to top where the black color represents 100 nm as the middle size. Figure **e**: Correlations between GEM and RGM, GEM and PHg, RGM and PHg. Figure **f**: Correlations between Temperature and GEM, RH and GEM, precipitation and GEM. Figure **g**: Correlations between aerosols and GEM as a function of particle size. Figure **h**: Concentrations of PHg and aerosols that correlate to GEM the most.

Figure 3.32 shows that GEM decreased from background level to around 0.2 ng m^{-3} with in only half a day, and then gradually rose back to 1.5 ng m^{-3} at the end of the episode. Both RGM and PHg concentration were actually below the MDL during the whole period, so they did not show any correlations with GEM concentration.

Temperature showed a decreasing trend at the beginning, and then it rose up a bit and kept relatively stable. It showed a positive correlation with GEM concentration, and the correlation coefficient equaled to 0.66. Relative humidity and precipitation did now show clear correlations with GEM concentration.

Total aerosol had an increasing trend all the time, and it had a relatively low concentration. Particle size distributions were rather equal between large particles and small ones, and none of the particles with specific size showed clear correlations with GEM concentration in this case.

3.8.9 AMDE episode 9

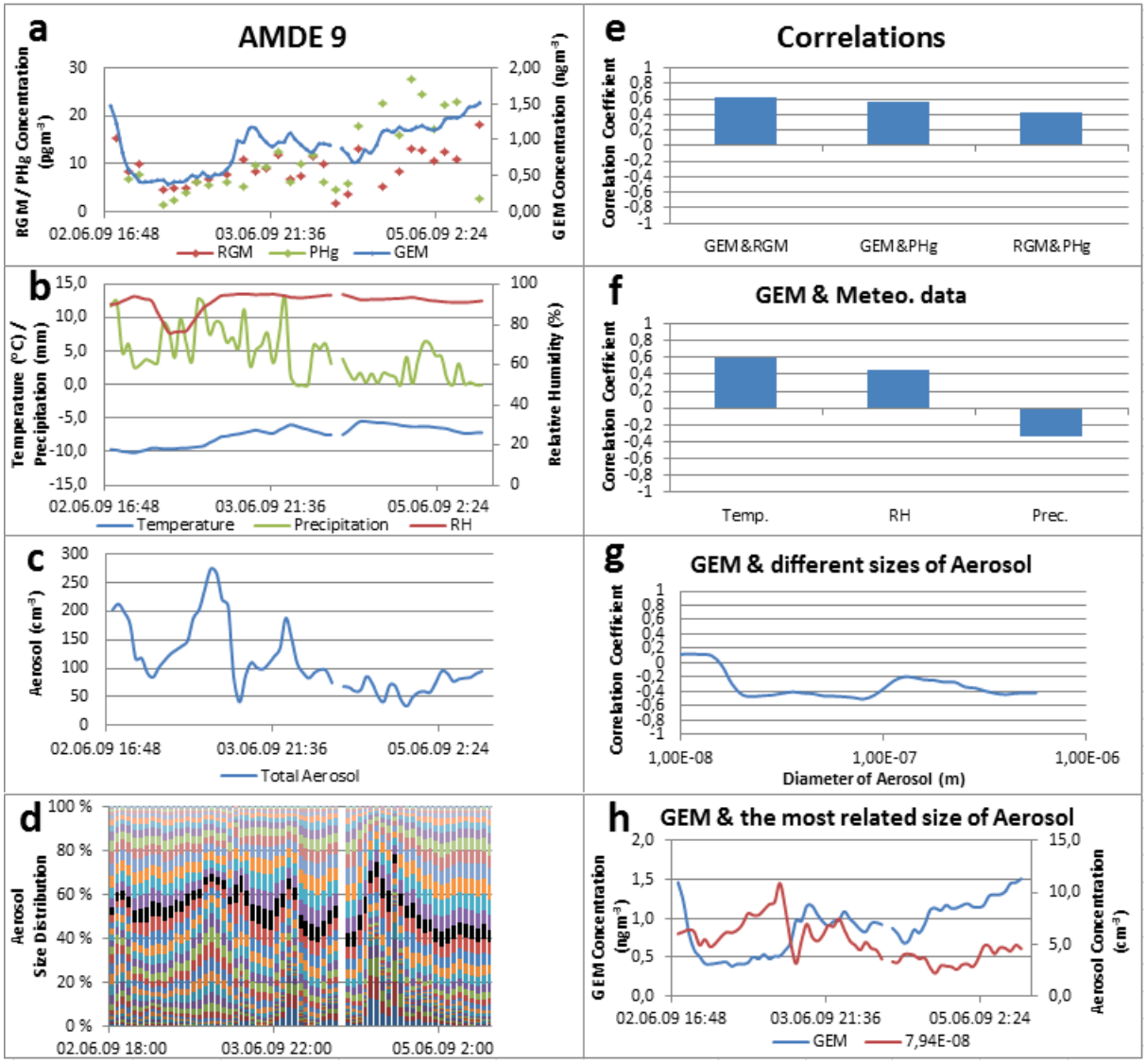

Figure 3.33: AMDE episode 9. Figure **a**: Concentrations of GEM, RGM and PHg. Figure **b**: Temperature, relative humidity and 10-day accumulated precipitation. Figure **c**: Number concentration of total detected aerosol. Figure **d**: Aerosol size distribution along time, different size interval of aerosols are colored and small to large sizes are shown from bottom to top where the black color represents 100 nm as the middle size. Figure **e**: Correlations between GEM and RGM, GEM and PHg, RGM and PHg. Figure **f**: Correlations between Temperature and GEM, RH and GEM, precipitation and GEM. Figure **g**: Correlations between aerosols and GEM as a function of particle size. Figure **h**: Concentrations of PHg and aerosols that correlate to GEM the most.

In Figure 3.33, it can be seen that GEM concentration decreased quickly from around 1.5 to below 0.5 ng m^{-3} within a few hours, and then gradually increased to back to 1.5 ng m^{-3}. Most data points of RGM and PHg were below MDL, so the correlations between mercury species were not precise enough.

Temperature slowly increased and then decreased between a range of -10 to $-5\,^{\circ}$C, and it showed a positive correlation with GEM concentration. Relative humidity decreased from more than 90 to below 80% in the beginning, and then increased and kept stable above 90%. It showed a small positive correlation with GEM concentration. Precipitation did not show much correlation with GEM concentration.

Total aerosol concentration vibrated a lot, while large and small particles had fairly balanced concentrations. Particles in some size ranges showed small negative correlations with GEM concentration. The largest correlation coefficient equaled to -0.50 where particles had a size of around 80 nm in diameter.

3.8.10 AMDE episode 10

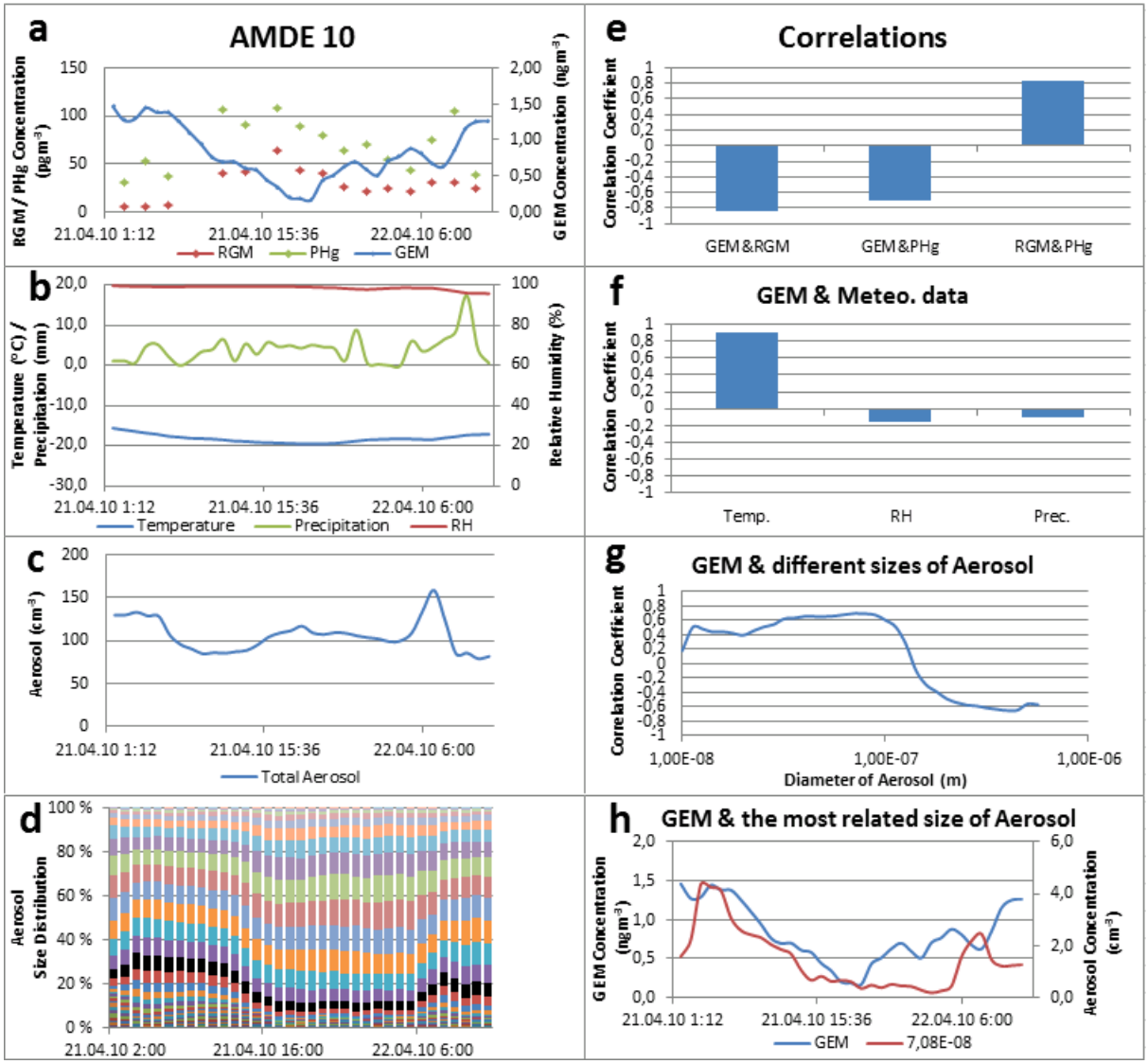

Figure 3.34: AMDE episode 10. Figure **a**: Concentrations of GEM, RGM and PHg. Figure **b**: Temperature, relative humidity and 10-day accumulated precipitation. Figure **c**: Number concentration of total detected aerosol. Figure **d**: Aerosol size distribution along time, different size interval of aerosols are colored and small to large sizes are shown from bottom to top where the black color represents 100 nm as the middle size. Figure **e**: Correlations between GEM and RGM, GEM and PHg, RGM and PHg. Figure **f**: Correlations between Temperature and GEM, RH and GEM, precipitation and GEM. Figure **g**: Correlations between aerosols and GEM as a function of particle size. Figure **h**: Concentrations of PHg and aerosols that correlate to GEM the most.

Figure 3.34 shows that GEM concentration gradually decreased from around 1.5 ng m^{-3} to as low as 0.2 ng m^{-3}, and then increased to around 1.3 ng m^{-3} with some vibrations. Both RGM and PHg showed an opposite trend to GEM concentration, and they had a significant positive correlation. GEM had negative correlations with both RGM and PHg.

Temperature slowly decreased from around -16 to −20 °C, and then gradually increased to −17 °C. It showed a significant positive correlation with GEM concentration with a correlation coefficient of 0.90. Relative humidity kept a very high level during the whole episode, but neither RH nor precipitation showed a clear correlation with GEM concentration.

Total aerosol concentration was around annual median value, and accumulation mode particles dominated the total concentration. It showed that particles smaller than 100 nm in diameter generally had positive correlations with GEM concentration, and the correlation curve in Figure **g** decreased quickly to negative with increasing size. The highest correlation coefficient was 0.70 where particles had a size of around 71 nm in diameter.

To sum up, AMDEs happened several times each year from March to June of 2007-2011. Every year, GEM concentrations during AMDE periods were different, but they showed similar decreasing patterns in GEM level general. Berg et al. (2013) reported that AMDEs were equally distributed between April and May with noly a few observed in March and June from 2000 to 2009 at Zeppelin station. In this AMDE episodes' study, it covered the whole AMDE periods from March to June.

From the 10 chosen AMDE episodes, the median temperature was calculated to be −16.1 °C which was more than 9 °C lower than the median value for the whole dataset. The median relative humidity was 97.6%, and it was 6% higher than the median value for the whole dataset. The median of 10-day accumulated precipitation was 2.7 mm which is less than a half of the median value for the whole dataset. All of the three meteorological parameters showed significant differences with the median for the whole dataset, which indicated that the happening of AMDE might need a low temperature, high RH and relatively low precipitation. Berg et al. (2013) reported a negative correlation between AMDEs and temperature, and the lowest GEM levels appeared when the RH was between 80 and 90% at Zeppelin station. In this study, low temperature during AMDEs corresponded to previous study very well, but the relative humidity was found much higher than previous reports.

Many researchers reported that the concentration of GEM had a close relationship with temperature, precipitation and relative humidity (Osawa et al., 2007). Moen (2012) reported that temperature and relative humidity were positively correlated with GEM concentration. Steen et al. (2011) reported that the low GEM concentrations correlated with air temperature in January, March and April, and anti correlated with temperature in August at Zeppelin station. In this study, it was found that temperature was positively correlated with GEM concentration during AMDE period in general, which corresponded to the previous studies well. While RH was generally anti-correlated with GEM concentrations, which did not correspond to Moen (2012) well.

Moen (2012) reported that the concentration of aerosols were more correlated with GEM concentration than PHg, In this thesis, some correlations between the concentrations of particles and GEM were also found, but they varied a lot during each AMDE episode. In general, accumulation mode particles had a higher number concentration compared with Aitken mode particles during most of the episodes, which corresponded to the haze period (Tunved et al., 2013).

3.9 Post-AMDE episodes

During the study of AMDEs in this thesis, it was found that GEM concentrations could increase to very high levels soon after the depletion events. GEM concentration sometimes could reach at around 2 ng m^{-3} during the spring, and the high level of GEM could appear between several depletion events. Lalonde et al. (2002); Steffen et al. (2002) reported that Hg (II) deposited on snow could be rapidly re-emitted, and GEM concentrations in the interstitial air of a snowpack elevated above those in ambient air during AMDEs. There are 2 episodes chosen and they are shown in Table 3.19.

post-AMDE episode	Start time	End time	Duration	Highest Conc.	Lowest Conc.	Median Conc.
1	25.05.2007 00:00	08.06.2007 23:00	15d	2.47	0.26	1.98
2	15.04.2008 00:00	02.05.2008 23:00	18d	1.96	<MDL	1.25

Table 3.19: Post-AMDE episodes chosen during 2007 to 2011. The unit is in ng m^{-3}.

Both of the episodes have a duration of more than half a month, and the concentration range is large. To look into detail, they are shown as Figure 3.35 and Figure 3.36.

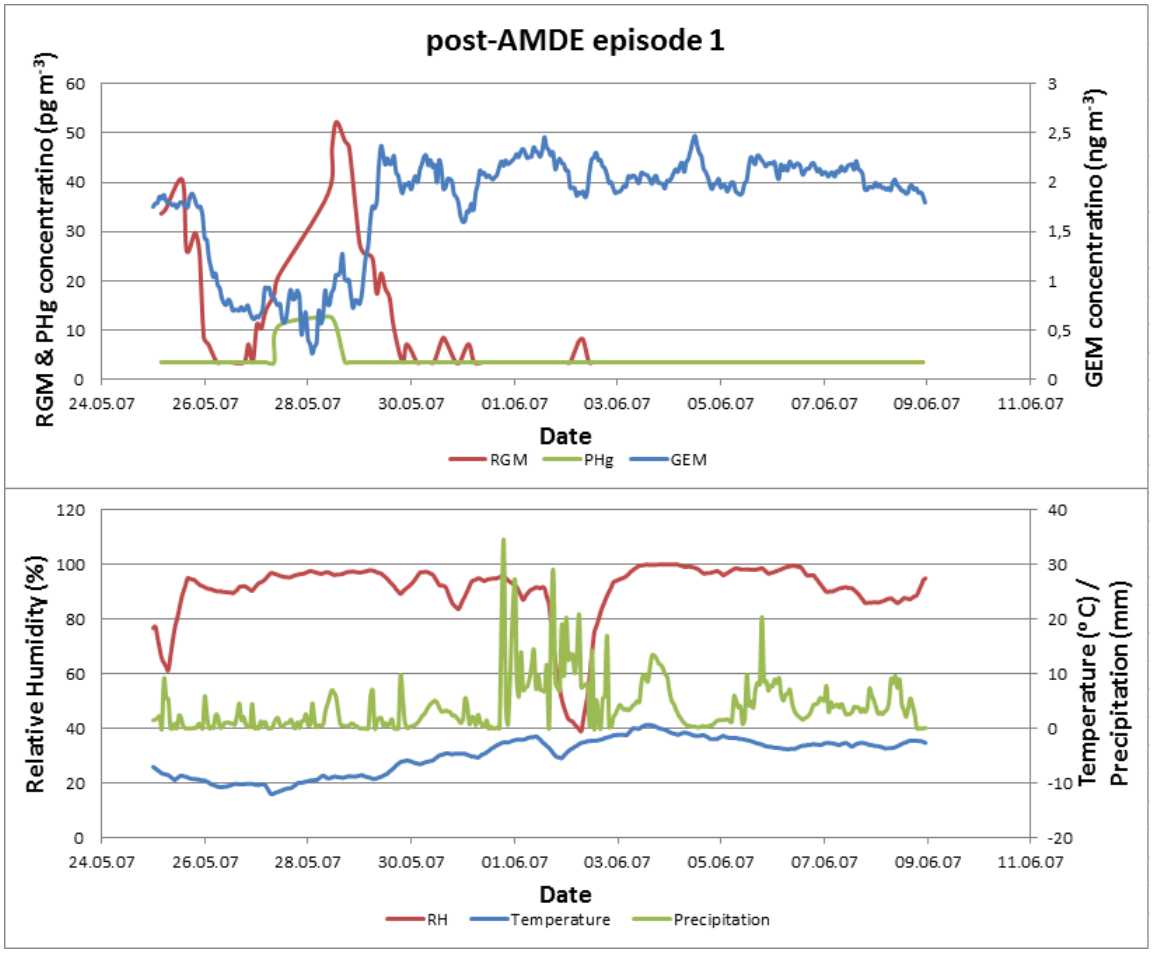

Figure 3.35: post-AMDE episode 1.

Figure 3.35 shows that GEM concentration decreased from background level to only around 0.26 ng m^{-3}, and then suddenly rose to a very high level which was above 2 ng m^{-3}. It kept a high concentration for around 10 days, and then decreased back to background level. Both RGM and PHg increased corresponding to the decreasing of GEM. The quick increasing of GEM after the depletion seemed to be contributed by the re-emission of RGM which was decreasing fast at the same time. PHg did not contribute much to the rising of GEM due to its low concentration. During the whole period, temperature showed a strong positive correlation with GEM concentration, and the correlation coefficient was calculated to be 0.78. Relative humidity and precipitation did not show much correlation with GEM concentration.

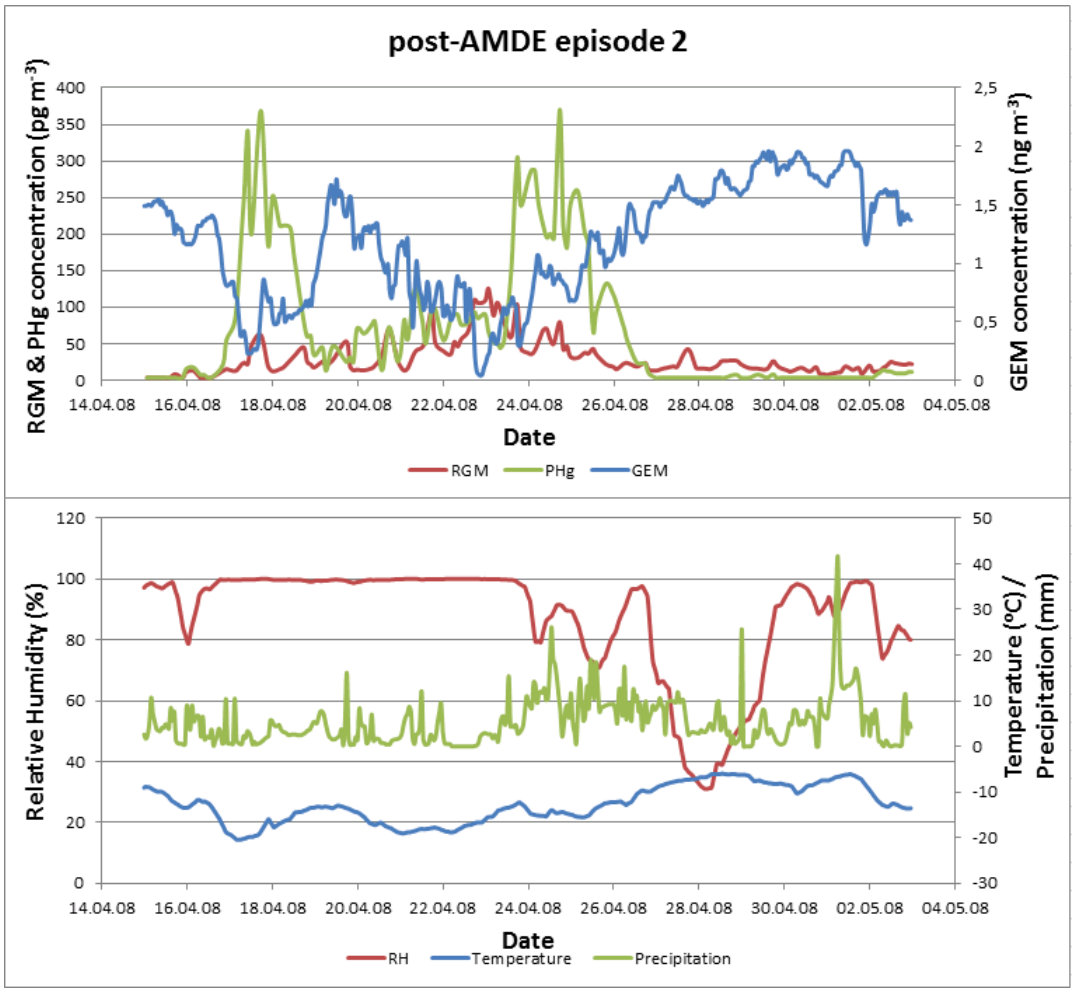

Figure 3.36: post-AMDE episode 2.

From Figure 3.36, it can be seen that AMDEs happened twice, first it decreased from around 1.5 ng m^{-3} to as low as 0.23 ng m^{-3}. And then it suddenly rose up to 1.7 ng m^{-3} before the second decrease to below the detection limit. After the second AMDE, GEM concentration gradually rose to around 2 ng m^{-3}, and kept the high level for several days. During the first AMDE, PHg concentration increased significantly corresponding to the increase of GEM. And the decreasing of PHg corresponded to the increasing of GEM very well after the first depletion.

During the second period of GEM depletion, RGM concentration gradually increased to more than 100 pg m^{-3}. And it started decreasing while both GEM and PHg were increasing. After the decrease of RGM, PHg also decreased, and in this period both decreasing trends of RGM and PHg might contribute to the increasing of GEM and caused a high level of GEM concentration.

This time, temperature had a strong positive correlation with GEM again, and the correlation coefficient was calculated to be 0.80.

To sum up, the high GEM concentrations after AMDEs were probably due to the reemission of Hg following photo-reduction of Hg (II) in snow right after AMDEs, and Hg (II) lost back to the atmosphere as GEM (Kirk et al., 2006).

3.10 AMEE episodes

The AMEEs were less studied than AMDEs, and they were found every year from 2007 to 2011 in this thesis. Aspmo et al. (2006) also reported increased concentrations of GEM in summertime in the North Atlantic Ocean. To investigate this phenomenon, 4 episodes have been chosen as shown in Table 3.20.

AMEE episode	Start time	End time	Duration	Highest Conc.	Lowest Conc.	Median Conc.
1	15.07.2007 00:00	22.07.2007 23:00	8d	2.11	1.43	1.77
2	26.06.2008 00:00	08.07.2008 23:00	13d	2.09	1.25	1.57
3	08.09.2008 00:00	11.09.2008 23:00	4d	2.19	1.68	1.90
4	17.07.2009 00:00	21:07:2009 23:00	5d	2.19	1.54	1.83

Table 3.20: AMEE episodes chosen during 2007-2011. The unit is in $\mathrm{ng\,m^{-3}}$.

During all of the 4 AMEE episodes, GEM concentrations passed over $2\,\mathrm{ng\,m^{-3}}$ which was much higher than the yearly median value (1.57-1.70 $\mathrm{ng\,m^{-3}}$). The details of each episode are shown from Figure 3.37 to Figure 3.40.

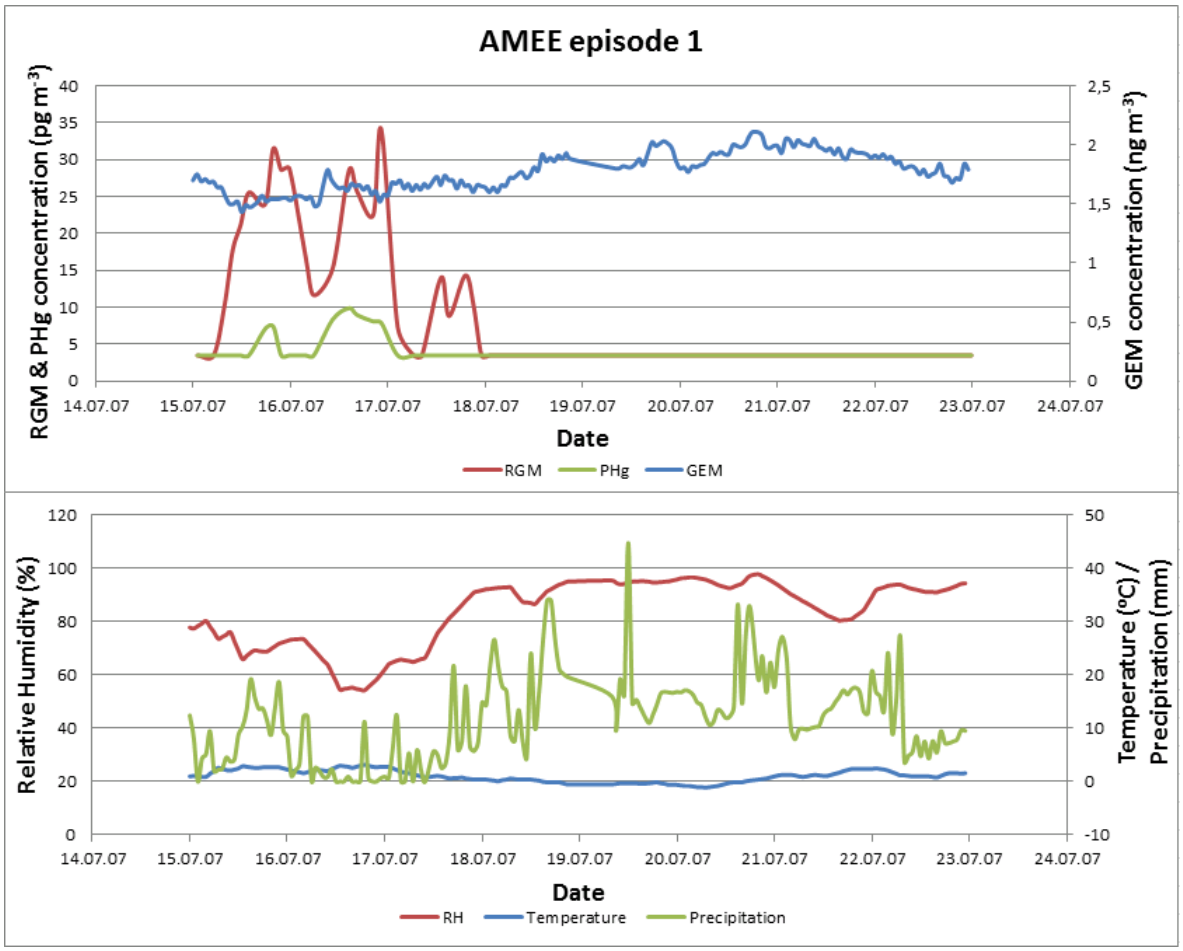

Figure 3.37: AMEE episode 1.

In Figure 3.37, it can be seen that GEM concentration decreased a little in the beginning from background level, and RGM concentration increased immediately at the same time. Then GEM concentration gradually increased to above 2 ng m^{-3}, and it kept for a while before decreasing back to background level. Both RGM and PHg concentrations were below detection limit when GEM concentration rose above background level. Steen et al. (2011) reported that the elevated concentrations of RGM in summer were possibly due to the in situ ozone mediated oxidation of GEM.

Relative humidity showed a positive correlation with GEM concentration, and the correlation coefficient equaled to 0.66. Temperature was around 0 °C, and it did not show very clear correlations with GEM concentration.

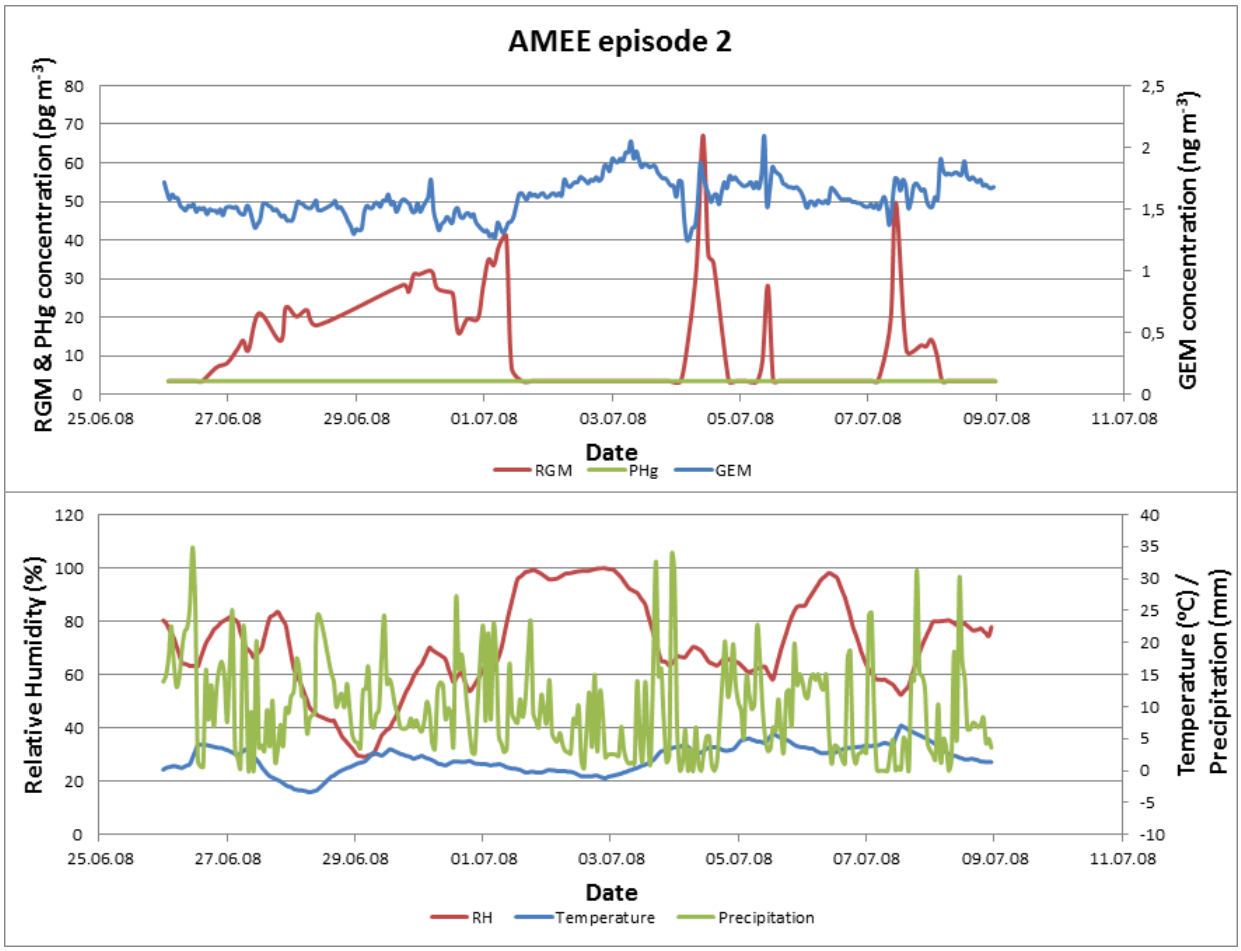

Figure 3.38: AMEE episode 2.

Figure 3.38 showed that GEM was slightly decreasing in the beginning from background level, and it reached at around 2 ng m^{-3} for a few times. RGM concentration vibrated many times, and sometimes it suddenly increased when GEM concentration was decreasing. However, PHg concentration stayed below the MDL for the whole period. The decreasing trends for GEM concentration were relatively small compared with AMDEs, and that might be due to either a strong reemission of GEM from surface waters (Sommar et al., 2007; Aspmo et al., 2006) and/or the arrival of air masses with increased GEM concentrations (Durnford et al., 2010). In this episode, temperature was generally above 0 °C, and RH had an anti-correlation trend with the elevated RGM concentration.

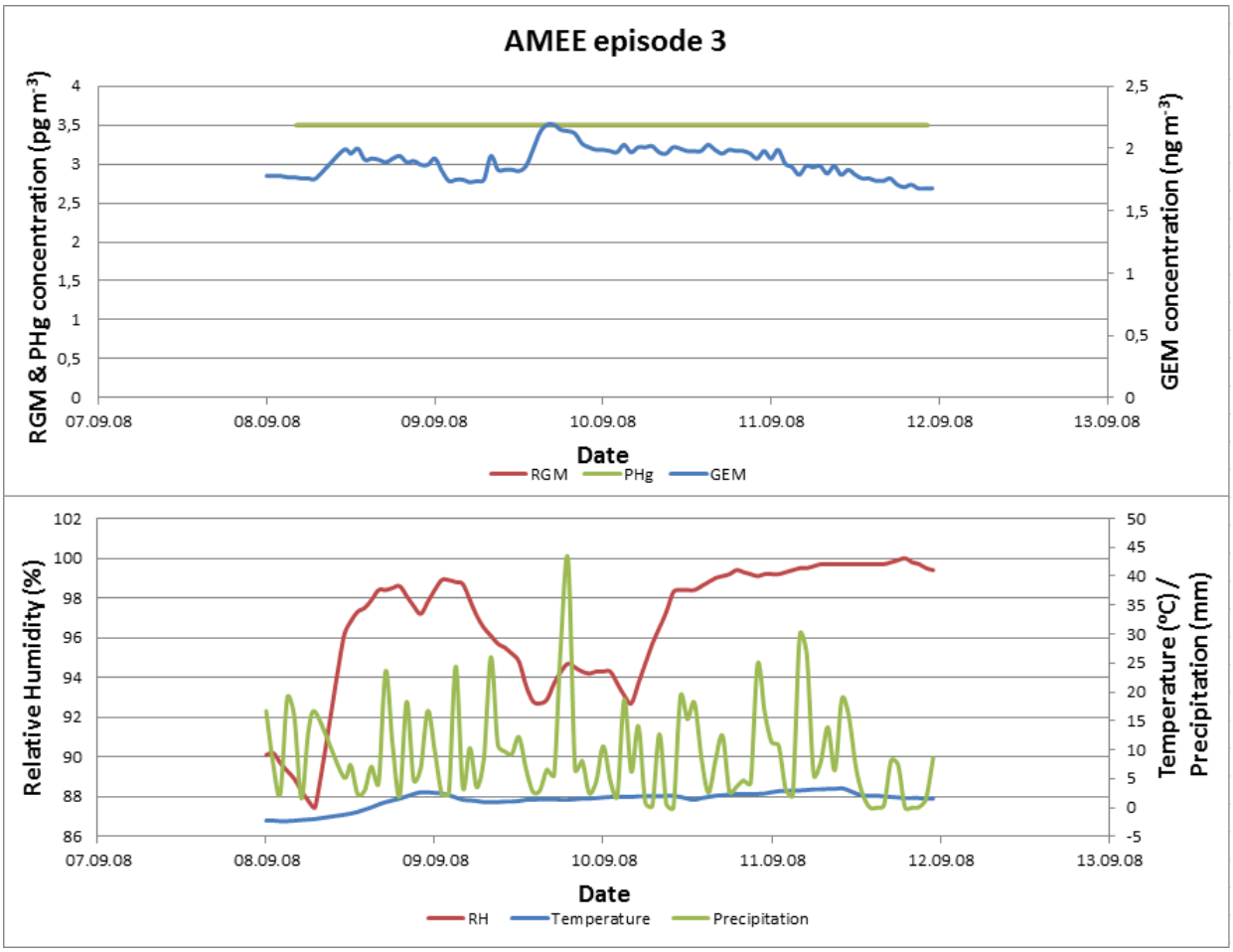

Figure 3.39: AMEE episode 3.

In Figure 3.39, it can be seen that GEM concentration was relatively stable. It rose gradually in the beginning, and kept at around 2 ng m^{-3} for more than one day. RGM and PHg concentrations were below the MDL during the whole period. Temperature was at around 0 °C, and the meteorological conditions did not show much correlations with GEM concentrations.

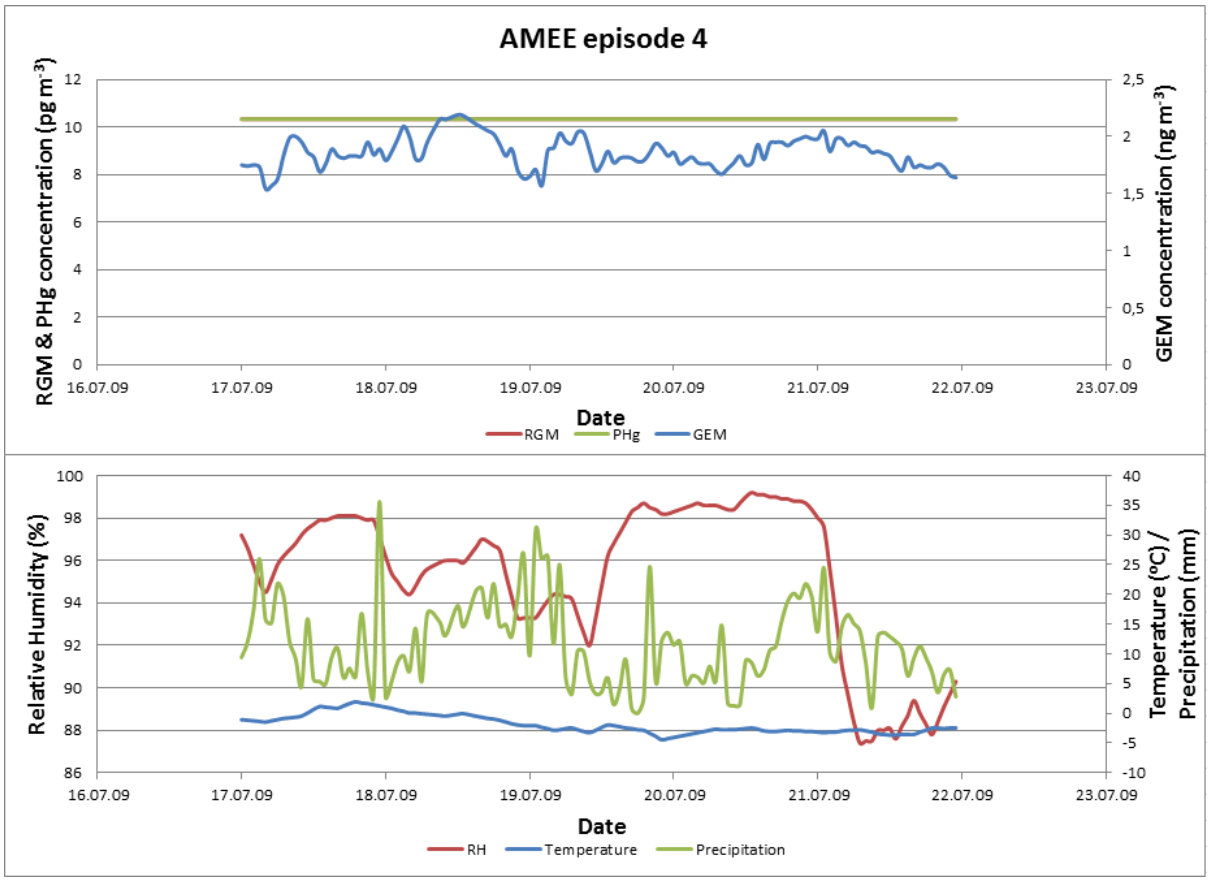

Figure 3.40: AMEE episode 4.

Figure 3.40 shows a similar pattern of GEM concentration as in Figure 3.39, and GEM concentration was generally very stable but reached above 2 ng m^{-3} several times. RGM and PHg concentrations were all below the detection limit, and meteorological conditions did not have much correlation with GEM concentration. Temperature was at around 0 °C during the whole period, and meteorological conditions did not show clear correlations with GEM concentrations.

To summarize the conditions of AMEEs, GEM frequently showed very high concentrations (around 2.0 ng m^{-3}) from the late of June to September every year in the period of 2007 to 2011. The AMEEs happened typically at around 0 °C, which corresponded to Cole and Steffen (2010) very well. Cole and Steffen (2010) explained that the mechanism for increasing AMEEs with temperature might be an increase in the photoreduction of oxidized mercury to gaseous GEM in the snowpack as the snow melted and sunlight penetrated further.

In the episode study, the decreases of GEM concentrations in summertime would sometimes increase RGM concentrations, but PHg concentrations normally did not increase. The elevated concentrations of RGM in summertime was probably caused by the in situ ozone mediated oxidation of GEM (Steen et al., 2011). In the first 2 AMEE episodes, RH showed a positive correlation with GEM concentration, and it was anti-correlated with elevated RGM concentration. This corresponded to Steen et al. (2011); Moen (2012) well in summertime. The low PHg concentrations were probably due to the lack of accumulation mode particle in the atmosphere in summertime (Ström et al., 2003; Tunved et al., 2013). When GEM concentration is very high, it is hardly found much RGM or PHg in summertime. Unlike the AMDEs, AMEEs have a trend to happen at temperature of around 0 °C. On the other hand, it is not found clear correlations between the temperature change and GEM concentration.

Chapter 4

Conclusion

In this thesis, it has been found that temperature, relative humidity and precipitation were intimately correlated with the concentrations of GEM, RGM and PHg. A full AMDE appeared only at a temperature range of -23 to $-12\,^{\circ}$C, and it often occurred at a high RH and low precipitation during 2007-2011 at Zeppelin station, Ny-Ålesund. Relative humidity had an anti-correlation with PHg concentration in general, however, RH was also found to be anti-correlated with GEM during AMDEs. Through detailed case studies, it has been found that either very high relative humidity (around 98%) or no accumulated precipitation during the recent few hours backward trajectory would provide a good condition for the high PHg concentrations to occur.

The accumulation mode aerosols which have a size range between 100 and 562 nm in diameter had the most significant positive correlations with PHg concentration. The concentration of Aitken mode particles had no clear correlations with PHg concentration. It indicated that the particle size range of 100-562 nm was most characteristic for hosting PHg. The number concentration of accumulation mode particles dominated during AMDEs, and high PHg values often occurred high RH and low precipitation. It indicated that PHg might consist of much cloud associated Hg during AMDEs.

High GEM concentration quite often occurred right after each AMDE, and also occurred in summertime when the temperature was around $0\,^{\circ}$C during 2007-2011 at Zeppelin station. RGM concentration was often elevated to a high level in summertime and it was anti-correlated with RH. High PHg concentration was found in winter-spring period. Concentrations of RGM and PHg were positively correlated with each other in general.

Further research may need to confirm the high relative humidity found during AMDEs, because it was found to be much higher than that of previous study. The high PHg concentrations in wintertime may also need to be further studied. The correlations between the concentrations of RGM and PHg may need to be further studied due to the different trends reported previously. This thesis contained mostly statistic work and literature work, with no laboratory work. So the knowledge about the composition of PHg during the study period was limited, and it might need to be investigated for the future study.

Appendix A

Acronyms

AMAP Arctic monitoring and assessment programme

AMDEs Atmospheric mercury depletion events

AMEEs Atmospheric mercury emission events

ARL Air resources laboratory

CCN Cloud condensation nuclei

CPC Condensation particle counter

DMA Differential mobility analyzer

DMPS Differential mobility particle sizer

GAWSIS Global atmosphere watch station information system

GEM Gaseous elemental mercury

HYSPLIT Hybrid single-particle Lagrangian integrated trajectory model

MDL Method detection limit

MECCA Module efficiently calculating the chemistry of the atmosphere

NILU Norwegian institute for air research

NIVA Norwegian institute for water research

NOAA National oceanic and atmospheric administration

NPI Norwegian polar institute

NTNU Norwegian university of science and technology

PHg Particulate bound mercury

RGM Reactive gaseous mercury

RH Relative humidity

RPF Regenerable particulate filter

SD Standard deviation

SU Stockholm university

TGM Total gaseous mercury

Appendix B

HYSPLIT trajectory

The air parcel trajectories were simulated by HYSPLIT model, and it was simulated for the periods of all PHg episodes and AMDE episodes. The simulations started at the end of each episode at Zeppelin station, and tracked backwards to the start of each episode. The time period of each trajectory was in integer days.

B.1 HYSPLIT trajectories during PHg episodes

Figure B.1 to Figure B.10 are the trajectories during PHg episodes.

B.2 HYSPLIT trajectories during AMDE episodes

Figure B.11 to Figure B.20 are the trajectories during AMDEs episodes.

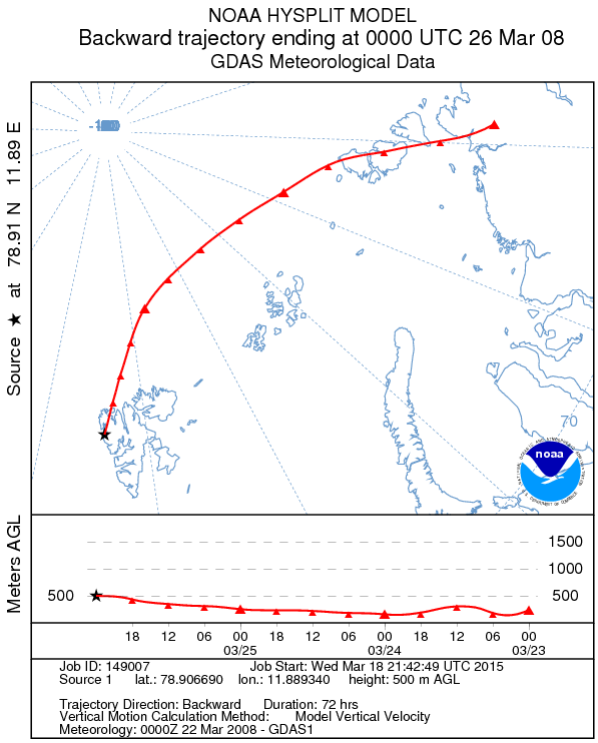

Figure B.1: PHg episode 1

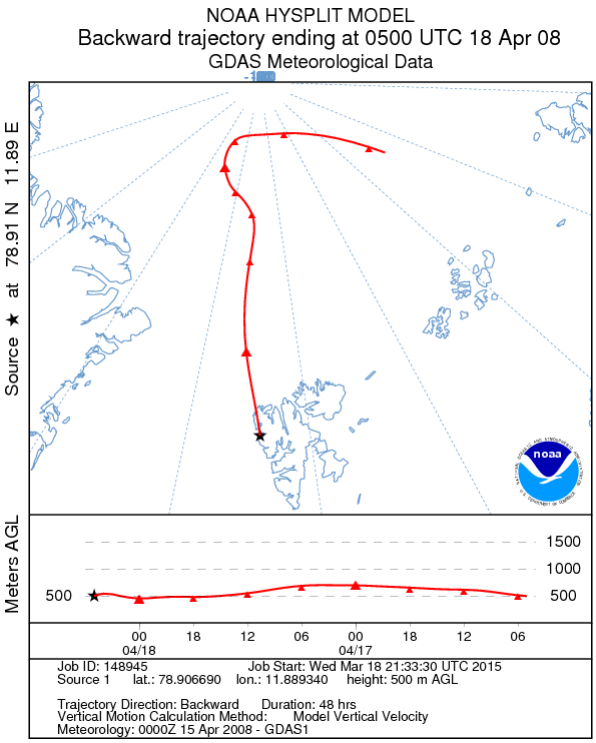

Figure B.2: PHg episode 2

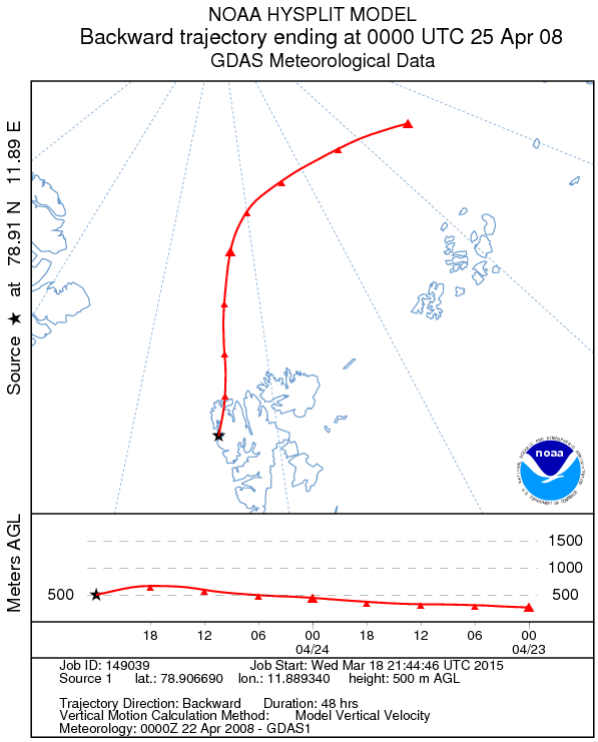

Figure B.3: PHg episode 3

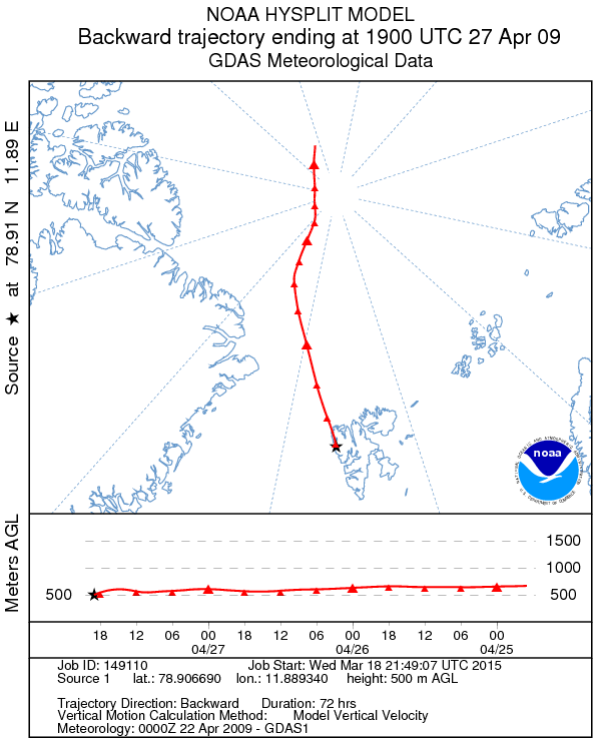

Figure B.4: PHg episode 4

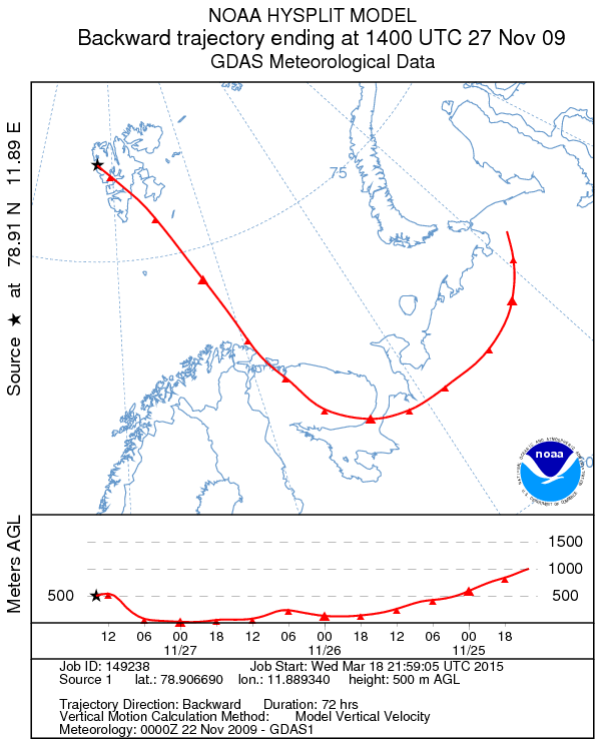

Figure B.5: PHg episode 5

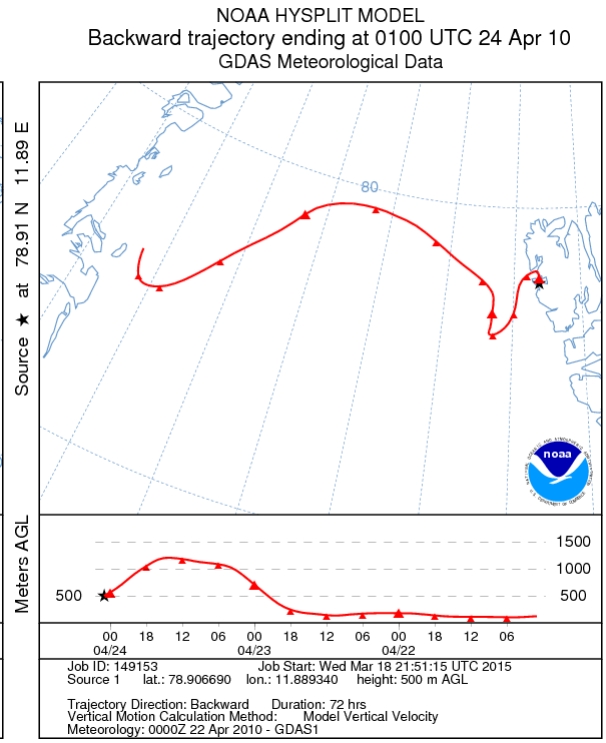

Figure B.6: PHg episode 6

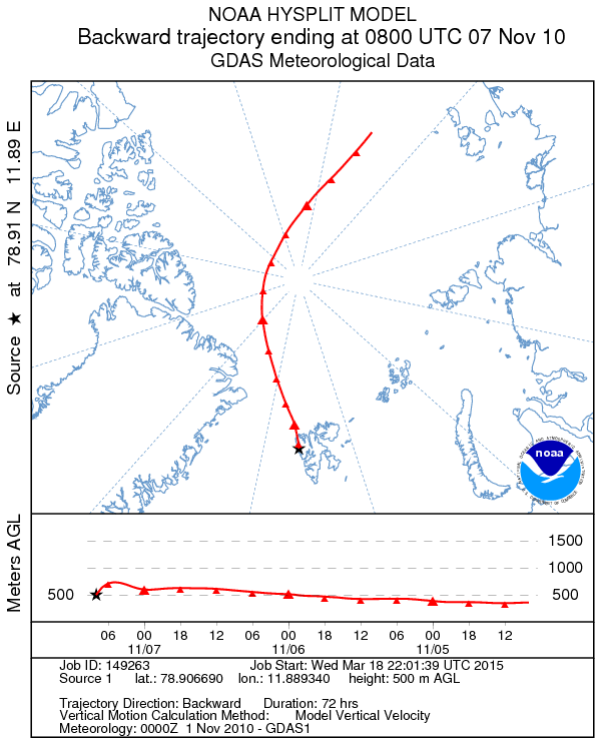

Figure B.7: PHg episode 7

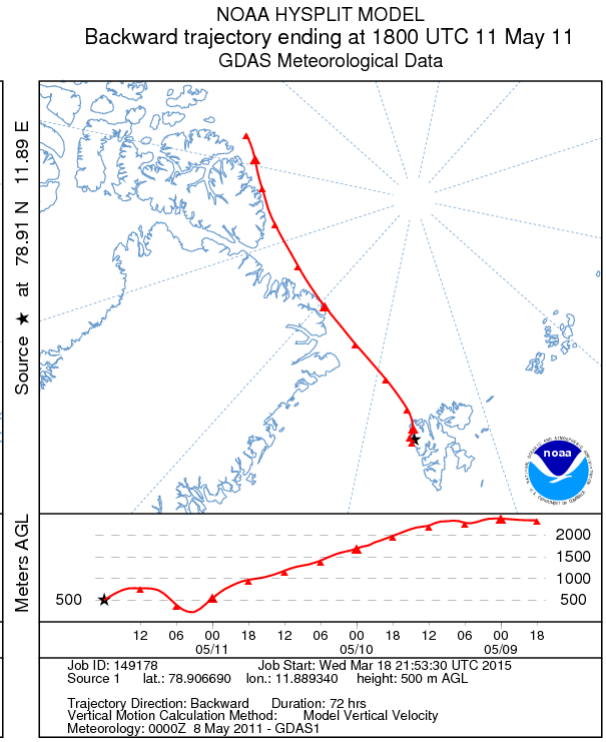

Figure B.8: PHg episode 8

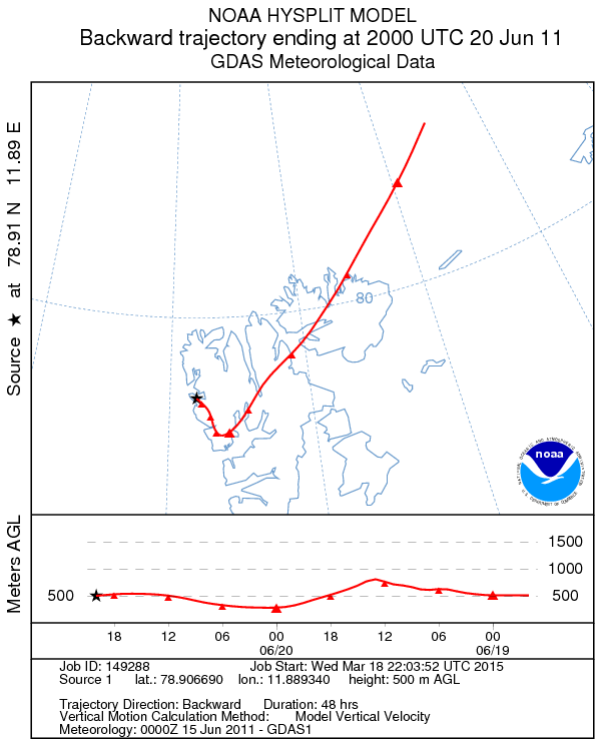

Figure B.9: PHg episode 9

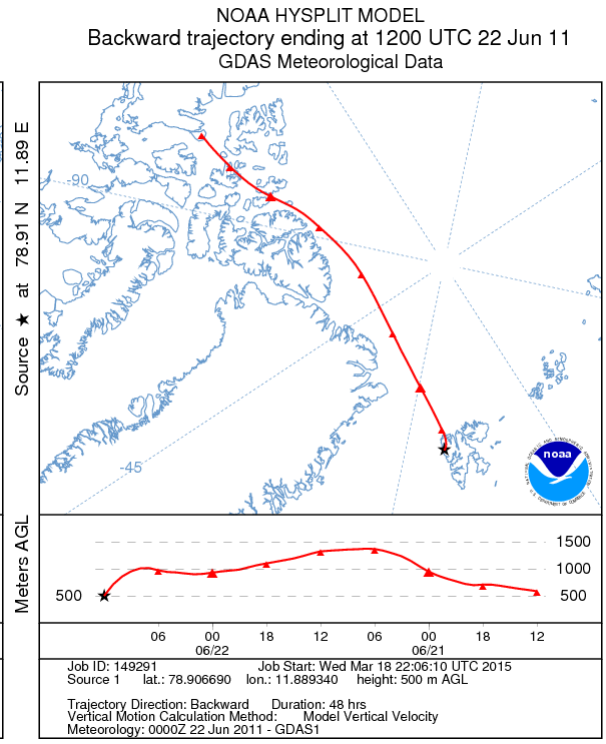

Figure B.10: PHg episode 10

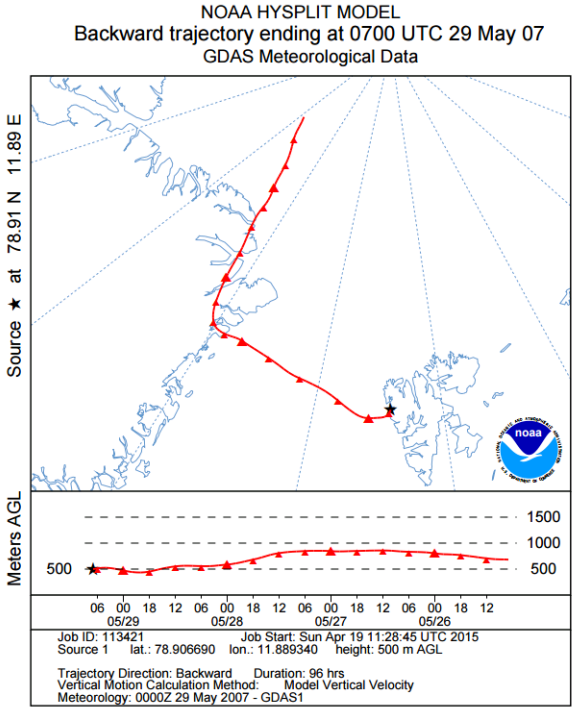

Figure B.11: AMDE episode 1

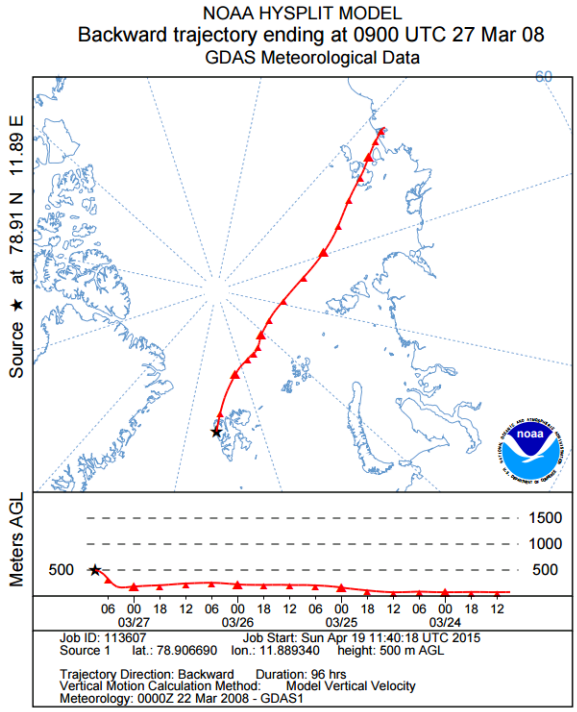

Figure B.12: AMDE episode 2

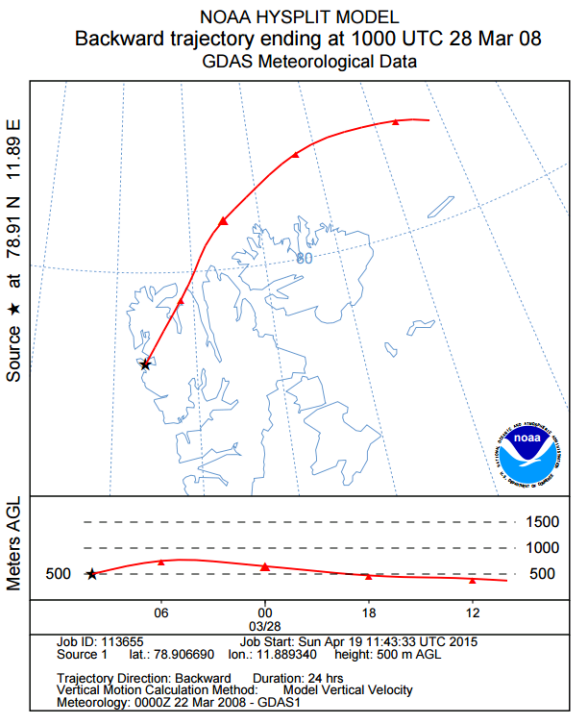

Figure B.13: AMDE episode 3

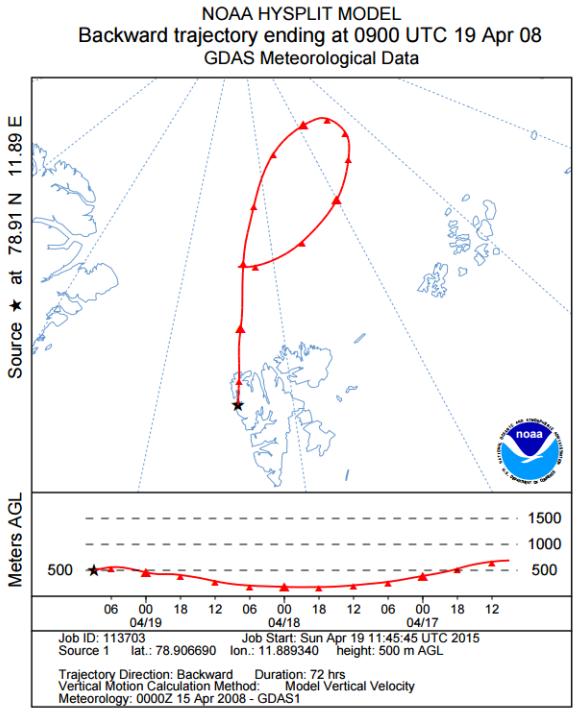

Figure B.14: AMDE episode 4

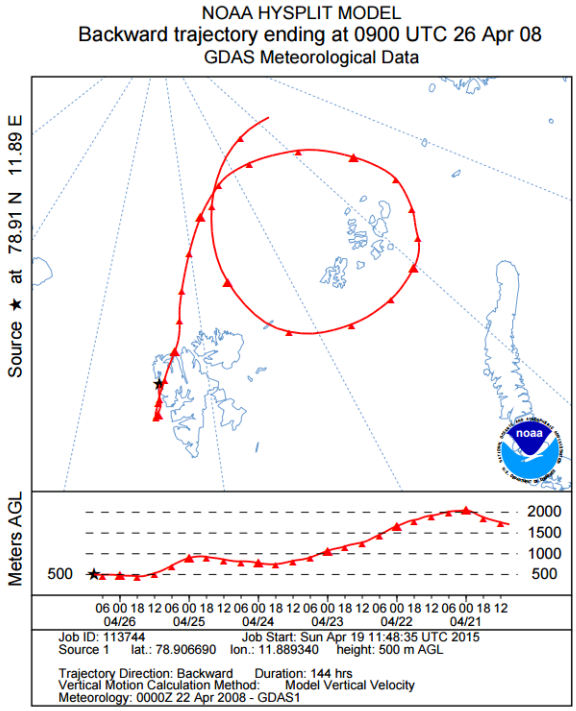

Figure B.15: AMDE episode 5

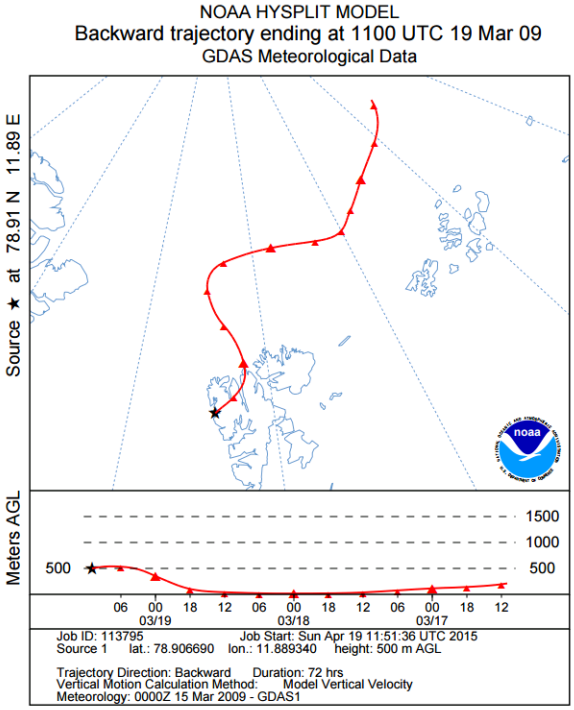

Figure B.16: AMDE episode 6

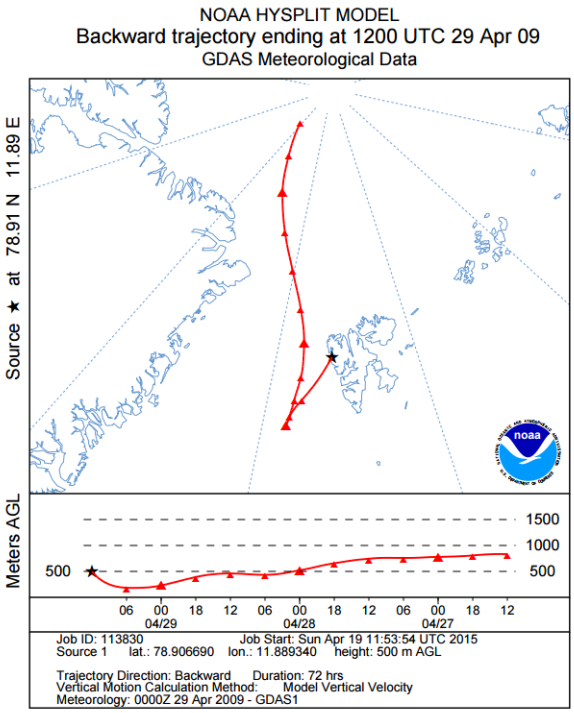

Figure B.17: AMDE episode 7

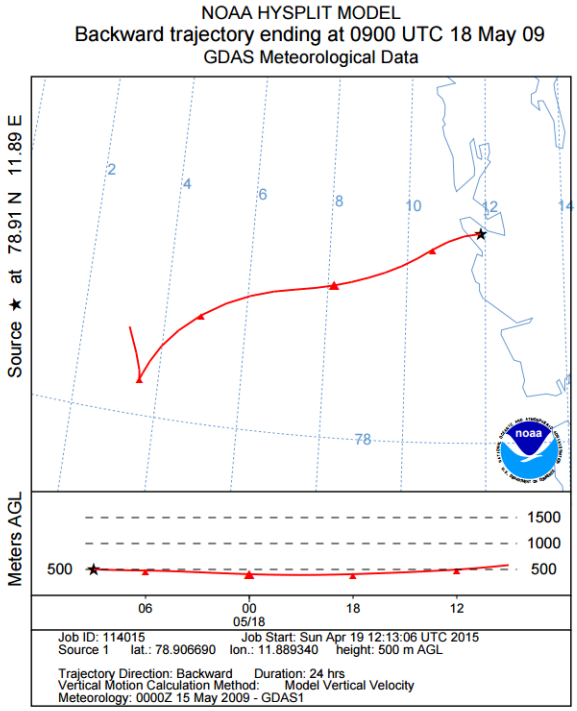

Figure B.18: AMDE episode 8

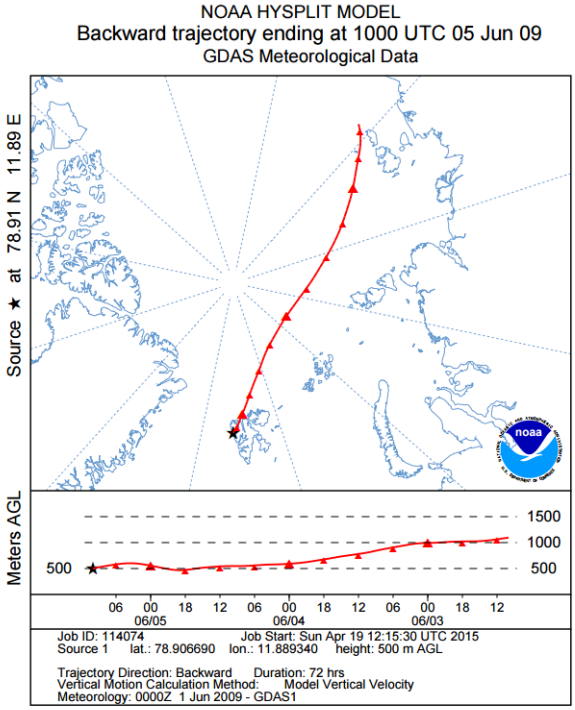

Figure B.19: AMDE episode 9

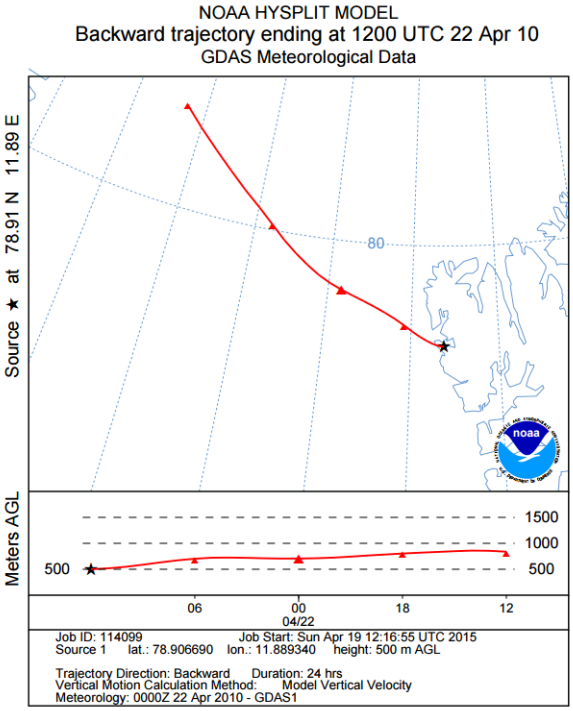

Figure B.20: AMDE episode 10

Bibliography

AMAP (2011). Arctic Pollution 2011. *Arctic Monitoring and Assessment Programme (AMAP)*, (ISBN-13978-82-7971-066-0). vi38 pp.

Amos, H. M., Jacob, D. J., Holmes, C., Fisher, J. A., Wang, Q., Yantosca, R. M., Corbitt, E. S., Galarneau, E., Rutter, A., Gustin, M., et al. (2012). Gas-particle partitioning of atmospheric Hg (II) and its effect on global mercury deposition. *Atmospheric Chemistry and Physics*, 12(1):591–603.

ARL (2015). Hybrid single-particle lagrangian integrated trajectory - (HYSPLIT) model. http://www.arl.noaa.gov/HYSPLIT_info.php.

Aspmo, K., Temme, C., Berg, T., Ferrari, C., Gauchard, P.-A., Fain, X., and Wibetoe, G. (2006). Mercury in the atmosphere, snow and melt water ponds in the North Atlantic Ocean during Arctic summer. *Environmental science & technology*, 40(13):4083–4089.

Balabanov, N. B. and Peterson, K. A. (2003). Mercury and reactive halogens: the thermochemistry of Hg+{Cl_2, Br_2, BrCl, ClO, and BrO}. *The Journal of Physical Chemistry A*, 107(38):7465–7470.

Barrie, L. A. (1986). Arctic air pollution: an overview of current knowledge. *Atmospheric Environment (1967)*, 20(4):643–663.

Baukal Jr, C. E. (2004). *Industrial combustion pollution and control*. CRC Press.

Berg, T., Aas, W., Pacyna, J., Uggerud, H. T., and Vadset, M. (2008). Atmospheric trace metal concentrations at Norwegian background sites during 25 years and its relation to European emissions. *Atmospheric Environment*, 42(32):7494–7501.

Berg, T., Pfaffhuber, K., Cole, A., Engelsen, O., and Steffen, A. (2013). Ten-year trends in atmospheric mercury concentrations, meteorological effects and climate variables at Zeppelin, Ny-Ålesund. *Atmospheric Chemistry and Physics*, 13(13):6575–6586.

Berg, T., Sekkesæter, S., Steinnes, E., Valdal, A.-K., and Wibetoe, G. (2003). Springtime depletion of mercury in the European Arctic as observed at Svalbard. *Science of the total environment*, 304(1):43–51.

Bernstein, L., Bosch, P., Canziani, O., Chen, Z., Christ, R., Davidson, O., Hare, W., Huq, S., Karoly, D., Kattsov, V., et al. (2007). IPCC, 2007: Climate Change 2007-synthesis Report. Contribution of Working Groups I, II and III to the Fourth Assessment Report of the Intergovernmental Panel on Climate Change. *IPCC, Geneva, Switzerland*.

Calmorin, L. (2006). *Statistics in education and the sciences*. Rex Bookstore, Inc.

Calvert, J. G. and Lindberg, S. E. (2005). Mechanisms of mercury removal by O_3 and OH in the atmosphere. *Atmospheric Environment*, 39(18):3355–3367.

CFR (1986). *40 CFR Part 136, Appendix B to Part 136 - Definition and Procedure for the Determination of the Method Detection Limit-Revision 1.11*, 1.11 edition.

Cobbett, F. D., Steffen, A., Lawson, G., and Van Heyst, B. J. (2007). Gem fluxes and atmospheric mercury concentrations (GEM, RGM and Hgp) in the Canadian Arctic at Alert, Nunavut, Canada (February–June 2005). *Atmospheric Environment*, 41(31):6527–6543.

Cole, A. and Steffen, A. (2010). Trends in long-term gaseous mercury observations in the Arctic and effects of temperature and other atmospheric conditions. *Atmospheric Chemistry and Physics*, 10(10):4661–4672.

Cole, A. S., Steffen, A., Eckley, C. S., Narayan, J., Pilote, M., Tordon, R., Graydon, J. A., St Louis, V. L., Xu, X., and Branfireun, B. A. (2014). A survey of mercury in air and precipitation across Canada: Patterns and trends. *Atmosphere*, 5(3):635–668.

Corbitt, E. S., Jacob, D. J., Holmes, C. D., Streets, D. G., and Sunderland, E. M. (2011). Global source–receptor relationships for mercury deposition under present-day and 2050 emissions scenarios. *Environmental science & technology*, 45(24):10477–10484.

Dietz, R., Outridge, P. M., and Hobson, K. A. (2009). Anthropogenic contributions to mercury levels in present-day arctic animals-a review. *Science of the Total Environment*, 407(24):6120–6131.

Durnford, D., Dastoor, A., Figueras-Nieto, D., and Ryjkov, A. (2010). Long range transport of mercury to the Arctic and across Canada. *Atmospheric Chemistry and Physics*, 10(13):6063–6086.

Ebinghaus, R., Kock, H. H., Temme, C., Einax, J. W., Löwe, A. G., Richter, A., Burrows, J. P., and Schroeder, W. H. (2002). Antarctic springtime depletion of atmospheric mercury. *Environmental Science & Technology*, 36(6):1238–1244.

Ehrlich, H. L. and Newman, D. K. (2008). *Geomicrobiology*. CRC press.

Engvall, A.-C., Krejci, R., Ström, J., Treffeisen, R., Scheele, R., Hermansen, O., and Paatero, J. (2008). Changes in aerosol properties during spring-summer period in the Arctic troposphere. *Atmospheric Chemistry and Physics*, 8(3):445–462.

Feddersen, D., Talbot, R., Mao, H., and Sive, B. (2012). Size distribution of particulate mercury in marine and coastal atmospheres. *Atmospheric Chemistry and Physics*, 12(22):10899–10909.

Gauchard, P.-A., Aspmo, K., Temme, C., Steffen, A., Ferrari, C., Berg, T., Ström, J., Kaleschke, L., Dommergue, A., Bahlmann, E., et al. (2005). Study of the origin of atmospheric mercury depletion events recorded in Ny-Ålesund, Svalbard, spring 2003. *Atmospheric Environment*, 39(39):7620–7632.

GAWSIS (2014). Zeppelin Mountain (Ny-Ålesund) (Norway). http://gaw.empa.ch/gawsis/reports.asp?StationID=18.

Guentzel, J. L., Landing, W. M., Gill, G. A., and Pollman, C. D. (2001). Processes influencing rainfall deposition of mercury in Florida. *Environmental science & technology*, 35(5):863–873.

Gustin, M. and Jaffe, D. (2010). Reducing the uncertainty in measurement and understanding of mercury in the atmosphere. *Environmental science & technology*, 44(7):2222–2227.

Hall, B. (1995). The gas phase oxidation of elemental mercury by ozone. In *Mercury as a Global Pollutant*, pages 301–315. Springer.

Hari, P. and Kulmala, L. (2008). Boreal forest and climate change. advances in global change research, vol. 34.

Hedgecock, I. M. and Pirrone, N. (2004). Chasing quicksilver: Modeling the atmospheric lifetime of Hg0 (g) in the marine boundary layer at various latitudes. *Environmental science & technology*, 38(1):69–76.

Hirdman, D., Aspmo, K., Burkhart, J., Eckhardt, S., Sodemann, H., and Stohl, A. (2009). Transport of mercury in the Arctic atmosphere: Evidence for a spring-time net sink and summer-time source. *Geophysical Research Letters*, 36(12).

Holmes, C. D., Jacob, D. J., Corbitt, E. S., Mao, J., Yang, X., Talbot, R., and Slemr, F. (2010). Global atmospheric model for mercury including oxidation by bromine atoms. *Atmospheric Chemistry and Physics*, 10(24):12037–12057.

Holmes, C. D., Jacob, D. J., and Yang, X. (2006). Global lifetime of elemental mercury against oxidation by atomic bromine in the free troposphere. *Geophysical Research Letters*, 33(20).

Keeler, G., Glinsorn, G., and Pirrone, N. (1995). Particulate mercury in the atmosphere: its significance, transport, transformation and sources. *Water, Air, and Soil Pollution*, 80(1-4):159–168.

Kim, P.-R., Han, Y.-J., Holsen, T. M., and Yi, S.-M. (2012). Atmospheric particulate mercury: Concentrations and size distributions. *Atmospheric Environment*, 61:94–102.

Kirk, J. L., St. Louis, V. L., and Sharp, M. J. (2006). Rapid reduction and reemission of mercury deposited into snowpacks during atmospheric mercury depletion events at Churchill, Manitoba, Canada. *Environmental science & technology*, 40(24):7590–7596.

Kock, H., Bieber, E., Ebinghaus, R., Spain, T., and Thees, B. (2005). Comparison of long-term trends and seasonal variations of atmospheric mercury concentrations at the two european coastal monitoring stations Mace Head, Ireland, and Zingst, Germany. *Atmospheric Environment*, 39(39):7549–7556.

Lalonde, J. D., Poulain, A. J., and Amyot, M. (2002). The role of mercury redox reactions in snow on snow-to-air mercury transfer. *Environmental science & technology*, 36(2):174–178.

Landis, M. S., Stevens, R. K., Schaedlich, F., and Prestbo, E. M. (2002). Development and characterization of an annular denuder methodology for the measurement of divalent inorganic reactive gaseous mercury in ambient air. *Environmental science & technology*, 36(13):3000–3009.

Lindberg, S., Brooks, S., Lin, C., Scott, K., Meyers, T., Chambers, L., Landis, M., and Stevens, R. (2001). Formation of reactive gaseous mercury in the arctic: evidence of oxidation of Hg to gas-phase Hg-II compounds after arctic sunrise. *Water, Air and Soil Pollution: Focus*, 1(5-6):295–302.

Lindberg, S., Bullock, R., Ebinghaus, R., Engstrom, D., Feng, X., Fitzgerald, W., Pirrone, N., Prestbo, E., and Seigneur, C. (2007). A synthesis of progress and uncertainties in attributing the sources of mercury in deposition. *AMBIO: A Journal of the Human Environment*, 36(1):19–33.

Lindberg, S. and Stratton, W. (1998). Atmospheric mercury speciation: concentrations and behavior of reactive gaseous mercury in ambient air. *Environmental Science & Technology*, 32(1):49–57.

Lindberg, S. E., Brooks, S., Lin, C.-J., Scott, K. J., Landis, M. S., Stevens, R. K., Goodsite, M., and Richter, A. (2002). Dynamic oxidation of gaseous mercury in the Arctic troposphere at polar sunrise. *Environmental Science & Technology*, 36(6):1245–1256.

Lu, J. Y. and Schroeder, W. H. (2004). Annual time-series of total filterable atmospheric mercury concentrations in the Arctic. *Tellus B*, 56(3):213–222.

Maxwell, J. A., Holsen, T. M., and Mondal, S. (2013). Gaseous elemental mercury (GEM) emissions from snow surfaces in northern New York. *PloS one*, 8(7):e69342.

Moen, I. M. (2012). Fraksjonering av atmosfærisk kvikksølv på Zeppelin, Ny-Ålesund. Master's thesis, Norwegian University of Science and Technology.

Nabi, S. (2014). *Toxic Effects of Mercury*. Springer.

NPI (2014). The Zeppelin Observatory in Ny-Ålesund. http://www.npolar.no/en/about-us/stations-vessels/zeppelin/.

Oliver, J. E. (2005). *The encyclopedia of world climatology*. Springer Science & Business Media.

Osawa, T., Ueno, T., and Fu, F. (2007). Sequential variation of atmospheric mercury in Tokai-mura, seaside area of eastern central Japan. *Journal of Geophysical Research: Atmospheres (1984–2012)*, 112(D19).

Pacyna, E. G., Pacyna, J., Sundseth, K., Munthe, J., Kindbom, K., Wilson, S., Steenhuisen, F., and Maxson, P. (2010). Global emission of mercury to the atmosphere from anthropogenic sources in 2005 and projections to 2020. *Atmospheric Environment*, 44(20):2487–2499.

Pandis, S. N. and Seinfeld, J. H. (2006). *Atmospheric chemistry and physics: From air pollution to climate change*. Wiley.

Penner, J. E., Andreae, M., Annegarn, H., Barrie, L., Feichter, J., Hegg, D., Jayaraman, A., Leaitch, R., Murphy, D., Nganga, J., et al. (2001). Aerosols, their direct and indirect effects. In *Climate Change 2001: The Scientific Basis. Contribution of Working Group I to the Third Assessment Report of the Intergovernmental Panel on Climate Change*, pages 289–348. Cambridge University Press.

Peterson, C., Gustin, M., and Lyman, S. (2009). Atmospheric mercury concentrations and speciation measured from 2004 to 2007 in Reno, Nevada, USA. *Atmospheric Environment*, 43(30):4646–4654.

Pfaffhuber, K., Berg, T., Hirdman, D., and Stohl, A. (2012). Atmospheric mercury observations from Antarctica: seasonal variation and source and sink region calculations. *Atmospheric Chemistry and Physics*, 12(7):3241–3251.

Pirrone, N., Cinnirella, S., Feng, X., Finkelman, R., Friedli, H., Leaner, J., Mason, R., Mukherjee, A., Stracher, G., Streets, D., et al. (2010). Global mercury emissions to the atmosphere from anthropogenic and natural sources. *Atmospheric Chemistry and Physics*, 10(13):5951–5964.

Pirrone, N., Keeler, G., and Allegrini, I. (1996). Particle size distributions of atmospheric mercury in urban and rural areas. *Journal of Aerosol Science*, 27:S13–S14.

Pirrone, N. and Mahaffey, K. R. (2005). *Dynamics of mercury pollution on regional and global scales: atmospheric processes and human exposures around the world*. Springer Science & Business Media.

Poissant, L. and Pilote, M. (2003). Time series analysis of atmospheric mercury in Kuujjuarapik/Whapmagoostui (Quebec). In *Journal de Physique IV (Proceedings)*, volume 107, pages 1079–1082. EDP sciences.

Poissant, L., Pilote, M., Xu, X., Zhang, H., and Beauvais, C. (2004). Atmospheric mercury speciation and deposition in the bay st. francois wetlands. *Journal of Geophysical Research: Atmospheres (1984–2012)*, 109(D11).

Rubin, A. (2012). *Statistics for evidence-based practice and evaluation*. Cengage Learning.

Sander, R., Kerkweg, A., Jöckel, P., and Lelieveld, J. (2005). Technical note: The new comprehensive atmospheric chemistry module MECCA. *Atmospheric Chemistry and Physics*, 5(2):445–450.

Schroeder, W., Anlauf, K., Barrie, L., Lu, J., Steffen, A., Schneeberger, D., and Berg, T. (1998). Arctic springtime depletion of mercury. *Nature*, 394(6691):331–332.

Schroeder, W. H. and Munthe, J. (1998). Atmospheric mercury-an overview. *Atmospheric Environment*, 32(5):809–822.

Selin, N. E., Jacob, D. J., Park, R. J., Yantosca, R. M., Strode, S., Jaeglé, L., and Jaffe, D. (2007). Chemical cycling and deposition of atmospheric mercury: Global constraints from observations. *Journal of Geophysical Research: Atmospheres (1984–2012)*, 112(D2).

Shannon, J. D. and Voldner, E. C. (1995). Modeling atmospheric concentrations of mercury and deposition to the Great Lakes. *Atmospheric Environment*, 29(14):1649–1661.

Sharma, S., Ishizawa, M., Chan, D., Lavoué, D., Andrews, E., Eleftheriadis, K., and Maksyutov, S. (2013). 16-year simulation of Arctic black carbon: Transport, source contribution, and sensitivity analysis on deposition. *Journal of Geophysical Research: Atmospheres*, 118(2):943–964.

Sheu, G.-R. and Mason, R. P. (2004). An examination of the oxidation of elemental mercury in the presence of halide surfaces. *Journal of Atmospheric Chemistry*, 48(2):107–130.

Slemr, F., Brunke, E.-G., Ebinghaus, R., Temme, C., Munthe, J., Wängberg, I., Schroeder, W., Steffen, A., and Berg, T. (2003). Worldwide trend of atmospheric mercury since 1977. *Geophysical Research Letters*, 30(10).

Sommar, J., Gårdfeldt, K., Strömberg, D., and Feng, X. (2001). A kinetic study of the gas-phase reaction between the hydroxyl radical and atomic mercury. *Atmospheric Environment*, 35(17):3049–3054.

Sommar, J., Wängberg, I., Berg, T., Gårdfeldt, K., Munthe, J., Richter, A., Urba, A., Wittrock, F., and Schroeder, W. (2007). Circumpolar transport and air-surface exchange of atmospheric mercury at Ny-Ålesund (79 N), Svalbard, spring 2002. *Atmospheric Chemistry and Physics*, 7(1):151–166.

Steen, A., Berg, T., Dastoor, A., Durnford, D., Engelsen, O., Hole, L., and Pfaffhuber, K. (2011). Natural and anthropogenic atmospheric mercury in the European Arctic: a fractionation study. *Atmospheric Chemistry and Physics*, 11(13):6273–6284.

Steen, A. O., Berg, T., Dastoor, A. P., Durnford, D. A., Hole, L. R., and Pfaffhuber, K. A. (2009). Dynamic exchange of gaseous elemental mercury during polar night and day. *Atmospheric Environment*, 43(35):5604–5610.

Steffen, A., Bottenheim, J., Cole, A., Douglas, T., Ebinghaus, R., Friess, U., Netcheva, S., Nghiem, S., Sihler, H., and Staebler, R. (2013). Atmospheric mercury over sea ice during the OASIS-2009 campaign. *Atmospheric Chemistry and Physics*, 13(14):7007–7021.

Steffen, A., Bottenheim, J., Cole, A., Ebinghaus, R., Lawson, G., and Leaitch, W. (2014). Atmospheric mercury speciation and mercury in snow over time at Alert, Canada. *Atmospheric Chemistry and Physics*, 14(5):2219–2231.

Steffen, A., Douglas, T., Amyot, M., Ariya, P., Aspmo, K., Berg, T., Bottenheim, J., Brooks, S., Cobbett, F., Dastoor, A., et al. (2008). A synthesis of atmospheric mercury depletion event chemistry in the atmosphere and snow. *Atmospheric Chemistry and Physics*, 8(6):1445–1482.

Steffen, A., Schroeder, W., Bottenheim, J., Narayan, J., and Fuentes, J. D. (2002). Atmospheric mercury concentrations: measurements and profiles near snow and ice surfaces in the Canadian Arctic during Alert 2000. *Atmospheric Environment*, 36(15):2653–2661.

Steffen, A., Schroeder, W., Macdonald, R., Poissant, L., and Konoplev, A. (2005). Mercury in the arctic atmosphere: An analysis of eight years of measurements of GEM at Alert (Canada) and a comparison with observations at Amderma (Russia) and Kuujjuarapik (Canada). *Science of the total environment*, 342(1):185–198.

Stephens, C. R., Shepson, P. B., Steffen, A., Bottenheim, J. W., Liao, J., Huey, L. G., Apel, E., Weinheimer, A., Hall, S. R., Cantrell, C., et al. (2012). The relative importance of chlorine and bromine radicals in the oxidation of atmospheric mercury at Barrow, Alaska. *Journal of Geophysical Research: Atmospheres (1984–2012)*, 117(D14).

Stern, G. A., Macdonald, R. W., Outridge, P. M., Wilson, S., Chetelat, J., Cole, A., Hintelmann, H., Loseto, L. L., Steffen, A., Wang, F., et al. (2012). How does climate change influence arctic mercury? *Science of the total environment*, 414:22–42.

Ström, J., Umegård, J., Tørseth, K., Tunved, P., Hansson, H.-C., Holmén, K., Wismann, V., Herber, A., and König-Langlo, G. (2003). One year of particle size distribution and aerosol chemical composition measurements at the Zeppelin Station, Svalbard, March 2000–March 2001. *Physics and Chemistry of the Earth, Parts A/B/C*, 28(28):1181–1190.

Tekran (2008a). *Model 1130 Mercury Speciation Unit (Patented)*. 330 Nantucket Boulevard, Toronto, Canada M1P 2P4, 041514 edition.

Tekran (2008b). *Model 1135 Particulate Mercury Unit (Patented)*. 330 Nantucket Boulevard, Toronto, Canada M1P 2P4, 041514 edition.

Tekran (2009). *New Tekran Pre-Packed and Batch Tested Soda lime Traps*. 330 Nantucket Boulevard, Toronto, Canada M1P 2P4, 1.00 edition.

Tekran (2015). http://www.tekran.com/products/ambient-air/overview/.

Temme, C., Ebinghaus, R., Einax, J. W., Steffen, A., and Schroeder, W. H. (2004). Time series analysis of long-term data sets of atmospheric mercury concentrations. *Analytical and bioanalytical chemistry*, 380(3):493–501.

Temme, C., Einax, J. W., Ebinghaus, R., and Schroeder, W. H. (2003). Measurements of atmospheric mercury species at a coastal site in the Antarctic and over the South Atlantic Ocean during polar summer. *Environmental science & technology*, 37(1):22–31.

TROPOS (2015). *SMPS - DMPS (Mobility Particle Size Spectrometer)*. http://wiki.tropos.de/index.php/SMPS_-_DMPS_%28Mobility_Particle_Size_Spectrometer%29.

Tunved, P., Ström, J., and Krejci, R. (2013). Arctic aerosol life cycle: linking aerosol size distributions observed between 2000 and 2010 with air mass transport and precipitation at Zeppelin station, Ny-Ålesund, Svalbard. *Atmospheric Chemistry and Physics*, 13(7):3643–3660.

Wang, P. K. (2013). *Physics and dynamics of clouds and precipitation*. Cambridge University Press.

Wierig, H.-J. (2004). *Properties of fresh concrete: proceedings of the international rilem colloquium*, volume 10. CRC Press.

Winklmayr, W., Reischl, G., Lindner, A., and Berner, A. (1991). A new electromobility spectrometer for the measurement of aerosol size distributions in the size range from 1 to 1000 nm. *Journal of Aerosol Science*, 22(3):289–296.

Xie, Z.-Q., Sander, R., Pöschl, U., and Slemr, F. (2008). Simulation of atmospheric mercury depletion events (AMDEs) during polar springtime using the MECCA box model. *Atmospheric Chemistry and Physics*, 8(23):7165–7180.

Zhang, L., Wright, L. P., and Blanchard, P. (2009). A review of current knowledge concerning dry deposition of atmospheric mercury. *Atmospheric Environment*, 43(37):5853–5864.